

8
9
6
3
0
6

WADD-TR-61-181

Part IV

COPY 2 of 3 COPIES

THE TENSILE DUCTILITY-TRANSITION IN MOLYBDENUM

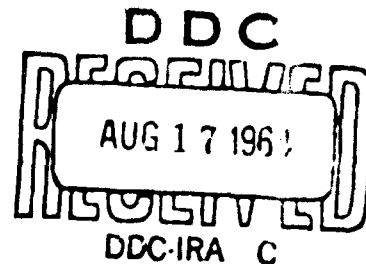
TECHNICAL DOCUMENTARY REPORT NO. WADD-TR-61-181

Part IV

July 1964

Air Force Materials Laboratory
Research and Technology Division
Air Force Systems Command
Wright-Patterson Air Force Base, Ohio

Project No. 7351, Task No. 735101



(Prepared under Contract No. AF 33(657)-8424
by ManLabs, Inc., Cambridge, Massachusetts:
B. S. Lement and K. Kreder, authors)

NOTICES

When Government drawings, specification, or other data are used for any purpose other than in connection with a definitely related Government procurement operation, the United States Government thereby incurs no responsibility nor any obligation whatsoever; and the fact that the Government may have formulated, furnished, or in any way supplied the said drawings, specification, or other data, is not to be regarded by implication or otherwise as in any manner licensing the holder or any other person or corporation, or conveying any rights or permission to manufacture, use or sell any patented invention that may in any way be related thereto.

Qualified requesters may obtain copies of this report from the Defense Documentation Center (DDC), (formerly ASTIA), Cameron Station, Bldg. 5, 5010 Duke Street, Alexandria, Virginia, 22314.

This report has been released to the office of Technical Services, U.S. Department of Commerce, Washington 25, D.C., for sale to the general public.

Copies of this report should not be returned to the Research and Technology Division Wright-Patterson Air Force Base, Ohio, unless return is required by security consideration, contractual obligations, or notice on a specific document.

FOREWORD

This report was prepared by ManLabs, Inc. under USAF Contract No. AF33(657)-8424. This contract was initiated under Project No. 7351 "Metallic Materials", Task No. 735101 "Refractory Metals". The work was administered under the AF Materials Laboratory, Metals and Ceramics Division with Mr. K. Elbaum acting as project engineer.

The period covered by this report is 30 April 1963 to 30 April 1964.

ABSTRACT

An investigation was carried out to determine the nature of the tensile ductility transition in recrystallized molybdenum strip of three interstitial contents. For a fine grain size, the tensile ductility transition temperature (T_d) and the brittleness transition temperature (T_b) were found to approximately coincide; whereas with increase in grain size T_d is raised and T_b is lowered. The occurrence of a minimum in the fracture stress (σ_F) at T_d appears to be associated with the temperature dependence of the necking stress (σ_n). Prestraining above T_d , was found to result in as much as a 20% increase in σ_F as determined at temperature below T_d . In general, the mode of fracture initiation was found to be intergranular at T_d or below and cleavage above T_d . For a test temperature above as well as below T_d , crack initiation appears to be the controlling step in fracture. Considering σ_F as a flow stress corresponding to the fracture strain (ϵ_F), the variation of σ_F with temperature above T_d was predicted within about 15%. Based on a modification of the Cottrell relation for crack initiation, the increase in σ_F above T_d is associated with a decrease in both the flow locking parameter (k_f) and the effective grain size.

This technical documentary report has been reviewed and is approved.



I. Perlmutter
Chief, Physical Metallurgy Branch
Metals and Ceramics Division
AF Materials Laboratory

TABLE OF CONTENTS

	Page
I. INTRODUCTION.	1
A. Background.	1
B. Scope of Investigation.	1
II. EXPERIMENTAL PROCEDURES.	3
A. Materials.	3
B. Recrystallization-Anneals.	3
C. Uniaxial Prestrain.	3
D. Mechanical Testing.	3
E. Precracked Charpy Slow Bend Tests.	6
F. Determination of Grain Size.	6
G. Fractography.	6
III. RESULTS AND DISCUSSION.	7
A. Flow and Fracture Characteristics of Mo-E2 Strip.	7
B. Flow and Fracture Characteristics of Mo-E3 Strip.	26
C. Flow and Fracture Characteristics of Mo-E4 Strip.	39
D. Fractographic Characteristics.	39
E. Theoretical Considerations.	60
IV. CONCLUSIONS.	80
REFERENCES.	81
APPENDIX I.	82

Illustrations

Figure		Page
1	Effect of Test Temperature on the Tensile Properties of Recrystallized Molybdenum (Mo-E2) Strip ($l = 0.026$ mm).	8
2	Effect of Test Temperature of Tensile Properties of Recrystallized Molybdenum (Mo-E2) Strip ($l = 0.044$ mm)	9
3	Effect of Test Temperature on Tensile Properties of Recrystallized Molybdenum (Mo-E2) Strip ($l = 0.174$ mm)	10
4	Variation of Yield Stress (σ_y) with Grain Size ($l^{-1/2}$) of Molybdenum (Mo-E2 Strip in Test Temperature Range of +25 to -150°C.	12
5	Variation of Yield Stress Parameter (k_y) and Frictional Stress (σ_i) of Molybdenum (Mo-E2) Strip with Test Temperature. The Parameter K_y and Frictional Stress σ_i are Based on Normal Stress (σ_y) and Full Grain Diameter (l).	13
6	Comparison of Predicted and Experimentally Observed Variations of the Fracture Stress (σ_F) and Fracture Strain (ϵ_F) with Grain Size ($l^{-1/2}$) of Recrystallized Molybdenum (Mo-E2 Strip for a Test Temperature of -40°C Based on Data Obtained for Fine Grain Size ($l = 0.026$ mm).	14
7	Variation of the Observed Fracture Stress (σ_F) at Constant Strain with Grain Size ($l^{-1/2}$) for Recrystallized Molybdenum Strip (Mo-E2).	16
8	Variation of Strain Hardening Exponent (n) and Strain Hardening Coefficient (K) with Test Temperature for Recrystallized Molybdenum (Mo-E2) Strip ($l = 0.026$ mm).	22
9	Variation of Strain Hardening Exponent (n) and Strain Hardening Coefficient (K) with Test Temperature for Recrystallized Molybdenum (Mo-E2) Strip ($l = 0.044$ mm).	23
10	Variation of Strain Hardening Exponent (n) and Strain Hardening Coefficient (K) with Test Temperature for Recrystallized Molybdenum (Mo-E2) Strip ($l = 0.174$ mm).	24
11	Effect of Test Temperature on Tensile Properties of Recrystallized Molybdenum (Mo-E3 Strip ($l = 0.023$ mm)).	28
12	Variation of Strain Hardening Exponent (n) and Strain Hardening Coefficient (K) with Test Temperature for Recrystallized Molybdenum (Mo-E3) Strip ($l = 0.023$ mm).	29

Illustrations (Continued)

Figure		Page
13	Effect of Uniform Prestraining Mo-E3 at -20°C and $+25^{\circ}\text{C}$ on the Fracture Stress at -100°C , -150°C , and -196°C	30
14	Effect of Prestraining Mo-E at -20°C and $+25^{\circ}\text{C}$ on Fracture Strain (ϵ_F) and Total Strain ($\epsilon_{pr} + \epsilon_F$) at -100°C	32
15	Effect of Prestraining Mo-E at -20°C and $+25^{\circ}\text{C}$ on Fracture Strain (ϵ_F) and Total Strain ($\epsilon_{pr} + \epsilon_F$) at -150°C	33
16	Effect of Prestraining Mo-E3 at -20°C and $+25^{\circ}\text{C}$ on Fracture Strain (ϵ_F) and Total Strain ($\epsilon_{pr} + \epsilon_F$) at -196°C	34
17	Effect of Test Temperature on Tensile Properties of Recrystallized Molybdenum (Mo-E4) Strip ($l = 0.020$ mm)	41
18	Variation of Strain Hardening Exponent (n) and Strain Hardening Coefficient (K) with Test Temperature for Recrystallized Molybdenum (Mo-E4) Strip ($l = 0.020$ mm).	42
19	Tensile Fracture of Mo-E2 (0.026 mm grain size) at $+25^{\circ}\text{C}$ Showing Several Cleavage Facets (with Cleavage steps) and Two Intergranular Facets (smooth).	43
20	Same Specimen as Fig. 19 - Showing Intergranular Facets Which Apparently Contains Fine Precipitates.	43
21	Tensile Fracture of Mo-E2 (0.026 mm grain size) at -30°C Showing Several Cleavage Facets.	44
22	Same Specimen as Fig. 21 - Showing Cleavage Steps and Smooth Intergranular Facets Which Apparently Contains Fine Precipitates.	44
23	Tensile Fracture of Mo-E2 (0.174 mm grain size) at $+25^{\circ}\text{C}$ Showing Highly Distorted Cleavage Facets.	46
24	Tensile Fracture of Mo-E2 (0.174 mm grain size) at $+25^{\circ}\text{C}$ Showing a Portion of a Smooth Intergranular Facet (Left) Which Apparently Contains Fine Precipitates.	46
25	Tensile Fracture of Mo-E2 (0.174 mm grain size) at 0°C Showing a Cleavage Facet (upper) and an Intergranular Facet (lower).	47
26	Tensile Fracture of Mo-E2 (0.174 mm grain size) at -40°C Showing a Cleavage Facet Containing Many Cleavage Steps.	47

Illustrations (Continued)

Figure		Page
27	Tensile Fracture of Mo-E2 (0.174 mm grain size at -100°C Showing One Intergranular Facet (Smooth) and Several Cleavage Facets.	48
28	Tensile Fracture of Mo-E2 (0.174 mm grain size) at -196°C Showing One Intergranular Facet (Smooth) Surrounded by Several Cleavage Facets with "River" Markings Radiating from Intergranular Facet (Possible Fracture Origin).	48
29	Tensile Fracture of Mo-E3 (0.023 mm grain size) at -20°C Showing Several Cleavage Facets and an Intergranular Facet (Smooth).	50
30	Tensile Fracture of Mo-E3 (0.023 mm grain size) at -100°C Showing Several Cleavage and Intergranular Facets.	50
31	Tensile Fracture of Mo-E3 (0.023 mm grain size) Uniformly Prestrained ($\epsilon = 0.115$) at $+25^{\circ}\text{C}$ and Broken at -100°C Showing Several Highly Distorted Cleavage Facets.	51
32	Tensile Fracture of Mo-E3 (0.023 mm grain size) Uniformly Prestrained ($\epsilon = 0.110$) at -25°C and Broken at -100°C Showing Several Cleavage Facets.	51
33	Tensile Fracture of Mo-E3 (0.023 mm grain size) Prestrained by Necking ($\epsilon = 0.28$) at $+25^{\circ}\text{C}$ and Broken at -100°C Showing Several Cleavage Facets.	52
34	Tensile Fracture of Mo-E3 (0.023 mm grain size) Prestrained by Necking ($\epsilon = 0.64$) at $+25^{\circ}\text{C}$ and Broken at -100°C Showing One Intergranular Facet (lower right) and Several Cleavage Facets.	52
35	Tensile Fracture of Mo-E3 (0.023 mm grain size) Prestrained by Necking ($\epsilon = 0.64$) at $+25^{\circ}\text{C}$, Recrystallized, and Broken at -100°C Showing Predominantly Intergranular Facets.	53
36	Tensile Fracture of Mo-E3 (0.023 mm grain size) Having Neck Machined Corresponding to a Necking Prestrain of $\epsilon = 0.64$, Recrystallized and Broken at -100°C Showing Predominantly Intergranular Facets.	53
37	Precracked Slow Bend Charpy Fracture of Mo-E3 (0.023 mm grain size) at -100°C Showing a Cleavage Facet Containing a Few Cleavage Steps.	56

Illustrations (Continued)

Figure		Page
38	Precracked Slow Bend Charpy Fracture of Mo-E3 (0.023 mm grain size) Prestrained (6% by rolling) at +25°C and Broken at -100°C Showing Cleavage Facets Containing Many Cleavage Steps.	56
39	Tensile Fracture of Mo-E4 (0.020 mm grain size) at +25°C Showing Several Cleavage Facets.	58
40	Tensile Fracture of Mo-E4 (0.020 mm grain size) at -35°C Showing Two Cleavage Facets and Many Intergranular Facets.	58
41	Schematic Plots of Variation of Fracture Stress (σ_F), Yield Stress (σ_y), Necking Stress (σ_n), Fracture Strain (ϵ_F) and Max. Uniform Strain (ϵ_u) with Temperature.	61
42	Plot of Stress and Strain Parameter Bands vs. Temperature for Mo-E2 ($l = 0.026$ mm).	61
43	Plot of Stress and Strain Parameter Bands vs. Test Temperature for Mo-E2 ($l = 0.044$ mm).	62
44	Plot of Stress and Strain Parameter Bands vs. Test Temperature for Mo-E2 ($l = 0.174$ mm)	62
45	Plot of Stress and Strain Parameter Bands vs. Test Temperature for Mo-E3 ($l = 0.023$ mm).	63
46	Plot of Stress and Strain Parameter Bands vs. Test Temperature for Mo-E4 ($l = 0.020$ mm).	63
47	Plots of Uniform Flow Stress (σ_{fs}) vs. Grain Size Parameter for Recrystallized Mo-E2 Strip at Plastic Strains (ϵ_p) of 0.2 and 0.4	67
48	Plots of Uniform Flow Stress (σ_{fs}) vs. Grain Size Parameter for Recrystallized Mo-E2 Strip at Plastic Strains (ϵ_p) of 0.7 and 1.0.	68
49	Variation of Elastic Modulus of Molybdenum (Mo-E1 Rod) with Temperature.	72

Tables

Table		Page
1	Chemical Composition.	4
2	Procedure Used for the Control of Grain Size.	5
3	Tensile Test Characteristics of Mo-E2, Mo-E3 and Mo-E4 Strip	11
4	Calculated Values of Fracture Stress Assuming Completely Uniform Elongation	25
5	Calculated Values of Fracture Stress Under Actual Necking Conditions.	27
6	Variation of Fracture Stress of Mo-E3 With Total Strain.	35
7	Effect of Necking Prestrains and Simulated Necks on the Fracture Stress of Mo-E3 at -100°C	36
8	Fracture Toughness of Mo-E3 at -100°C	38
9	Effect of Prestrain on the Fracture Stress of Mo-E4 Strip at -100°C and -196°C	40
10	Fractographic Characteristics of Mo-E2 Broken Tensile Specimens	49
11	Fractographic Characteristics of Mo-E3 Broken Tensile Specimens	55
12	Fractographic Characteristics of Mo-E3 Broken Precracked Charpy Slow Bend Test Specimens	57
13	Fractographic Characteristic of Mo-E4 Broken Tensile Specimens	59
14	Yield Locking Parameter (k_y) and Frictional Stress (σ_f) for Mo-E2, Mo-E3, and Mo-E4 Strip	65
15	Flow Locking Parameter (k_f) for Mo-E2 Strip	69
16	Approximate Values of Flow Locking Parameter (k_f) for Mo-E3 and Mo-E4 Strip	71
17	Calculated Effective Surface Energy for Crack Initiation in Mo-E2, Mo-E3 and Mo-E4 Strip	73
18	Calculated Effective Surface Energy for Crack Propagation in Mo-E2, Mo-E3, and Mo-E4 Strip	76

I. INTRODUCTION

A. Background

During the period of 1 November 1959 to 30 April 1963, ManLabs Inc. acted as prime contractor on a program entitled "Substructure and Mechanical Properties of Refractory Metals" under Contracts No. AF33(616)-6383 and AF33(657)-8424. Other research participants on this program were Massachusetts Institute of Technology, Rutgers the State University, University of Liverpool (England) and University of Cambridge (England). The results obtained were presented in three summary technical reports by Lement et al, (1, 2, 3)^{*}.

In connection with the above program, ManLabs concentrated on the relation of microstructure to the ductile-brittle transition in refractory metals. The results obtained on molybdenum that are considered pertinent to the present investigation are as follows:

a) For recrystallized as well as worked molybdenum strip of relatively high purity, the effective surface energy (γ') at the tensile ductility-transition temperature (T_d) as calculated on the basis of the Cottrell fracture relation is about 3000 ergs/cm²; and the corresponding critical crack length as calculated on the basis of the Griffith-Orowan fracture relation is equal to the first-order subgrain size.

b) The discontinuous change in both ductility and fracture stress that occurs at T_d does not appear to correlate with changes in fracture mode, mechanical twinning, or the occurrence of nil-ductility. Rather the tensile ductility-transition seems to be related to the phenomenon of necking which occurs above but not below T_d . Accordingly, a suggested criterion for the occurrence of a tensile ductility transition is the intersection of the fracture stress (σ_F) corresponding to uniform strain and the necking stress (σ_n) vs. test temperature curves, i. e. $\sigma_F = \sigma_n$ at T_d .

c) The concept of a strain-dependent (temperature-independent) critical fracture stress was used in an attempt to predict the grain size dependence of the observed fracture stress and fracture strain based on the variation of the quantities with test temperature as measured for a fine grain, recrystallized molybdenum. The predicted values of fracture stress and fracture strain for a selected test temperature of -40°C were both found to be appreciably lower than the corresponding values actually measured as a function of grain size. This raised the question as to whether a Cottrell-type fracture relation actually holds.

B. Scope of Investigation

The present investigation^{**} represents a continuation of the research conducted under Contract AF33(657)-8424. The objective was to elucidate both theoretically and experimentally some of the basic factors affecting

* Underscored numbers in parentheses designate References given at end of report.

** Manuscript released by the authors May, 1964 for publication as an R&D Technical Documentary Report.

fracture phenomena in molybdenum. The approach used was to study the effects of interstitial content, grain size, and prestraining on the tensile ductility-transition behavior. Attempts were made to determine the effects of plastic strain on both flow stress and fracture stress. Comparison were made between effective crack propagation energy values as determined by tensile tests and by precracked Charpy slow bend tests.

II. EXPERIMENTAL PROCEDURES

A. Materials

The interstitial contents of the four 30-mil thick molybdenum strip materials used in this investigation are listed in Table 1. The strip from ingot Mo-E2 is relatively high in carbon (about 60 ppm); from ingot Mo-E3 is relatively high in nitrogen (about 10 ppm) and possibly oxygen (about 20 ppm); and from ingot Mo-E4 is relatively high in oxygen (about 145 ppm).

B. Recrystallization-Anneals

All recrystallization runs were carried out in a purified argon atmosphere passing through a vertical Super-Kanthal element furnace controlled within $\pm 8^{\circ}\text{C}$. Specimens were wrapped in tantalum foil and suspended vertically in the heating zone of the furnace operating at the selected recrystallization temperature. After either 0.5 or 1.0 hour at temperature (allowing for heating-up time), the specimens were removed from the heating zone and then allowed to cool to room temperature in the atmosphere. Recrystallization temperatures and times for Mo-E2, Mo-E3, and Mo-E4 are given in Table 2.

C. Uniaxial Prestrain

In order to strain recrystallized Mo-E2 strips and thereby attain larger grain sizes on subsequent recrystallization anneal, uniaxial prestrains in tension were utilized. Flat tensile specimens 1 inch wide and 10 inches long were machined from the molybdenum strips with the specimen axis parallel to the rolling direction. These specimens were stress-relieved for 1 hr. at 800°C in a vacuum furnace and then prestrained in uniaxial tension to about 10-15% elongation in a Baldwin tensile machine. Subsequent recrystallizations were carried out at 1300°C (medium grain size) and 1600°C (coarse grain size).

D. Mechanical Testing

1. Tensile Tests

In general, the tensile tests were carried out in the range of $+25^{\circ}\text{C}$ to -190°C as described in the second summary technical report(2). The applied strain rate was maintained at $2.8 \times 10^{-4} \text{ sec}^{-1}$. In analyzing the stress-strain curves, relatively large discrepancies were found between the measured elastic modulus and the 1961 Metals Handbook value for molybdenum ($E \approx 47 \times 10^6 \text{ psi}$), which appears to be relatively constant in the test temperature range of 25°C to at least -80°C . In order to correct for these discrepancies, it was decided to algebraically add the difference in elastic strain (as calculated by dividing the measured stress level by the known elastic modulus and by the measured elastic modulus) to the measured strain value (elastic plus plastic).

Table i

Chemical Composition

<u>Ingot No.</u>	<u>Strip No.</u>	<u>Initial Condition</u>	<u>C ppm</u>	<u>N ppm</u>	<u>O ppm</u>	<u>Others</u>
Mo-E2	H	recrystallized at 1200°C and rolled 87% at 1600 to 400°C	65	4	12	*
	D	recrystallized at 1200°C and rolled 44% at 1250 to 900°C	65	2	11	*
	F	recrystallized at 1200°C and rolled 52% at 1250 to 400°C	56	3	8	*
Mo-E3	H	recrystallized at 1200°C and rolled 88% at 1000 to 400°C	19	7-15	12-29	--
Mo-E4	C	rolled 64% at 1250°C and rolled 28% at 900 to 600°C	12	3	145	--

*Other elements in ppm are as follows:

<u>Al</u>	<u>Cr</u>	<u>Cu</u>	<u>Fe</u>	<u>Mg</u>	<u>Mn</u>	<u>Ni</u>	<u>Pb</u>	<u>Si</u>	<u>Sn</u>	<u>Ti</u>	<u>V</u>
< 50	< 5	1	30	< 1	< 1	< 10	< 100	10	< 50	< 10	< 10

Table 2

Procedure Used for the Control of Grain Size

<u>Ingot No.</u>	<u>Strip No.</u>	<u>Amount of As-Rolled Deformation</u>	<u>Primary Recrystallization Treatment</u>	<u>Uniaxial Prestrain</u>	<u>Secondary Recrystallization Treatment</u>	<u>Average Grain Diameter mm.</u>
Mo-E2	H	87%	1200°C, 0.5 hr.	---	---	0.026
	D	44%	1300°C, 1 hr.	---	---	0.044
	E	52%	1200°C, 1 hr.	15%	1300°C, 1 hr.	0.174
	F	52%	1400°C, 1 hr.	12%	1600°C, 1 hr.	0.310
Mo-E3	H	88%	1200°C, 0.5 hr.	---	---	0.023
Mo-E4	C	28%	1400°C, 0.5 hr.	---	---	0.020

E. Precracked Charpy Slow Bend Tests

Precracked Charpy slow bend tests at -100°C were carried out on specimens about 0.030 inch thick, 0.394 inch wide and 2 inches long containing a 45° V-notch. Fatigue precracking to produce an initial crack about 0.025 inch long at the V-notch was accomplished by bending in compression using a ManLabs precracking machine with the specimen in the reverse position. The slow bend tests were carried out using three point loading to determine load vs deflection characteristics.

F. Determination of Grain Size

Grain size measurements were carried out on both longitudinal and transverse sections of the recrystallized molybdenum strips. After mounting, the specimens were electropolished in a solution of 75 cc methyl alcohol and 25 cc H_2SO_4 at a current density of about 1 amp./ cm^2 . Etching was carried out using Murakami's reagent. Grain diameter measurements were made using the linear intercept method on photomicrographs taken at 100X.

G. Fractography

Fractured surface of tensile and slow bend test specimens were examined by both light and electron fractography. Light microscopic examination at magnifications up to 800X was used to determine where fracture initiated, mode of fracture, and facet size. Electron microscopy was carried out at 2000X on shadowed carbon replicas of the fractured surface as obtained by a) stripping a parlodion replica from the fractured surface, b) shadowing with chromium, c) depositing a carbon film by evaporation at 90° , and d) dissolving the parlodion in butyl acetate.

III. RESULTS AND DISCUSSION

A. Flow and Fracture Characteristics of Mo-E2 Strip

1. Tensile Properties vs. Test Temperature

Plots of yield stress (σ_y), fracture stress (σ_F) and fracture strain (ϵ_F) for Mo-E2 molybdenum strip of fine, intermediate and coarse grain size (t) are shown in Figs. 1, 2 and 3. Discontinuous yielding was found to occur in both the fine and intermediate grain size materials and σ_y represents the lower yield stress. On the other hand, discontinuous yielding was not observed in the coarse grain material and it was decided to use the proportional limit for σ_y . This seems justified on the basis that the proportional limits of the fine and coarse grain materials were found to be approximately equal to their respective lower yield stress values.

Based on Figs. 1, 2 and 3, the brittleness-transition (T_b), ductility-transition (T_d), and fracture stress maximum (T_m) temperatures* as well as both the corresponding fracture strains (ϵ_F) and ratios of σ_F to σ_y at T_d are given in Table 3. The values obtained for the fine and intermediate grain sizes of the Mo-E2 strip are about the same except that T_b is lower for the intermediate grain size. For the fine grain Mo-E2, it was found that T_b approximately coincides with T_d . The coarse grain size has the lowest T_b and the highest T_d and T_m temperatures. Also, the values of ϵ_F and σ_F/σ_y at T_d are highest for the coarse grain size.

2. Dependence of Yield Stress on Grain Size

Based on Figs. 1, 2 and 3, plots of σ_y vs $t^{-1/2}$ are shown in Fig. 4 for the Mo-E2 strip subjected to test temperatures in the range of +25 to -150°C. The corresponding k_y values (based on normal stress and full grain size) are given by the slopes of these plots. As shown in Fig. 5, k_y appears to increase linearly with decrease in test temperature, and the extrapolated value at -196°C is about six times higher than at +25°C. The k_y ratio at -80°C is about three, which is about twice that reported for molybdenum by Wronski (4) (about 1.6). This is tentatively attributed to the fact that the interstitial level of the molybdenum (Mo-E2) used in the present investigation is significantly lower than that used by Wronski.

3. Prediction of Dependence of Fracture Stress on Grain Size

In the previous report (3), a method of predicting the variation of observed fracture stress with grain size over the test temperature range of T_d to T_m based on data for a single grain size was presented. It was assumed that the critical fracture stress (σ_c) is strain-dependent but temperature-independent, and that the Cottrell (5) relation is obeyed if σ_c at given fracture strain (ϵ_F) is determined as a function of the grain size (t):

$$[\sigma_c]_{\epsilon_F} = C_t t^{-1/2} \quad (1)$$

*These temperatures are defined in Appendix I.

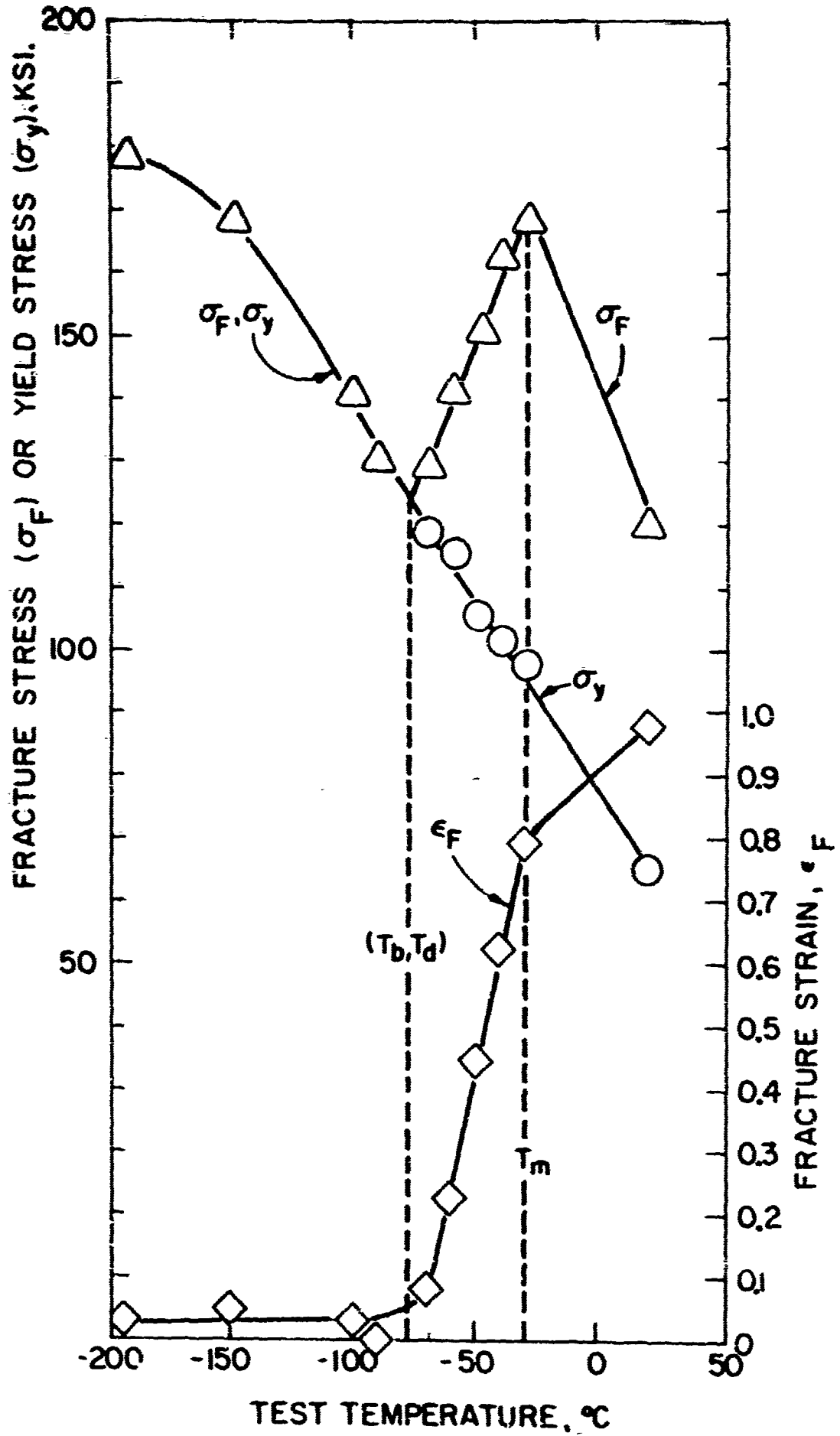


Fig. 1 - Effect of Test Temperature on the Tensile Properties of Recrystallized Molybdenum (Mo-E2) Strip ($t = 0.026$ mm).

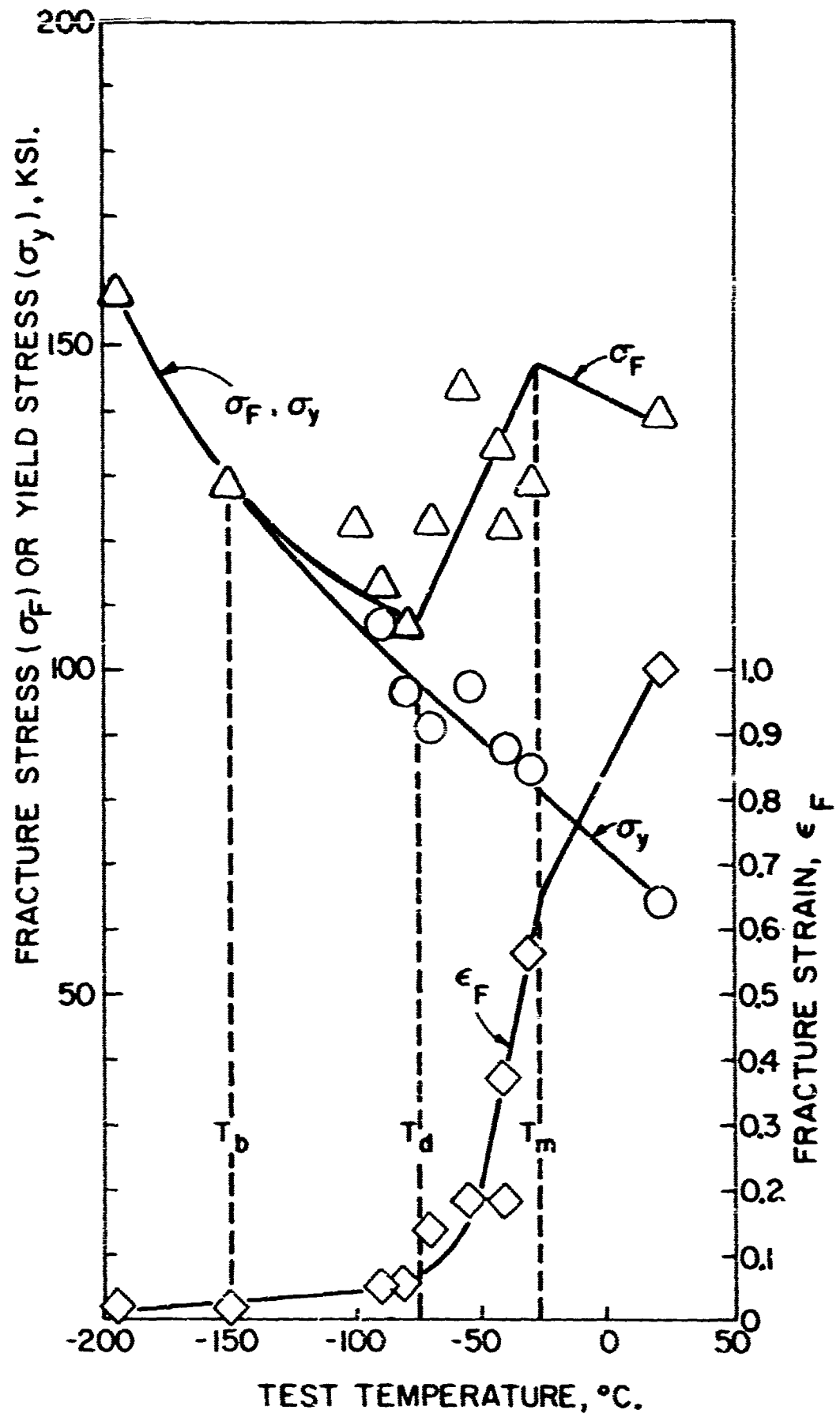


Fig. 2 - Effect of Test Temperature on Tensile Properties of Recrystallized Molybdenum (Mo-E2) Strip ($t = 0.044$ mm).

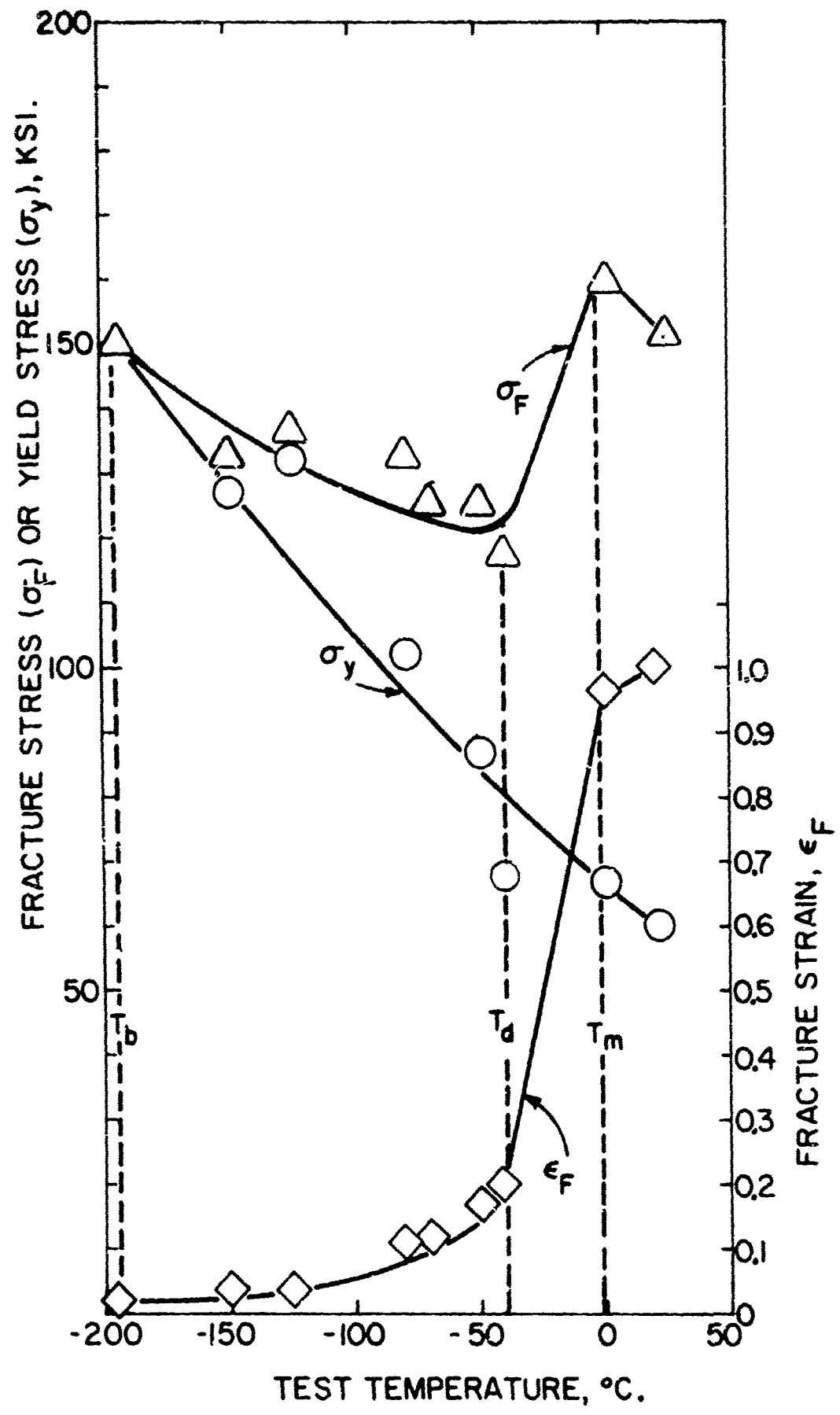


Fig. 3 - Effect of Test Temperature on Tensile Properties of Recrystallized Molybdenum (Mo-E2) Strip ($l = 0.174$ mm).

Table 3

Tensile Test Characteristics of Mo-E2, Mo-E3 and Mo-E4 Strip

<u>Strip</u>	<u>Average Grain Size</u> mm	T_b °C	ϵ_F at T_b	T_d °C	ϵ_F at T_d	T_m °C	ϵ_F at T_m	σ_F/σ_y at T_d
Mo-E2	0.026	-80	0.04	-80	0.04	-30	0.80	1.00
	0.044	-150	0.02	-75	0.07	-25	0.65	1.10
	0.174	-195	0.02	-40	0.18	0	0.95	1.44
Mo-E3	0.023	-80	0.03	-80	0.03	-20	0.90	1.00
Mo-E4	0.020	-35	0.00	-35	0.00	+25	0.62	1.00

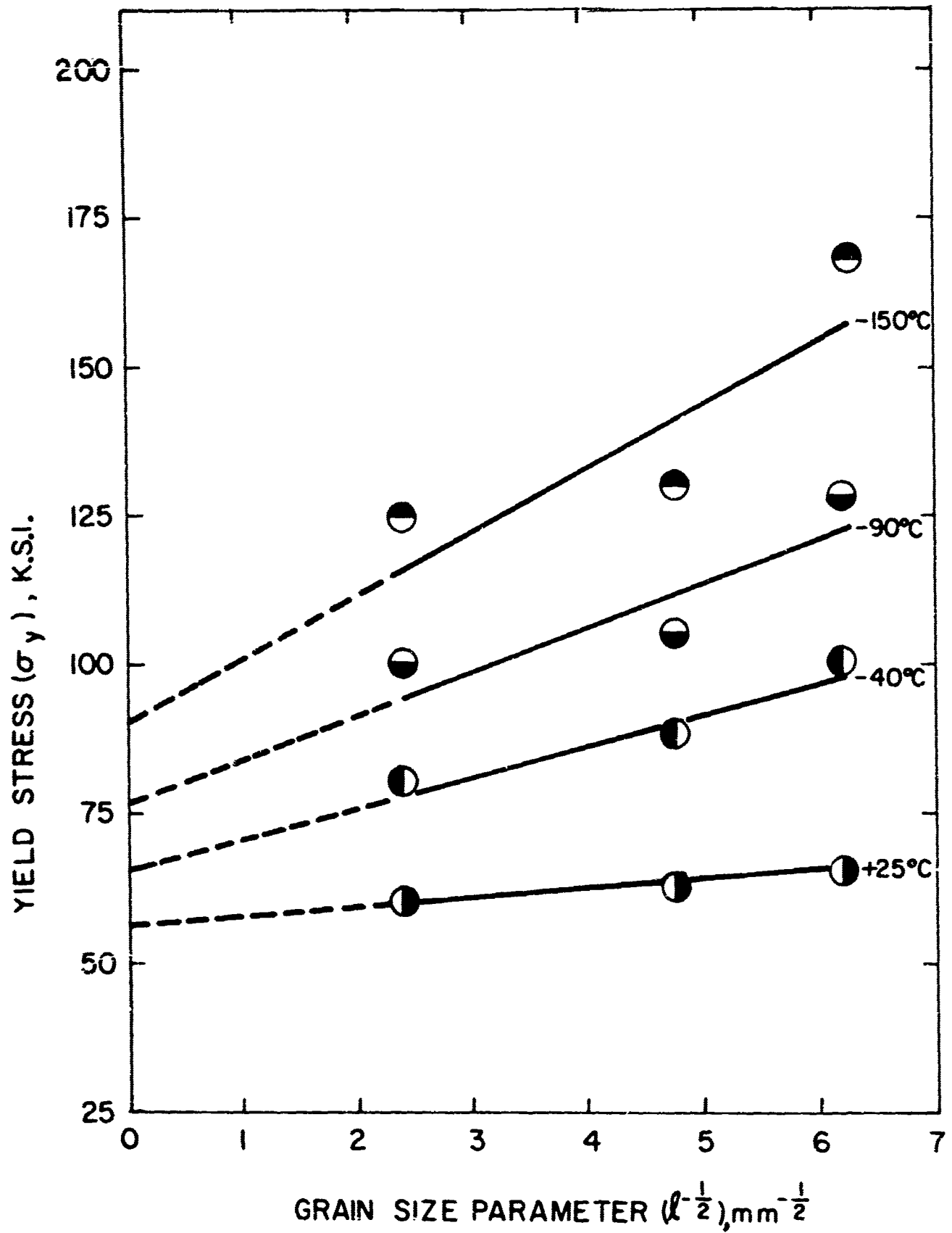


Fig. 4 - Variation of Yield Stress (σ_y) with Grain Size ($l^{-1/2}$) of Molybdenum (Mo-E2) Strip in Test Temperature Range of +25 to -150°C.

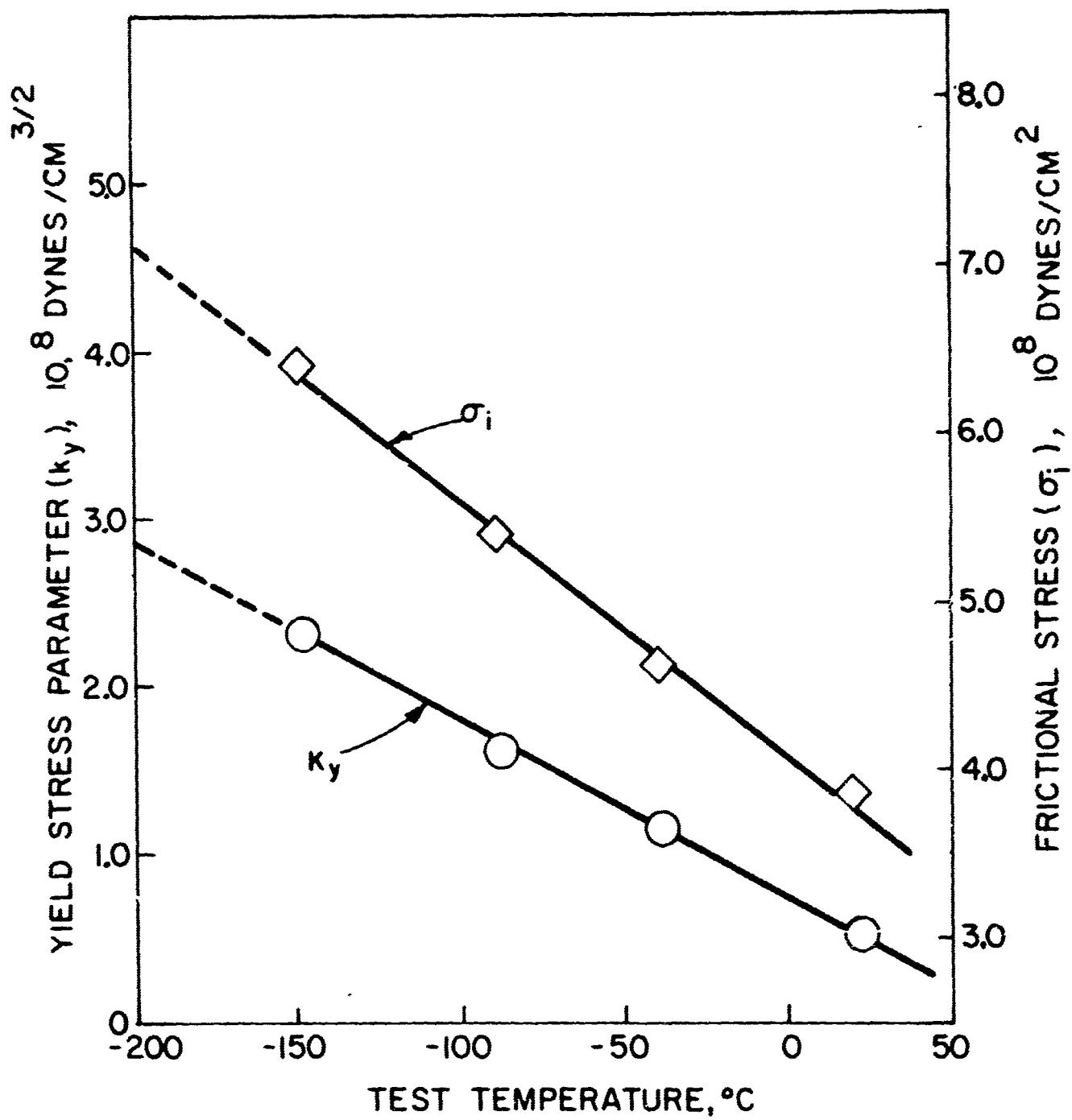


Fig. 5 - Variation of Yield Stress Parameter (k_y) and Frictional Stress (σ_i) of Molybdenum (Mc-E2) Strip with Test Temperature. The Parameter k_y and Frictional Stress σ_i are Based on Normal Stress (σ_y) and Full Grain Diameter (l).

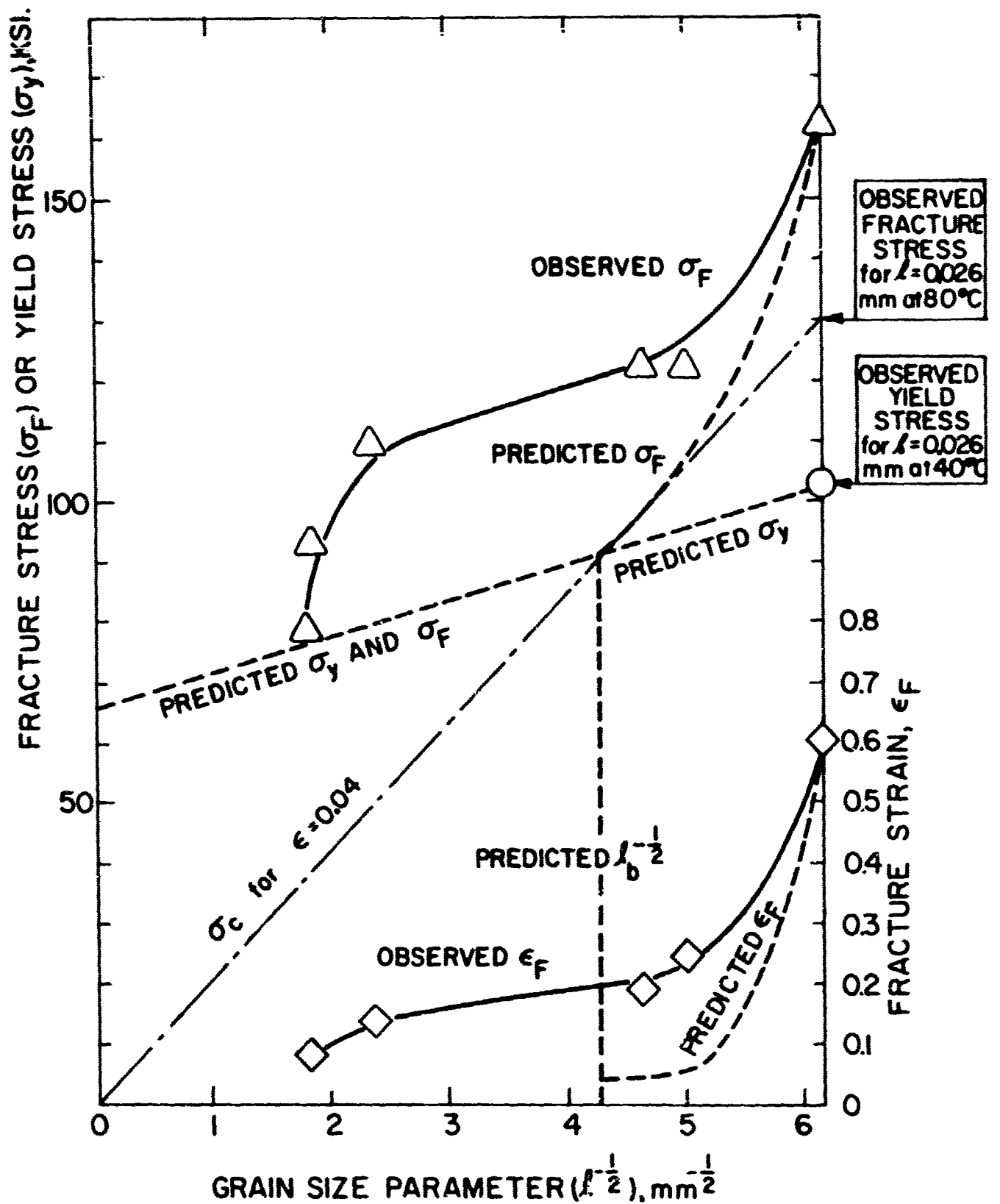


Fig. 6 - Comparison of Predicted and Experimentally Observed Variations of the Fracture Stress (σ_F) and Fracture Strain (ϵ_F) with Grain Size ($l^{-1/2}$) of Recrystallized Molybdenum (Mo-E2) Strip for a Test Temperature of -40°C Based on Data Obtained for Fine Grain Size ($l = 0.026$ mm).

Fig. 6 is a revised plot showing both the observed and predicted values of the fracture stress (σ_F) and fracture strain (ϵ_F) as function of $t^{-1/2}$. The observed fracture stresses are as much as 30% higher than predicted; and the observed fracture strain are as much as four times the predicted values. This raised the question as to whether the critical fracture stress actually follows the relation given in Eq. (1). In order to clarify this question, plots of σ_F vs $t^{-1/2}$ corresponding to ϵ_F values of 0.2, 0.4 and 0.6 were made based on Figs. 1, 2 and 3. As shown in Fig. 7, the slopes (k_F) are all about 0.9×10^8 cgs, and there is an intercept ($\sigma_{F\infty}$) corresponding to infinite grain size. It appears that the dependence of σ_F at constant fracture strain has the following form:

$$[\sigma_F]_{\epsilon} = \sigma_{F\infty} + k_F t^{-1/2} \quad (2)$$

Eq. (2) differs from the form of the Cottrell (5) fracture relation, Eq. (1), according to which σ_F or σ_C should equal zero at infinite grain size. Thus, it does not seem possible to accurately predict the dependence of σ_F on test temperature based on data obtained for a single grain size, as was attempted by this approach.

4. Prediction of Fracture Stress from Fracture Strain

4.1 Previous Approach

In the previous report (3), calculations were made of the ratio of the maximum to minimum fracture stress in the transition range for Mo-E1 strip (about 40 ppm carbon, 4 ppm nitrogen and 25 ppm oxygen) rolled 5, 46 and 88% (reduction in area) after recrystallization; and for recrystallized Mo-E2 strip in the fine grain condition. For the Mo-E1 strips, T_d and T_m appear to coincide; whereas for the Mo-E2 strip (Fig. 1) T_m is about 50°C higher than T_d . It was assumed that the over-all strengthening factor due to necking (q_n) is equal to the following product:

$$q_n = q_f \times q_p \times q_{\dot{\epsilon}} = (\sigma_F)_{\max} / (\sigma_F)_{\min} \quad (3)$$

q_p = plastic constraint factor
 $q_{\dot{\epsilon}}$ = strain rate factor

Calculated values of q_n based on Eq. (3) were found to agree within 10% of the corresponding measured values.

Subsequent analysis of this approach has led to the conclusion that the good agreement obtained between calculated and measured values of q_n is probably fortuitous. This is based on the following considerations:

- a) The strengthening factor associated with substructural

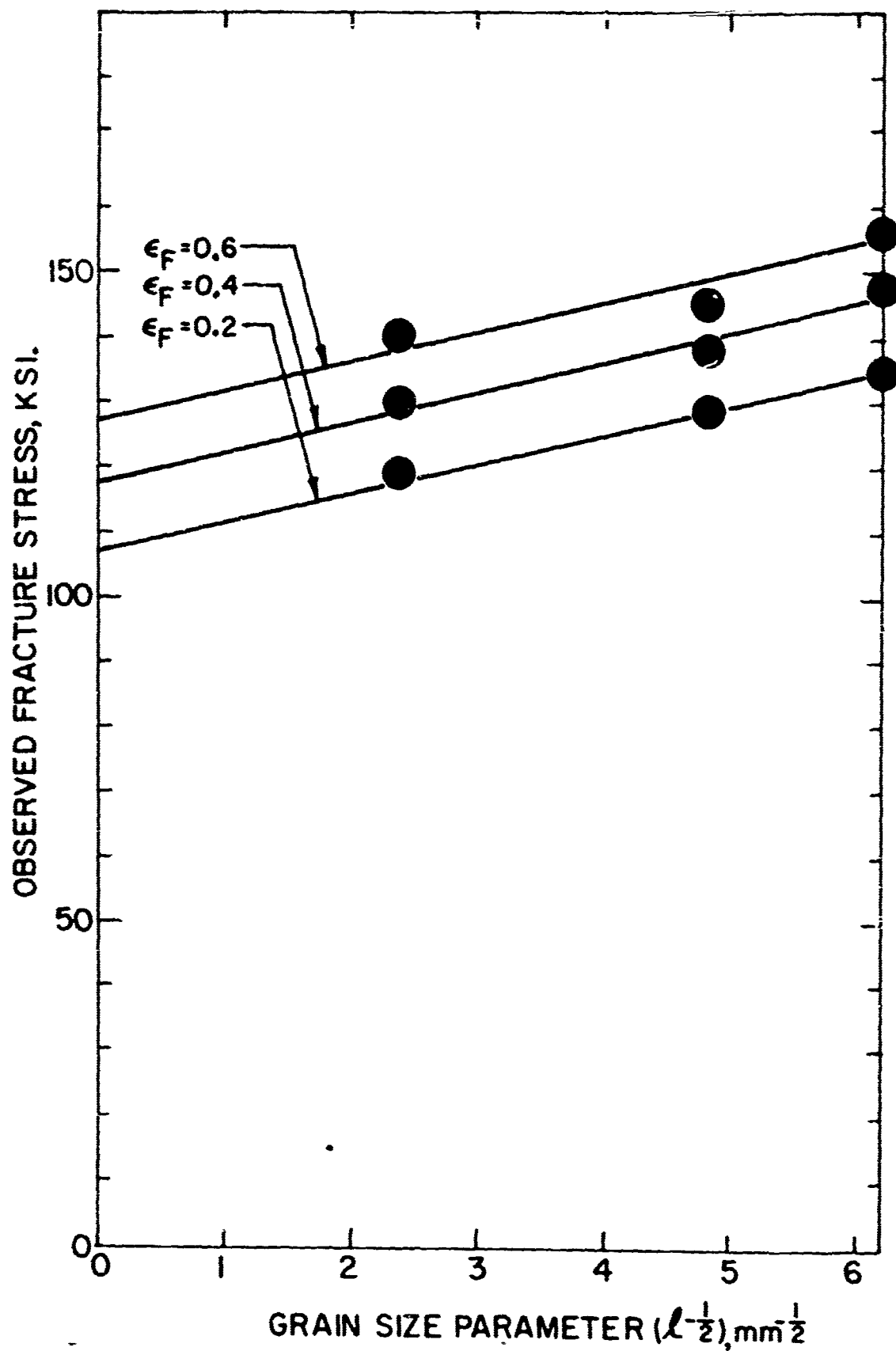


Fig. 7 - Variation of the Observed Fracture Stress (σ_F) at Constant Strain with Grain Size ($l^{-1/2}$) for Recrystallized Molybdenum Strip (Mo-E2).

changes during straining from the necking stress to the fracture stress, $(\sigma_F)_{\max}$, at T_{in} was not taken into account.

b) The calculated grain size factor (q_f) is probably too large since the fracture stress (which is the flow stress at fracture strain) was assumed to be directly proportional to $\epsilon^{-1/2}$ whereas the actual dependence of flow stress includes a term representing the flow stress at infinite grain size.

c) The strengthening factors are more likely to be additive rather than multiplicative.

4.2 Revised Approach

Based on the foregoing considerations, it was decided to modify Eq. (3) and attempt to predict the variation of fracture stress with test temperature above T_d . Since the fracture stress and the flow stress at the fracture strain are identical, the factors that influence flow stress can be utilized to calculate the fracture stress provided that the fracture strain is known. Assuming that the observed flow stress σ_f is equal to the flow stress due to substructural changes, σ_{fs} , plus the strengthening contributions of a) decreased grain size during straining, b) plastic constraint due to necking, and c) increased strain rate due to deformation being confined to the neck; the following relation should hold:

$$\sigma_f = \sigma_{fs} [1 + (q_f - 1) + (q_p - 1) + (q_\epsilon - 1)] \quad (4)$$

where q_f , q_p and q_ϵ are the strengthening factors due to grain size, plastic constraint and strain rate (in the necked region) respectively, corresponding to a given amount of strain ϵ (elastic plus plastic). As is subsequently discussed, $q_f \cong 1$ and therefore can be neglected. For the prediction of fracture stress (σ_F), the identity of σ_F and σ_f at ϵ_F is utilized and equation (4) takes the following form:

$$\sigma_F = \sigma_{Fs} [1 + (q_p - 1) + (q_\epsilon - 1)] \quad (5)$$

where σ_{Fs} is the contribution of substructural changes to the fracture stress, and q_p and q_ϵ are maximum values which occur at the fracture strain (ϵ_F).

(a) Substructural Strengthening

For the determination of σ_{Fs} it is necessary to know the relation of the true flow stress (σ_{fs}) to the true strain (ϵ). The simplest

assumption is that the so called power law holds:

$$\sigma_{fs} = K(\epsilon)^n \quad (6)$$

where ϵ = total strain (elastic plus plastic)
 K = strain hardening coefficient
 n = strain hardening exponent

In particular, σ_{Fs} is given by substituting ϵ_F for ϵ :

$$\sigma_{Fs} = K(\epsilon_F)^n \quad (7)$$

Thus it is possible to determine σ_{Fs} provided K , n and ϵ_F are known. The best way to determine K and n is from a plot of Eq. (6) in the form of $\log \sigma_{fs}$ vs $\log \epsilon$ using data corresponding to the portion of the stress-strain curve from the yield stress (σ_y) to the necking stress (σ_n). σ_{Fs} can then be determined using equation (7), which is effectively extrapolating the $\log \sigma_{fs}$ vs $\log \epsilon$ plot to $\log \epsilon_F$. This assumes that the power law continues to hold from σ_n to σ_F (or from the strain (ϵ_u) at σ_n to ϵ_F).

An alternative way to determine σ_{Fs} is to utilize the relation between the yield stress (σ_y) and the yield strain (ϵ_y):

$$\sigma_y = K(\epsilon_y)^n \quad (8)$$

Defining q_s as σ_{Fs}/σ_y at the fracture strain (ϵ_F) and utilizing Eq. (7) and (8) gives

$$q_s = \left(\frac{\epsilon_F}{\epsilon_y} \right)^n \quad (9)$$

Therefore, q_s represents the substructural strengthening factor and σ_{Fs} can be determined if n , ϵ_y and ϵ_F are known.

(b) Grain Size Strengthening Factor

The grain size factor (q_f) may be defined as follows:

$$q_f = \frac{\sigma_{fs} + \Delta\sigma_{fs}}{\sigma_{fs}} \quad (10)$$

where $\Delta\sigma_{fs}$ = increase in the flow stress due to the decrease in transverse grain dimensions. The dependence of flow stress σ_{fs} at a given strain and test temperature on grain diameter is given by the following relation:

$$\sigma_{fs} = \sigma_{f\infty} + k_f l^{-1/2} \quad (11)$$

where $\sigma_{f\infty}$ = flow stress at infinite grain size
 k_f = flow stress parameter

Since a decrease in grain size occurs because of the reduction in area during the tensile test, the increase in flow stress is at a given strain is given by

$$\Delta\sigma_{fs} = k_f \Delta(l^{-1/2}) \quad (12)$$

and therefore

$$q_f = 1 + \frac{k_f \Delta(l^{-1/2})}{\sigma_{fs}} \quad (13)$$

Assuming that $k_f = 0.3 k_y$ for molybdenum and using the measured value of k_y at 20°C for Mo-E2 ($1.8 \text{ ksi/mm}^{-1/2}$), the corresponding value of k_f at 20°C is $0.6 \text{ ksi/mm}^{-1/2}$. For a reduction of area as high as 69% ($\epsilon = 1.00$), $\Delta(l^{-1/2}) \approx 2 \text{ mm}^{-1/2}$. Since the approximate value of σ_{fs} at 20°C is 125 ksi, the value of q_f calculated on the basis of Eq. (13) is about 1.01. Since this represents a maximum value, q_f can in most cases be considered as equal to unity.

(c) Plastic Constraint Strengthening Factor

Based on the Bridgeman (6) correction, the plastic constraint factor $(q_p)_{rd}$ for a round tensile specimen is approximately given by the following relation in terms of the fracture strain $(\epsilon_F)_{rd}$.

$$(q_p)_{rd} - 1 = \frac{0.15 (\epsilon_F)_{rd}}{1 - 0.15 (\epsilon_F)_{rd}} \quad (14)$$

According to an analysis of Aronofsky's (7) results for a flat specimen, the following relations appear to hold between the plastic constraint factors, $(q_p)_{fl}$ and $(q_p)_{rd}$ and between the fracture strains, $(\epsilon_F)_{fl}$ and $(\epsilon_F)_{rd}$ for

a flat and round specimen, respectively:

$$(q_p)_{fl}^{-1} = 0.5 [(q_p)_{rd}^{-1}] \quad (15)$$

$$(\epsilon_F)_{fl} = 0.9 (\epsilon_F)_{rd} \quad (16)$$

Solving Eq. (14), (15) and (16) for $(q_p)_{fl}$ in terms of $(\epsilon_F)_{fl}$ and dropping the subscript fl gives

$$q_p = \frac{0.5}{0.5 - 0.08 \epsilon_F} \quad (17)$$

(d) Strain Rate Strengthening Factor

As discussed in the previous report (3) the strain rate $(\dot{\epsilon}_p)$ in the necked region of a tensile specimen is higher than the applied strain rate and the flow stress required to produce a given strain is increased by a factor (q_ϵ) given by the following equation:

$$q_\epsilon = \left[\frac{L_g (\epsilon_n - \epsilon_u)^{1/4}}{[8 a_o a_u \exp^{-\epsilon_n} - 8 a_o^2 \exp^{-2\epsilon_n} - 4 (\epsilon_n - \epsilon_u)^{1/2} (a_u - a_o \exp^{-\epsilon_n})^2]^{1/2}} \right]^r \quad (18)$$

where L_g = gage length

ϵ_n and ϵ_u = total necking strain and maximum uniform strain respectively

a_o and a_u = initial specimen semi-width and specimen semi-width corresponding to maximum uniform strain respectively

r = strain rate exponent (0.05 for molybdenum according to Bechtold's (8) results).

Based on the previous calculations (3), the factor q_ϵ has the following dependence on plastic strain as given by the difference between ϵ_F and the maximum uniform strain (ϵ_u):

$\epsilon_F - \epsilon_u$	q_ϵ
0.0001	1.03
0.0010	1.06
0.0100	1.09
0.1000	1.11
0.5000	1.11

Since the values of $\epsilon_F - \epsilon_u$ fall in the range of about 0.10 to 0.8 for the Mo-E2 strip tensile test results considered, it may be assumed that q_ϵ is equal to 1.11 for all the cases of interest.

4.3 Calculation of Fracture Stress Assuming Completely

Uniform Elongation

As previously defined, σ_{FS} represents the fracture stress due to substructural changes alone, i. e. the flow stress corresponding to the observed fracture strain assuming completely uniform elongation (no necking). In order to calculate σ_{FS} for a given test temperature, it is necessary to first determine the strain hardening exponent (n) and strain hardening coefficient (K) from a plot of $\log \sigma_{fs}$ vs $\log \epsilon$ at that temperature and then to utilize the power law as given in Eq. (8).

The variations of n and K with test temperature in the range from T_d to 20°C are shown in Figs. 8* to 10 for Mo-E2 (fine, intermediate and coarse grain sizes). Corresponding sets of n, K and ϵ_F values were used to calculate σ_{FS} at T_d , at half-way between T_d and T_m , at T_m and at 25°C . The results given in Table 4 indicate that σ_{FS} goes through a maximum with increase in test temperature above T_d just as does the observed fracture stress. However, the calculated maximum in σ_{FS} occurs at about half-way between T_d and T_m instead of at T_m as does the maximum in the observed fracture stress.

From the calculated values of σ_{FS} and corresponding values of observed yield stress (σ_y), it is possible to calculate the substructural strengthening factor (q_s) which was defined as σ_{FS}/σ_y . As shown in Table 4, the variation of q_s with increase in test temperature above T_d consists of a steady increase up to at least 25°C for the fine grain Mo-E2 strip; whereas q_s reaches a maximum and then decreases for the intermediate and coarse grain Mo-E2 strip.

4.4 Calculation of Fracture Stress Under Actual Necking

Conditions

Based on the revised approach, the relation between the fracture stress under actual necking conditions (σ_F) and the fracture stress due

*The values given in Fig. 8 for n and K at -90°C (i. e., below $T_d = T_b = -85^\circ\text{C}$) correspond to a specimen that actually necked at -90°C .

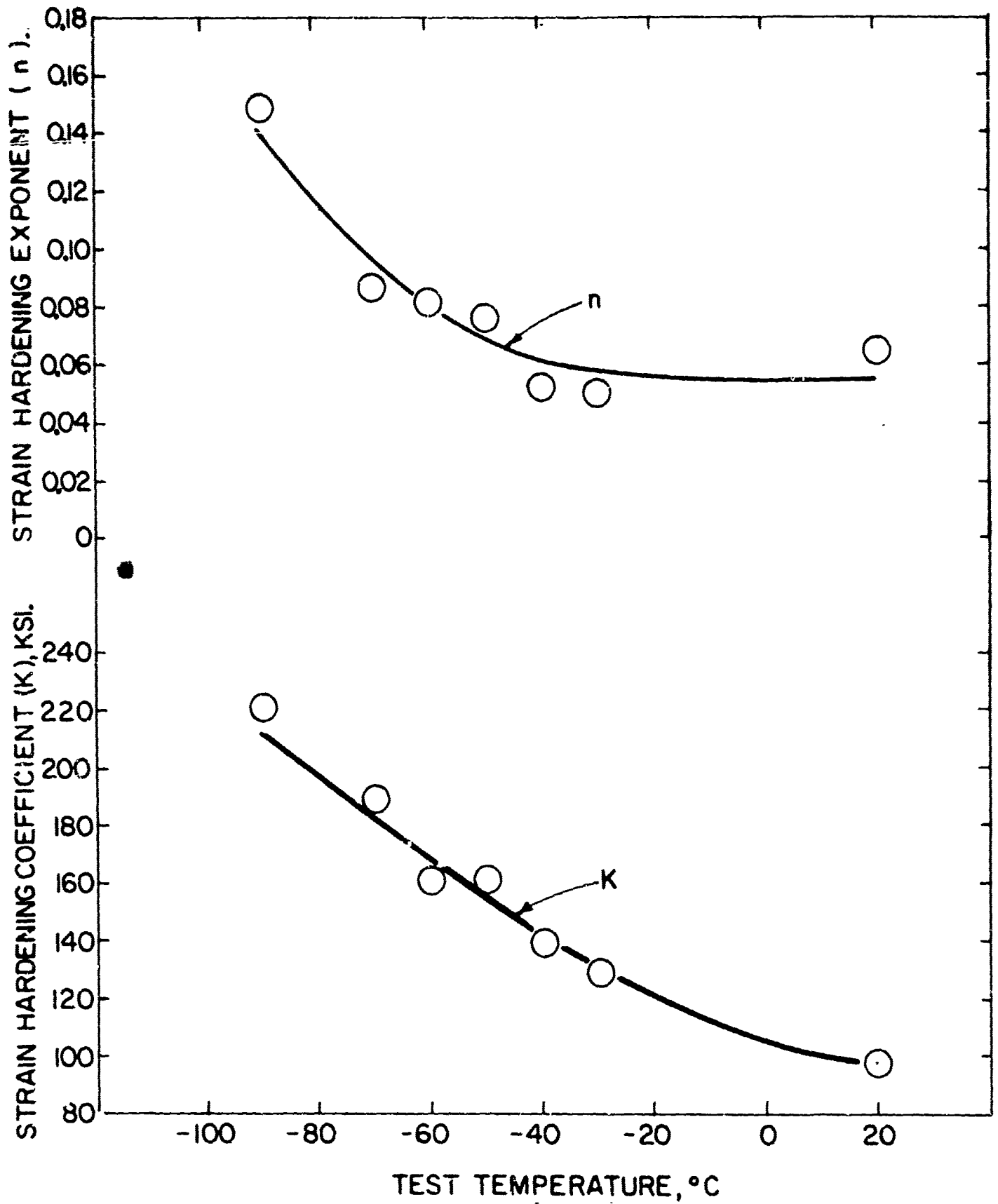


Fig. 8 - Variation of Strain Hardening Exponent (n) and Strain Hardening Coefficient (K) with Test Temperature for Recrystallized Molybdenum (Mo-E2) Strip ($l = 0.026$ mm).

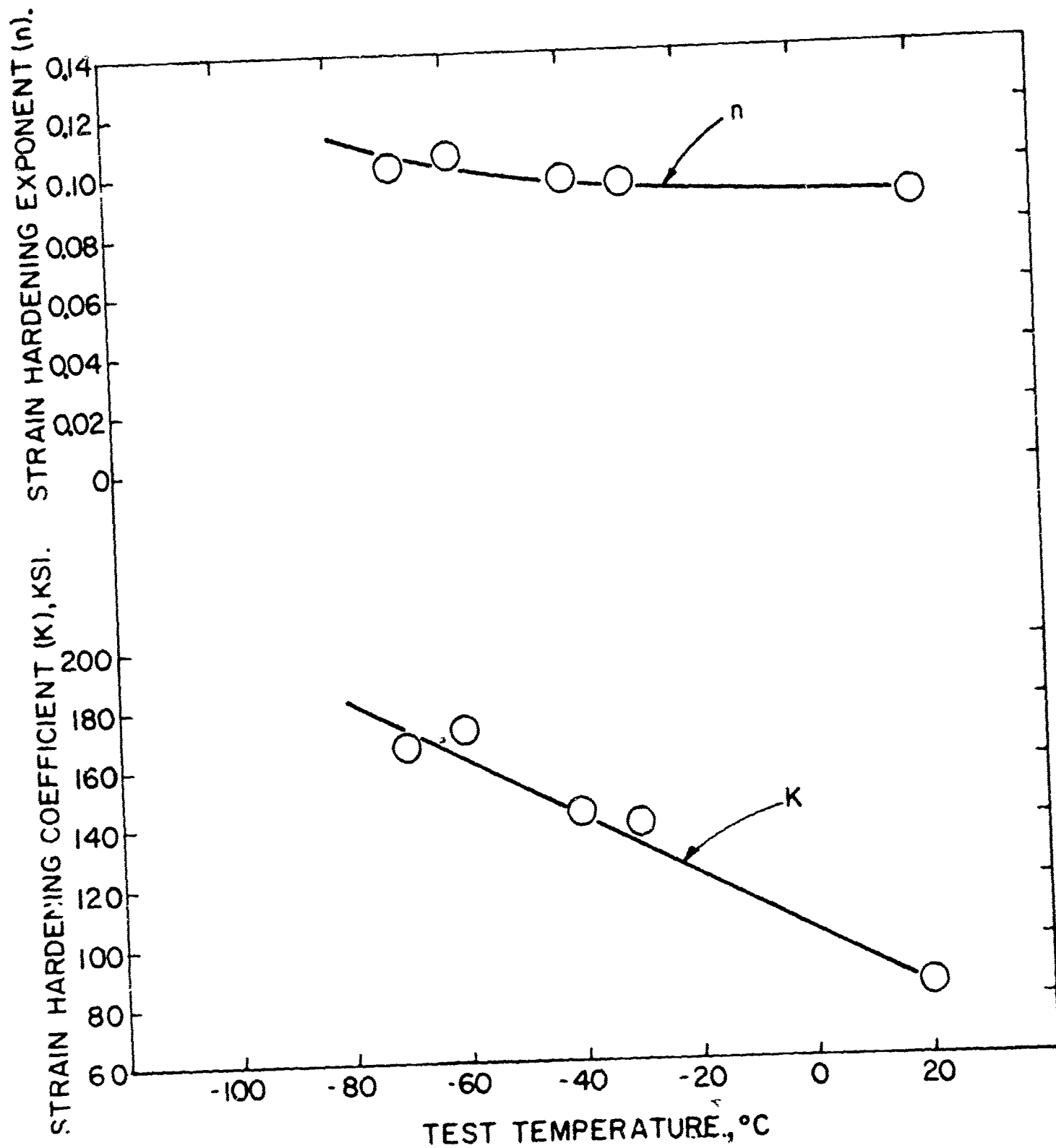


Fig. 9 - Variation of Strain Hardening Exponent (n) and Strain Hardening Coefficient (K) with Test Temperature for Recrystallized Molybdenum (Mo-E2) Strip ($l = 0.044$ mm).

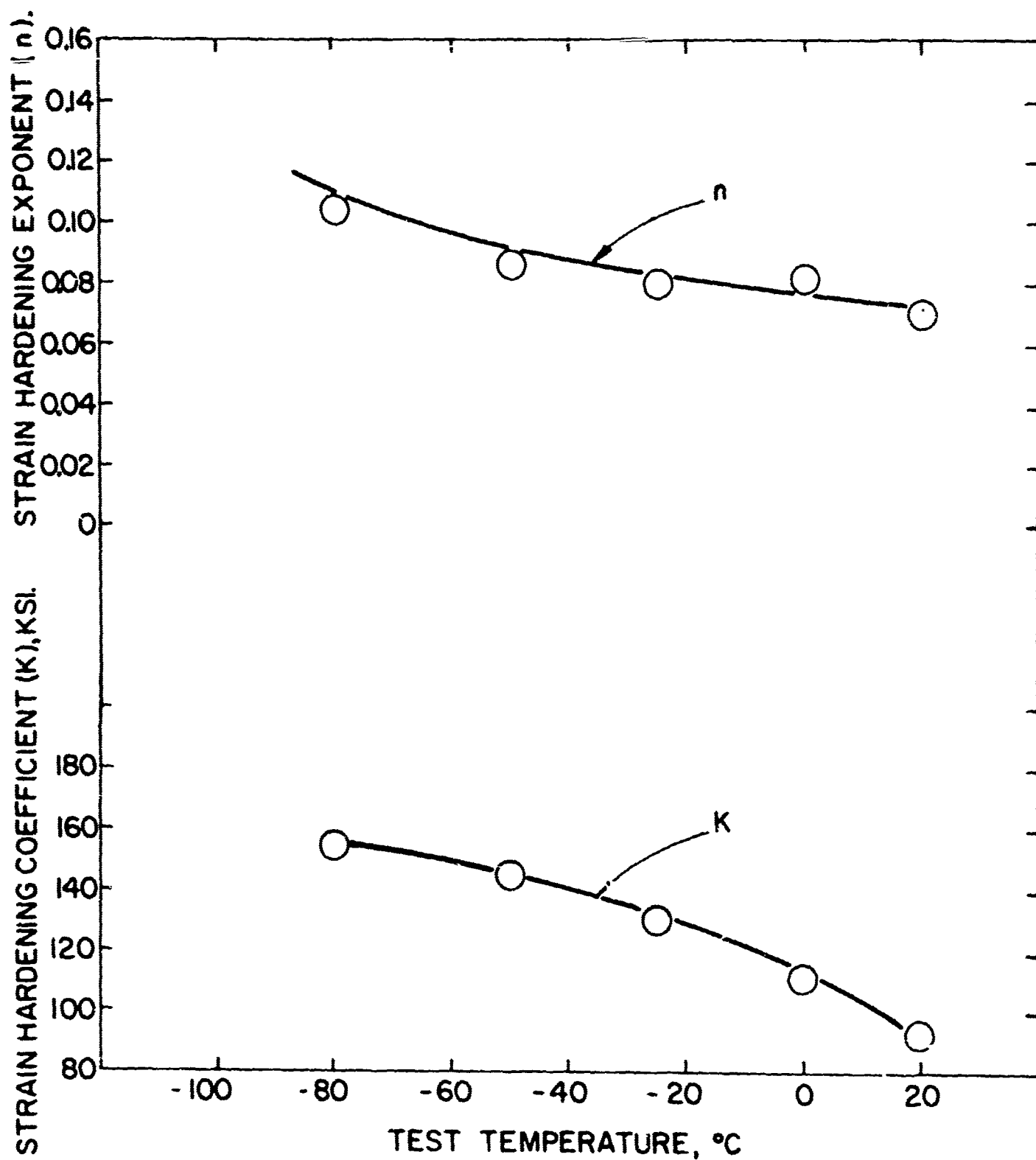


Fig. 10 - Variation of Strain Hardening Exponent (n) and Strain Hardening Coefficient (K) with Test Temperature for Recrystallized Molybdenum (Mo-E2) Strip ($l = 0.174$ mm).

Table 4

Calculated Values of Fracture Stress Assuming Completely Uniform Elongation

Material & Grain Size	Test Temp °C	Fracture Strain ϵ_F	Strain Hardening Exponent n	$(\epsilon_F)^n$	Strain Hardening Coefficient K ksi	Calculated Uniform Fracture Stress σ_{Fs} ksi	Observed Yield Stress σ_Y ksi	Substructural Strengthening Factor q_s
Mo-E2 (0.026mm)	-80	0.04	0.116	0.69	195	135	125	1.08
	-55	0.35	0.074	0.92	160	147	112	1.31
	-30	0.80	0.058	0.99	130	129	94	1.37
	+25	0.98	0.054	1.00	97	97	65	1.50
Mo-E2 (0.044mm)	-75	0.07	0.109	0.74	180	133	98	1.36
	-50	0.20	0.100	0.86	155	133	90	1.48
	-25	0.65	0.094	0.96	130	125	81	1.54
	+25	1.00	0.090	1.00	85	85	65	1.31
Mo-E2 (0.174mm)	-40	0.17	0.088	0.85	140	119	81	1.47
	-20	0.62	0.081	0.96	129	124	73	1.70
	0	0.95	0.077	1.00	111	111	66	1.68
	+25	1.00	0.072	1.00	92	92	60	1.54
Mo-E3 (0.023mm)	-85	0.03	0.090	0.73	216	158	132	1.20
	-45	0.54	0.062	0.95	156	148	109	1.36
	-20	0.91	0.052	1.00	126	126	97	1.30
	+25	1.06	0.046	1.00	100	100	83	1.20
Mo-E4 (0.020mm)	-25	0.10	0.200	0.63	164	104	74	1.41
	0	0.36	0.236	0.79	156	123	62	1.98
	+25	0.68	0.276	0.89	150	134	48	2.79
	+50	0.61	0.311	0.86	145	121	38	3.18

to substructural changes alone ($\bar{\sigma}_{F_s}$) is given by equation (5), which requires that q_p and q_s be known as a function of ϵ_F . Eq. (17) was used to calculate q_p at the same temperatures at which values of $\bar{\sigma}_{F_s}$ given in Table 4 were obtained for the three grain sizes of Mo-E2 strip. Taking q_s as approximately 1.11 based on Eq. (18), calculations were made of $\bar{\sigma}_F$ as a function of test temperature. The calculated values of $\bar{\sigma}_F$ shown in Table 5 agree with the observed fracture stress values within about 15% for 10 cases, and within about 20% for the other two cases. This is considered to be good agreement since the precision of measurement of fracture stress is about 10%.

The calculated maxima in $\bar{\sigma}_F$ occur about half-way between T_d and T_m similar to the calculated $\bar{\sigma}_{F_s}$ maxima. However, there is less of a difference between the calculated maximum in $\bar{\sigma}_F$ and the calculated value at T_m as compared to the corresponding values of $\bar{\sigma}_{F_s}$. It, therefore, appears that the method used to calculate $\bar{\sigma}_F$ is correct in principle but suffers from inaccuracies in determining values of q_p and q_s .

B. Flow and Fracture Characteristics of Mo-E3 Strip

1. Tensile Properties vs. Test Temperature

The effect of test temperature on the tensile properties of Mo-E3 strip of fine grain size (0.023 mm) is shown in Fig. 11. Similar to the fine grain Mo-E2 strip, it was found that T_b and T_d coincide. As indicated in Table 3, the tensile test characteristics of Mo-E2 and Mo-E3 are about the same.

The variations of the strain hardening exponent (n) and the strain hardening coefficient (K) of Mo-E3 with test temperature are shown in Fig. 12. This information was utilized to calculate the variation of fracture stress ($\bar{\sigma}_{F_s}$) assuming completely uniform elongation (Table 4) as well as the fracture stress ($\bar{\sigma}_F$) under actual necking conditions (Table 5). It was found that the substructural strengthening factor (q_s) goes through a maximum at about -45°C . This is reflected in the occurrence of the calculated maximum $\bar{\sigma}_F$ value at -45°C instead of at -20°C as actually observed.

2. Effect of Uniform Prestraining

Experiments were carried out on Mo-E3 to determine the effect of a uniform prestrain (ϵ_{pr}) at a temperature above T_d on the fracture stress ($\bar{\sigma}_F$) and fracture strain (ϵ_F) at a temperature below T_d . The temperatures selected for the prestraining, -20°C and $+25^\circ\text{C}$, correspond to the temperature at which $\bar{\sigma}_F$ goes through a maximum (T_m) and room temperature respectively. The procedure was to prestrain to increasing values of ϵ_{pr} up to about 0.19 at -20°C or $+25^\circ\text{C}$, decrease the load by about 90%, cool to a final test temperature (-100°C , -150°C , or -196°C), and load until fracture occurs.

As shown in Fig. 13, the fracture stress ($\bar{\sigma}_F$) at -100°C increases with prestrain (ϵ_{pr}) and goes through a maximum at $\epsilon_{pr} \cong 0.1$. The maximum in $\bar{\sigma}_F$ corresponds to an increase of about 30% as compared to $\bar{\sigma}_F$ for zero prestrain as measured at the same breaking temperature of -100°C . For a breaking

Table 5

Calculated Values of Fracture Stress Under Actual Necking Conditions

Material & Grain Size	Test Temp °C	Fracture Strain ϵ_F	Uniform Fracture Stress σ_{Fs} ksi	Strengthening Factors		Fracture Stress σ_F ksi		Ratio of Calc. to Obs. $\frac{\sigma_F}{\sigma_{Fs}}$
				q_p	q_c	calc. ksi	obs. ksi	
Mo-E2 (0.026mm)	-80	0.04	135	1.00	1.00	135	125	1.08
	-55	0.35	147	1.06	1.11	172	145	1.18
	-30	0.80	129	1.15	1.11	163	168	0.97
	+25	0.98	97	1.19	1.11	126	122	1.03
Mo-E2 (0.044mm)	-75	0.07	133	1.00	1.00	133	110	1.21
	-50	0.20	133	1.03	1.11	132	128	1.19
	-25	0.65	125	1.12	1.11	154	147	1.05
	+25	1.00	85	1.19	1.11	111	139	0.80
Mo-E2 (0.174mm)	-40	0.17	119	1.02	1.00	122	122	1.00
	-20	0.62	124	1.11	1.11	151	140	1.08
	0	0.95	111	1.18	1.11	143	160	0.89
	+25	1.00	92	1.19	1.11	120	152	0.79
Mo-E3 (0.023mm)	-85	0.03	158	1.00	1.00	150	132	1.13
	-45	0.54	148	1.10	1.11	179	162	1.10
	-20	0.91	126	1.17	1.11	162	180	0.90
	+25	1.06	100	1.21	1.11	132	155	0.85
Mo-E4 (0.020mm)	-25	0.10	104	1.02	1.10	117	90	1.30
	0	0.36	123	1.06	1.11	144	111	1.30
	+25	0.68	134	1.12	1.11	165	130	1.27
	+50	0.61	121	1.11	1.11	148	108	1.37

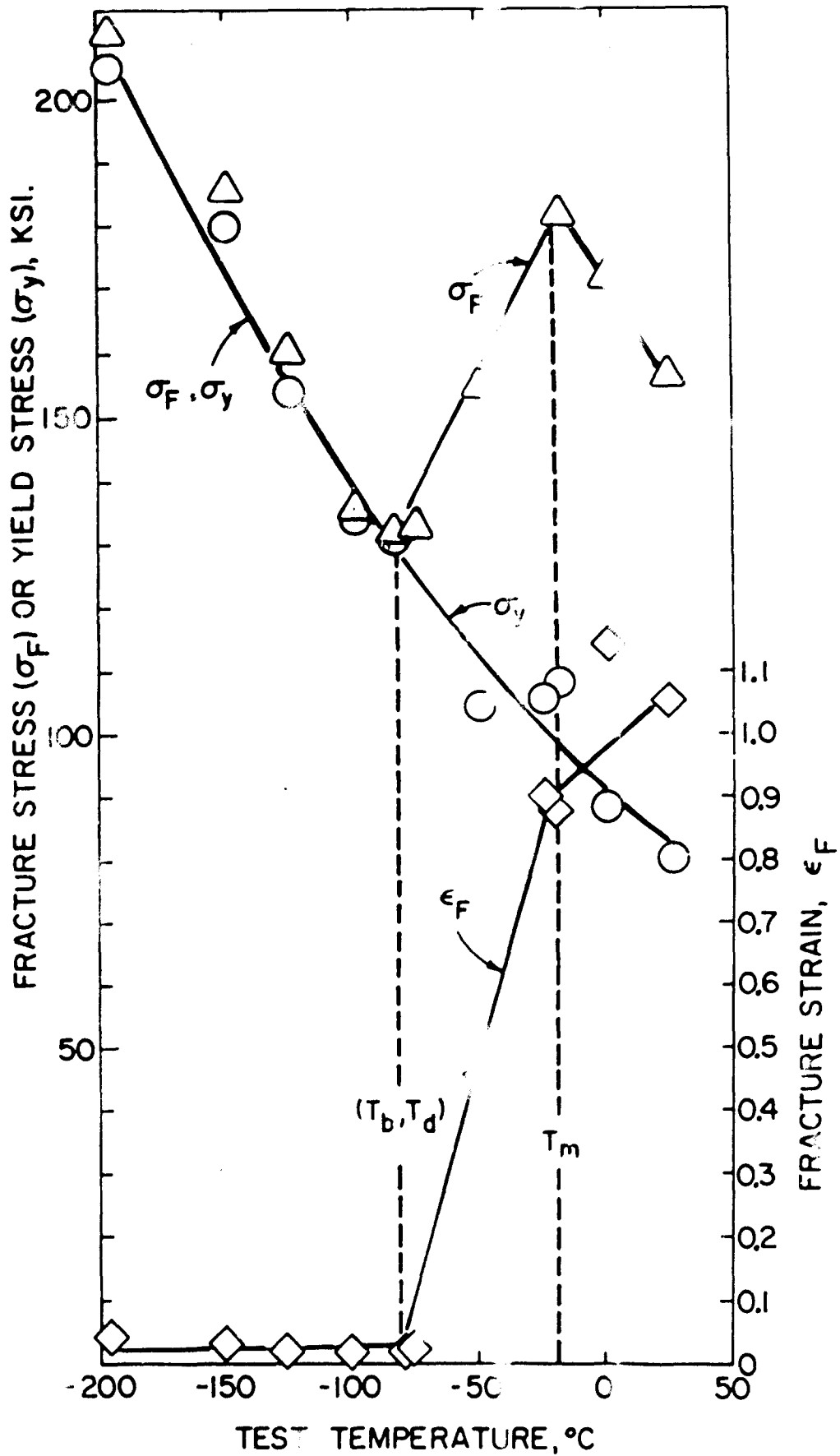


Fig. 11 - Effect of Test Temperature on Tensile Properties of Recrystallized Molybdenum (Mo-E3 Strip ($t = 0.023$ mm)).

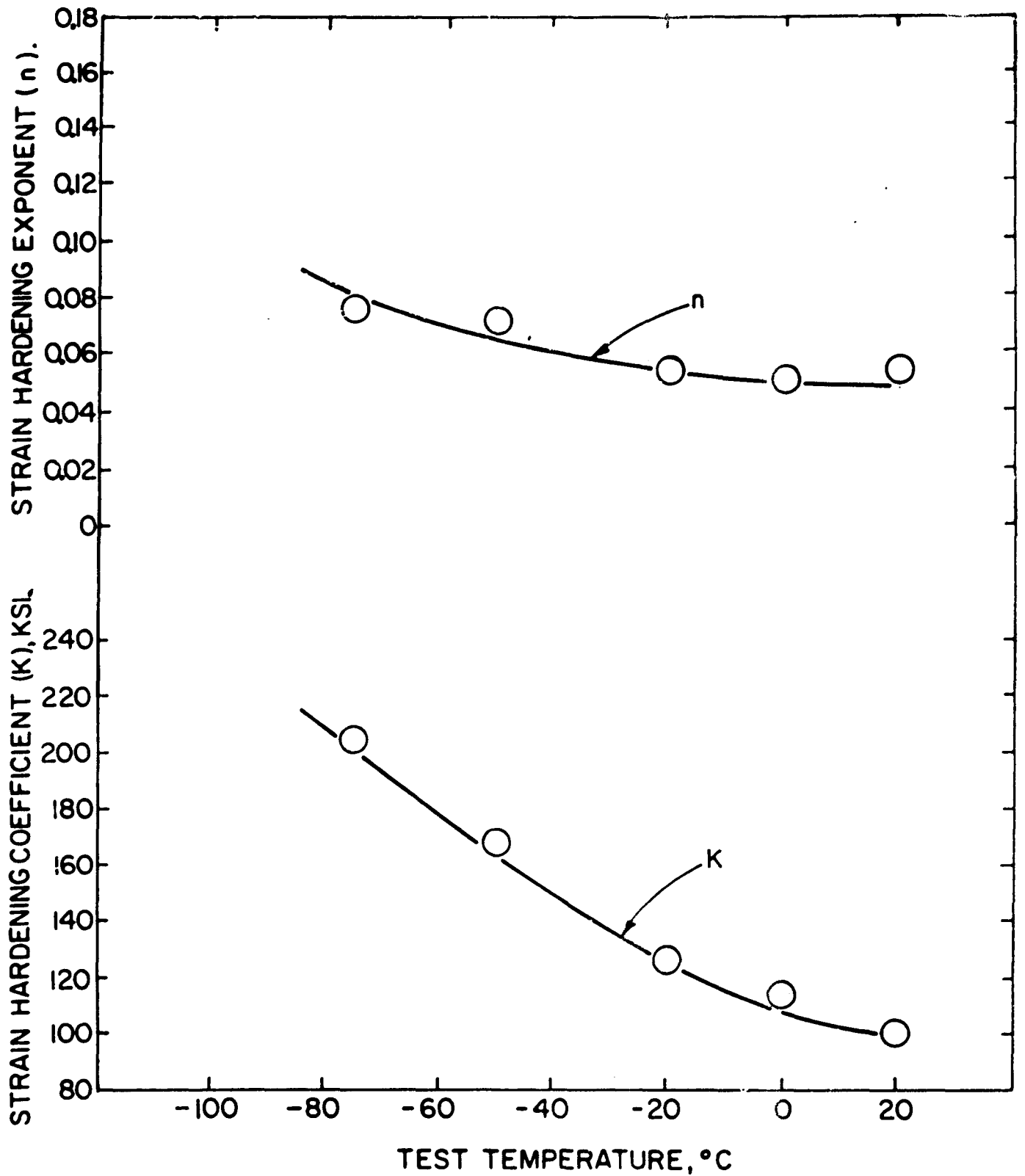


Fig. 12 - Variation of Strain Hardening Exponent (n) and Strain Hardening Coefficient (K) with Test Temperature for Recrystallized Molybdenum (Mo-E3) Strip ($t = 0.023$ mm).

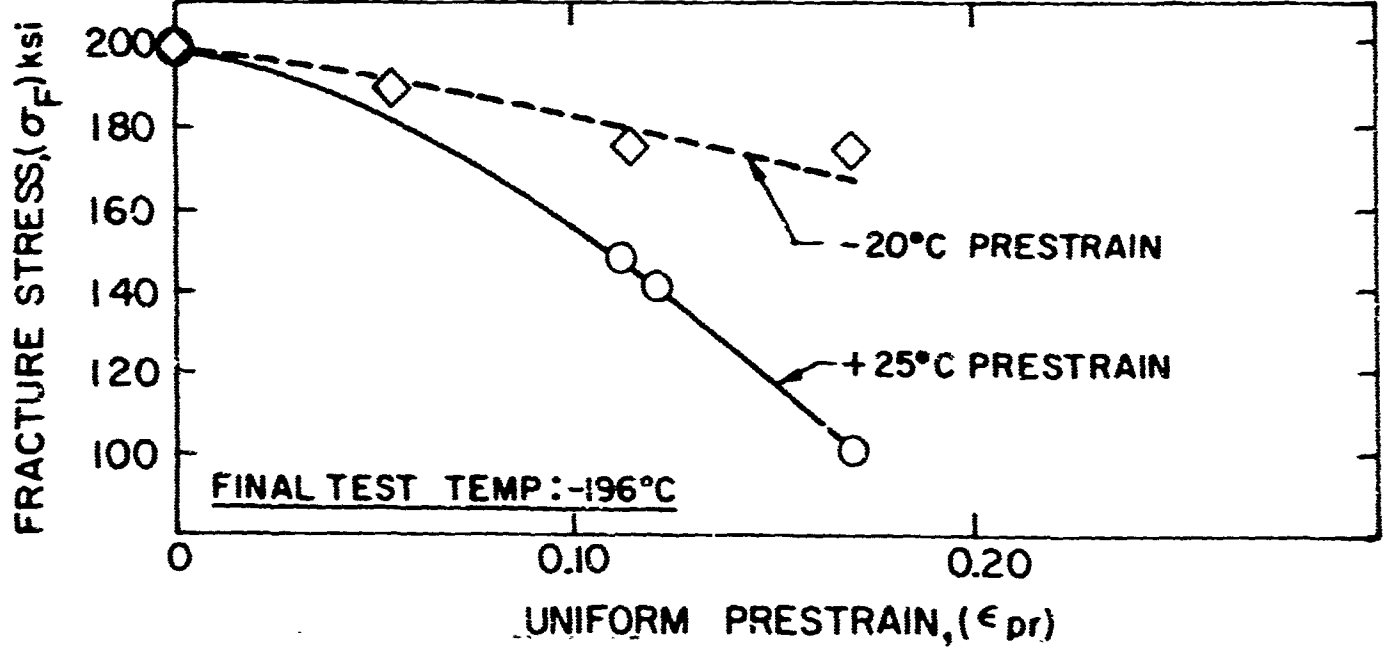
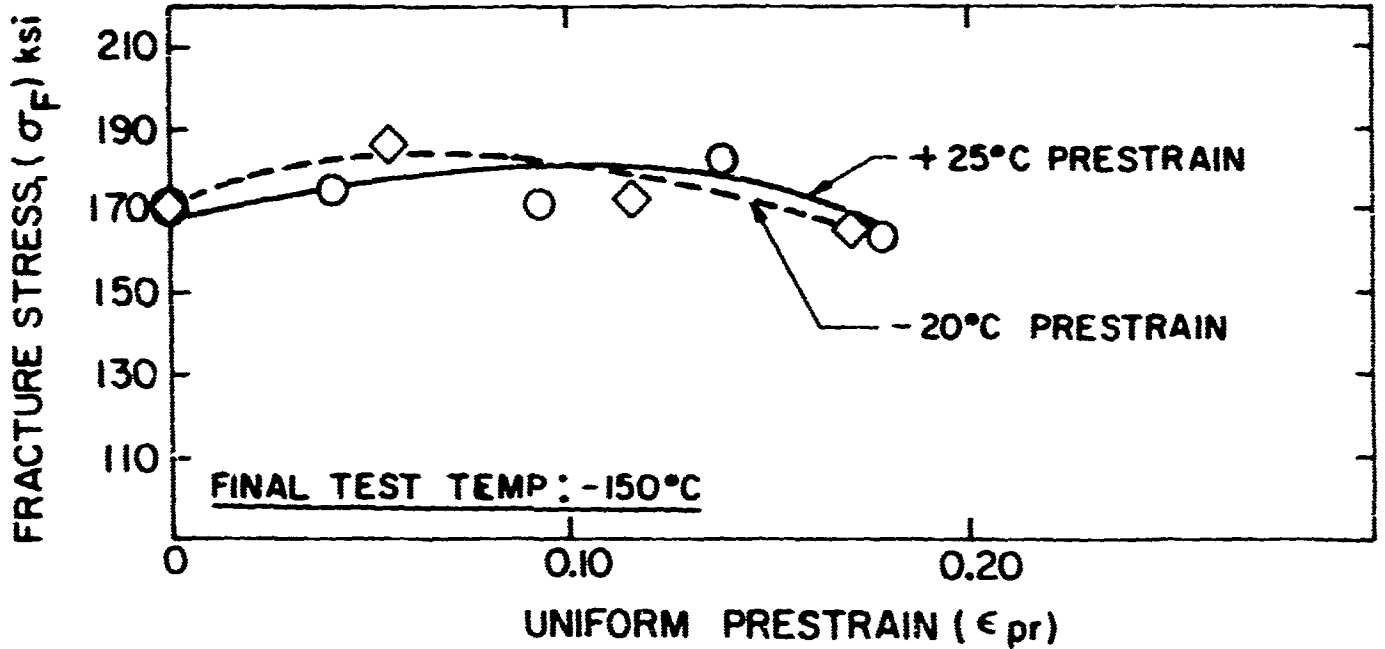
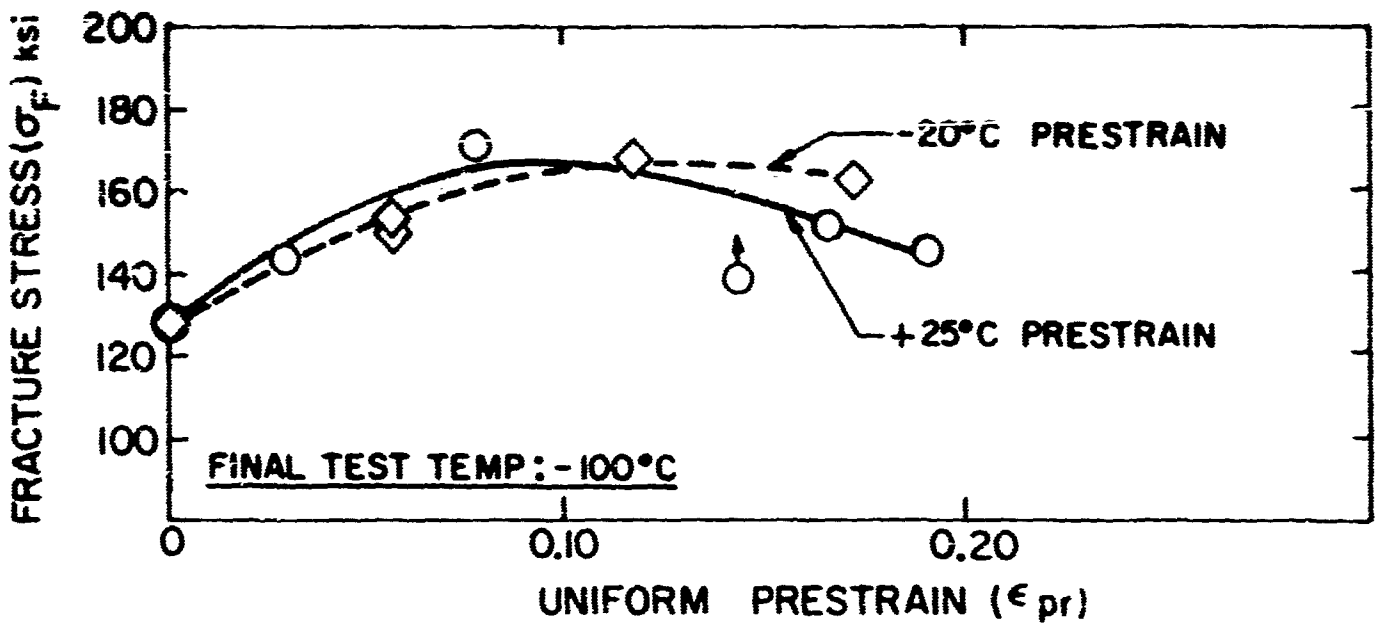


Fig. 13 - Effect of Uniform Prestraining Mo-E3 at -20°C and $+25^\circ\text{C}$ on the Fracture Stress at -100°C , -150°C , and -196°C .

temperature of -150°C there appears to be a slight maximum in σ_F at $\epsilon_{pr} \cong 0.06$ for a prestrain temperature of -20°C . A similar trend was found for prestraining at $+25^{\circ}\text{C}$ although the position of the maximum is in doubt because of the scatter in the data. At -196°C , σ_F decreases with prestrain and the rate of decrease is greater for the $+25^{\circ}\text{C}$ than for the -20°C prestrain temperature.

The corresponding variations of the fracture strain (ϵ_F) and the total strain ($\epsilon_{pr} + \epsilon_F$) with prestrain ϵ_{pr} are shown in Figs. 14, 15 and 16. After prestraining at either -20 or $+25^{\circ}\text{C}$, ϵ_F as a function of ϵ_{pr} goes through a maximum at all of the final test temperatures (-100°C , -150°C , and -196°C). The total strain ($\epsilon_{pr} + \epsilon_F$) increases with ϵ_{pr} and tends to level off at the higher values of ϵ_{pr} .

The variation of σ_F with total strain ($\epsilon_{pr} + \epsilon_F$) is shown in Table 6 for Mo-E3 strip prestrained at -20°C and broken at -100 , 150 , and -196°C . It was found that σ_F increases appreciably at -100°C , increases slightly at -150°C , and decreases at -196°C as the total amount of strain is increased. For the purpose of comparison, σ_F values obtained in the range of -80 to -67°C without any prestrain are listed in Table 6. The ratio of fracture stresses with and without any prestrain varies with both total strain and test temperature. This is further evidence that σ_F is not a unique function of strain alone.

3. Effect of Necking Prestrain

Studies were carried out to determine the effect of necking prestrains at $+25^{\circ}\text{C}$ on the fracture stress (σ_F) and fracture strain (ϵ_F) at -100°C . As shown in Table 7, a necking prestrain of 0.29 at $+25^{\circ}\text{C}$ results in an increase in σ_F at -100°C of about 20% and in ϵ_F at -100°C of about 500% (0.03 to 0.18). A larger necking prestrain (0.64) results in a slight increase in σ_F along with a 55% decrease in ϵ_F as compared to a 0.29 necking prestrain.

In order to determine to what extent the geometry of the neck affects σ_F and ϵ_F , simulated necking was studied using two procedures: a) prestraining at $+25^{\circ}\text{C}$ to produce a neck corresponding to a strain of 0.64 and recrystallizing to remove the deformation; b) machining a neck in the rolling plane section of the specimen that corresponds to 0.64 strain. As shown in Table 7 procedures a) and b) resulted in completely brittle fractures ($\epsilon_F = 0$) as well as decreases in σ_F of 30% and 12% respectively as compared to a non-prestrained specimen tested at -100°C ($\sigma_F = 140$ ksi). These results indicate that the geometrical effect of a neck corresponding to 0.64 strain is to provide a stress concentration which results in a lowering of σ_F . It should be noted that the simulated neck obtained by procedure b) was machined in only one plane, whereas during tensile deformation necking actually occurs along both the thickness and width dimensions. Therefore, a greater stress concentration is presumably present in a specimen that is pre-necked by tensile deformation, procedure a), than by machining, procedure b).

In view of the simulated necking results, it appears that the plastic deformation associated with prestraining has a greater effect on raising σ_F at -100°C than is indicated by the 30% increase shown in Table 7 for 0.64 necking prestrain.

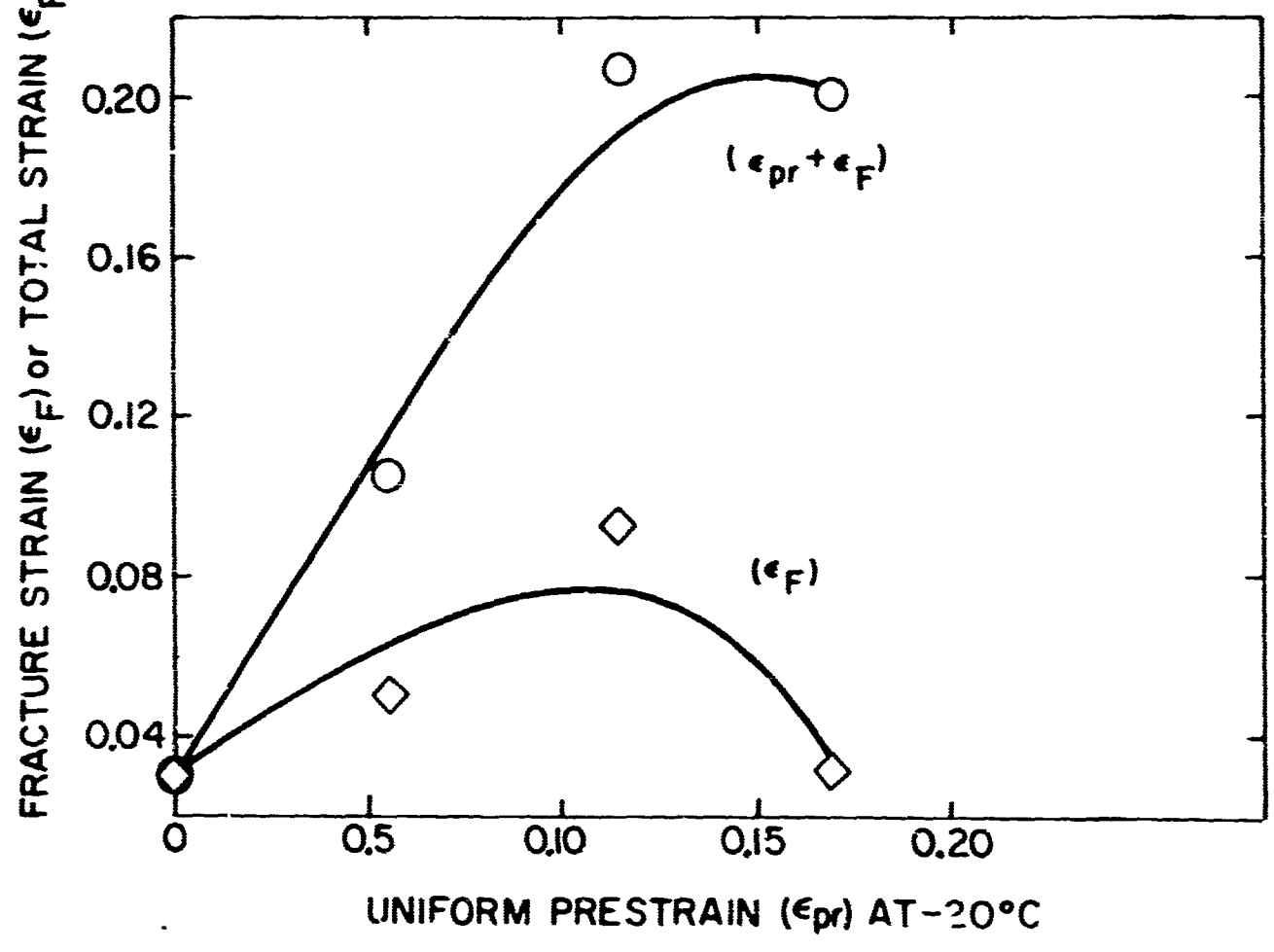
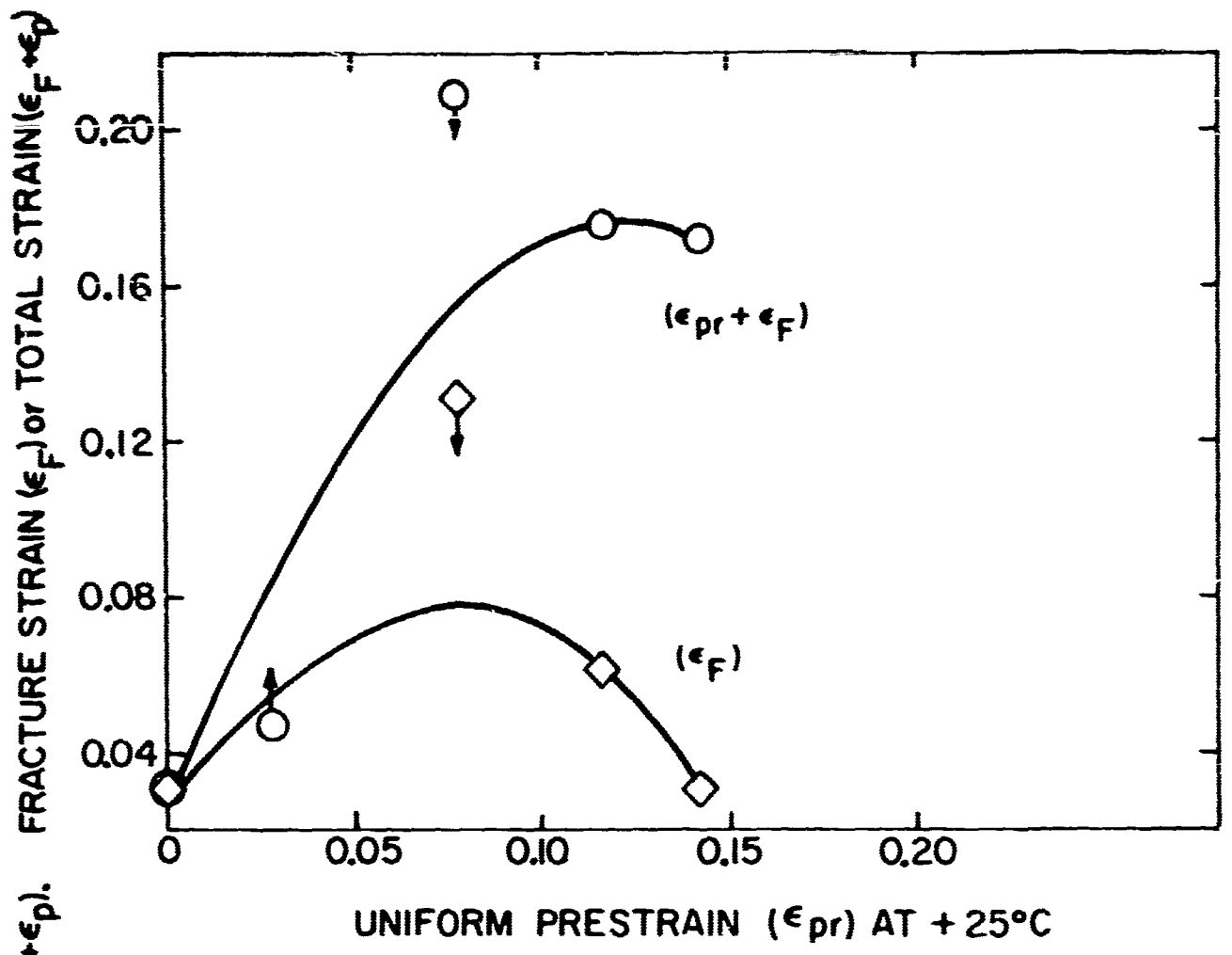


Fig. 14 - Effect of Prestraining Mo-E3 at -20°C and +25°C on Fracture Strain (ϵ_F) and Total Strain ($\epsilon_{pr} + \epsilon_F$) at -100°C.

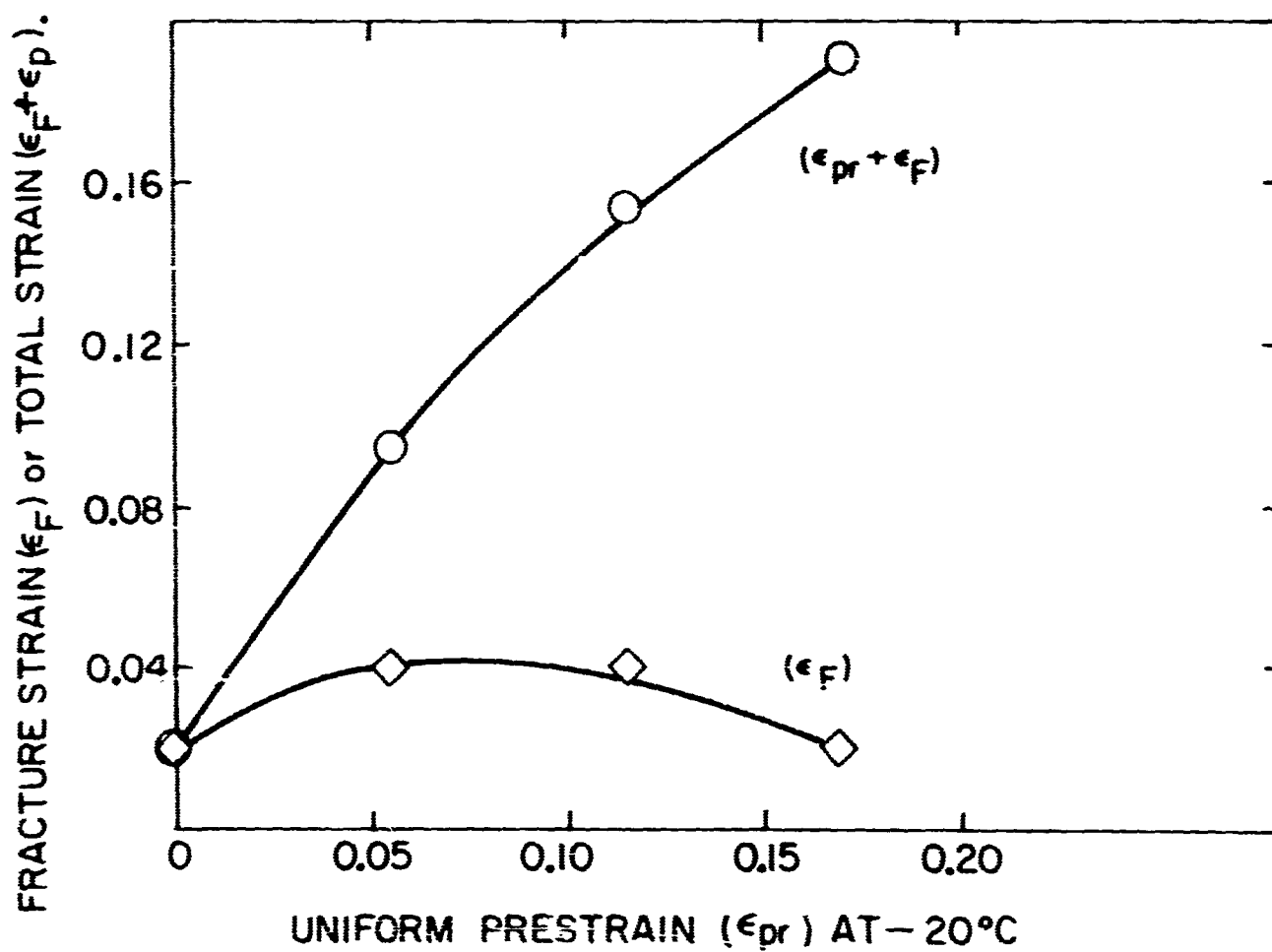
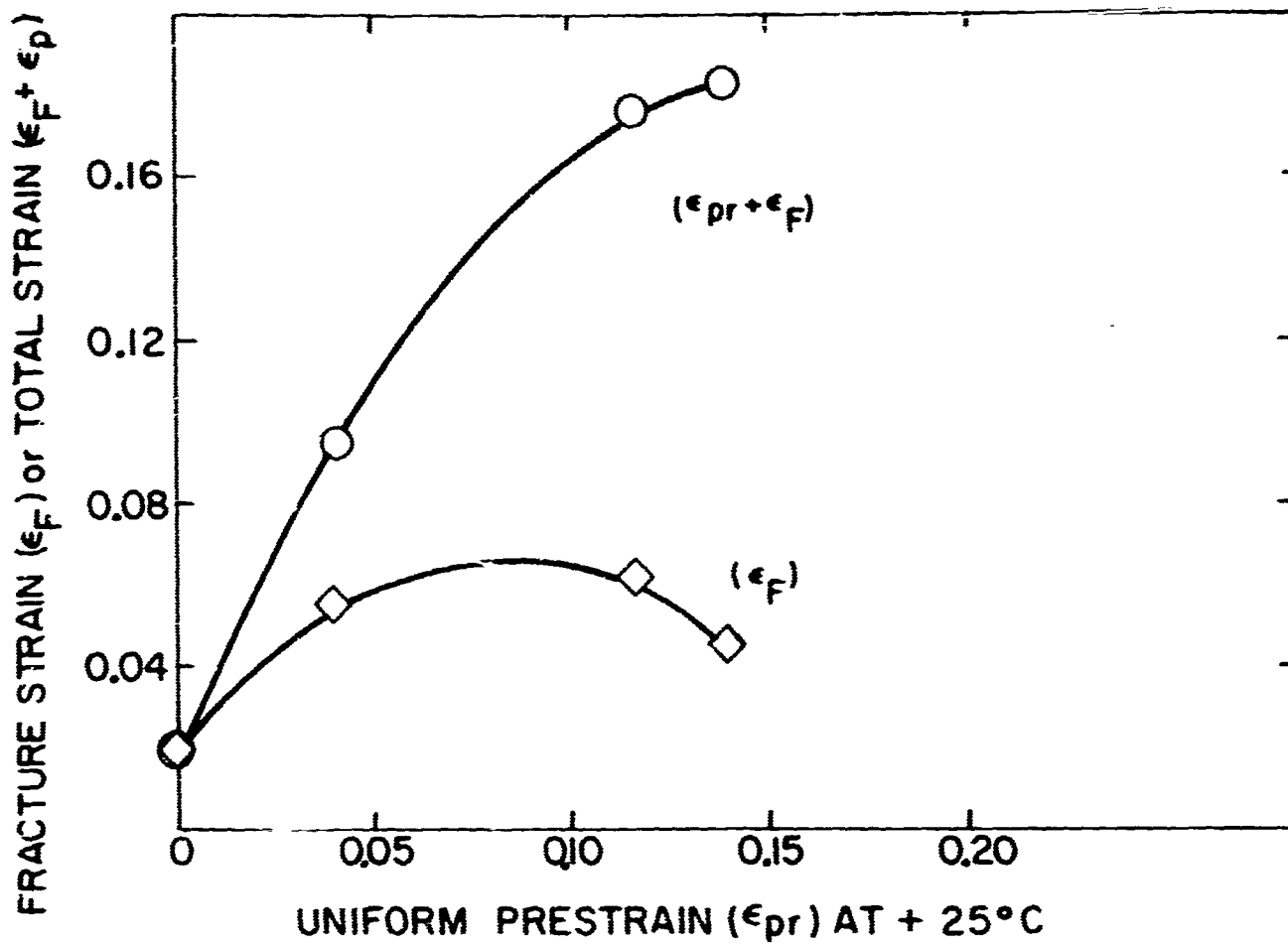


Fig. 15 - Effect of Prestraining Mo-E3 at -20°C and +25°C on Fracture Strain (ϵ_F) and Total Strain ($\epsilon_{pr} + \epsilon_F$) at -150°C.

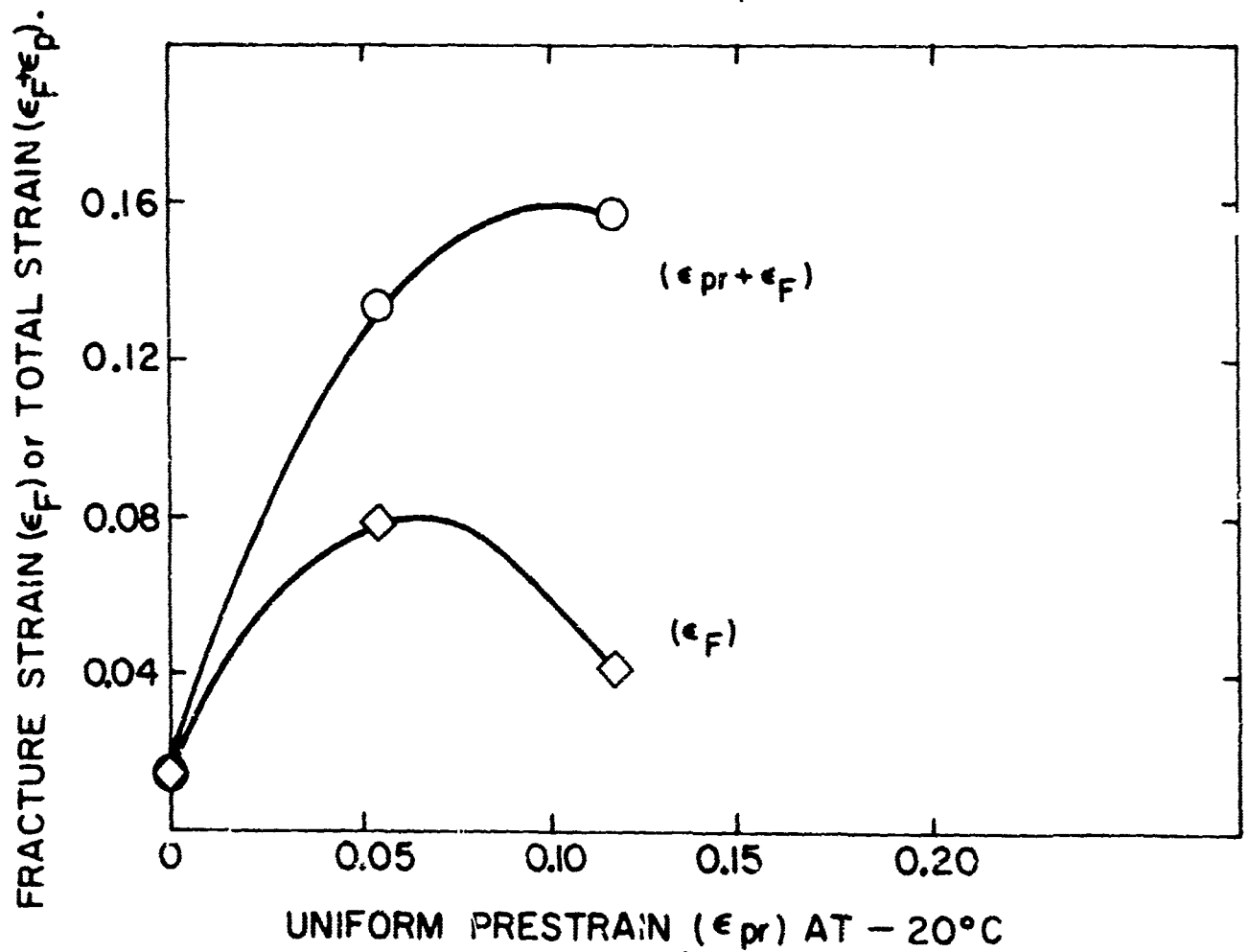
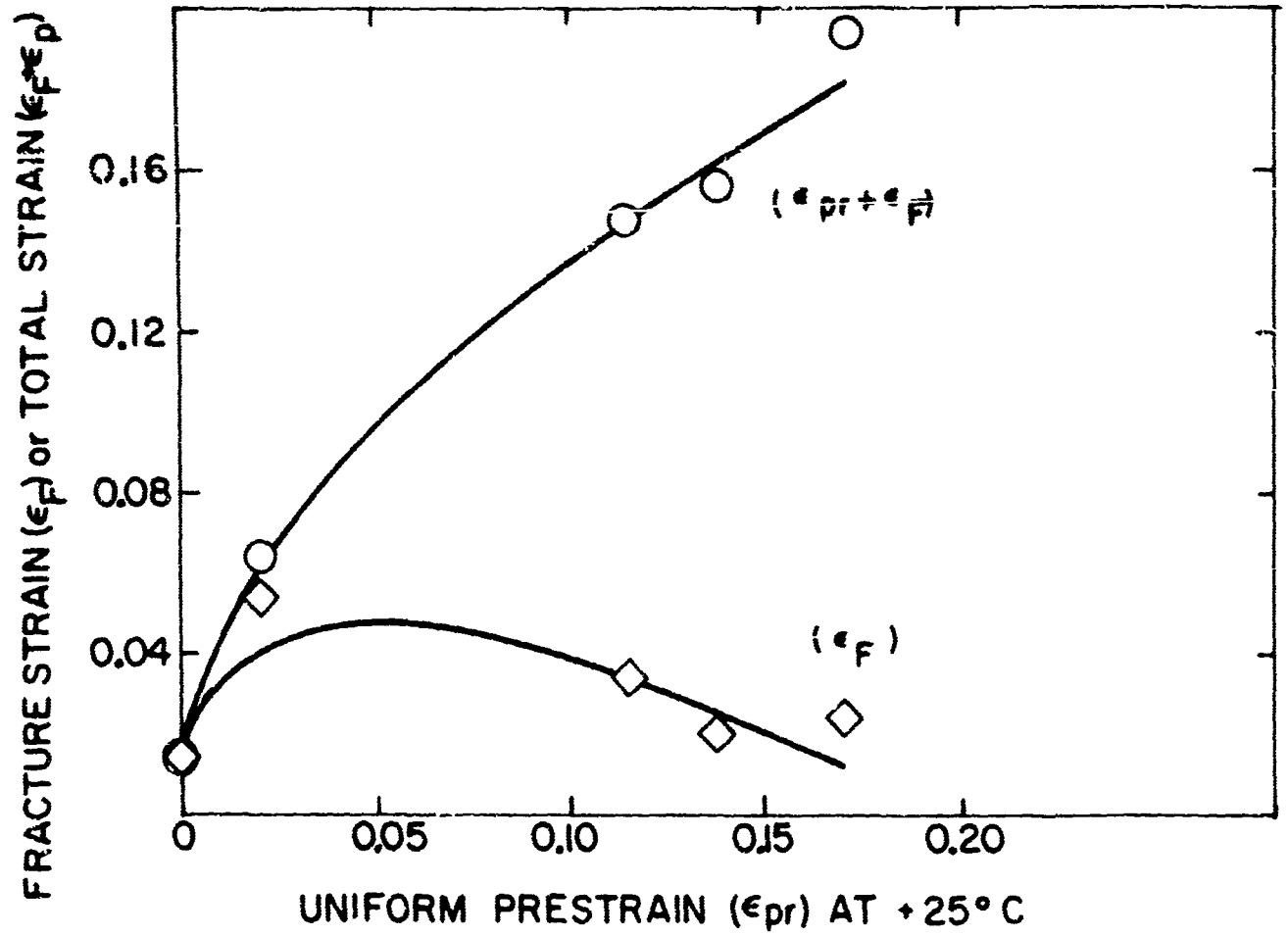


Fig. 16 - Effect of Prestraining Mo-E3 at -20°C and +25°C on Fracture Strain (ϵ_F) and Total Strain ($\epsilon_{pr} + \epsilon_F$) at -196°C.

Table 6

Variation of Fracture Stress of Mo-E3 With Total Strain

<u>Test Temperature</u>		<u>Prestrain</u>	<u>Total Strain</u>	<u>Fracture</u>	<u>Ratio*</u>
<u>Prestrain</u>	<u>Fracture</u>	<u>(ϵ_p)</u>	<u>($\epsilon_F + \epsilon_{pr}$)</u>	<u>Stress</u>	<u>of Fracture</u>
<u>$^{\circ}\text{C}$</u>	<u>$^{\circ}\text{C}$</u>			<u>(σ_F)</u>	<u>Stresses</u>
					<u>With and</u>
					<u>Without Prestrain</u>
-20 $^{\circ}\text{C}$	-100 $^{\circ}\text{C}$	-	0.03	138	1.06
		0.015	0.05	141	1.08
		0.05	0.10	151	1.13
		0.085	0.15	158	1.15
		0.13	0.20	164	1.16
-20 $^{\circ}\text{C}$	-150 $^{\circ}\text{C}$	0.015	0.05	177	1.35
		0.055	0.10	180	1.34
		0.11	0.15	178	1.29
		0.185	0.20	161	1.14
-20 $^{\circ}\text{C}$	-196 $^{\circ}\text{C}$	0.01	0.05	202	1.54
		0.05	0.10	193	1.44
		0.115	0.15	166	1.20
		0.21	0.20	160	1.11
-	-80 $^{\circ}\text{C}$	-	0.03	130	-
-	-79 $^{\circ}\text{C}$	-	0.05	131	-
-	-86 $^{\circ}\text{C}$	-	0.10	134	-
-	-73 $^{\circ}\text{C}$	-	0.15	138	-
-	-70 $^{\circ}\text{C}$	-	0.20	141	-
-	-67 $^{\circ}\text{C}$	-	0.25	144	-

* Values of fracture stress without any prestrain are given in this table for the temperature range of -80 to -67 $^{\circ}\text{C}$.

Table 7

Effect of Necking Prestrains and Simulated

Necks on the Fracture Stress of Mo-E3 at -100°C

<u>Amt. of Prestrain at +25°C</u>	<u>Procedure Prior to test at -100°C</u>	<u>Fracture Stress at -100°C</u> ksi	<u>Fracture Strain at -100°C</u>	<u>Total Strain</u>
0	no prestrain	140	0.03	0.03
0.29	necking prestrain	170	0.18	0.47
0.64	necking prestrain	173	0.10	0.74
* 0	prestrained 0.64 and recrystallized 0.5 hr. at 1200°C	98	0	0
** 0	machined with neck (in rolling plane section) equi- valent to 0.64 strain and recrystallized 0.5 hr at 1200°C.	123	0	0

* No prestrain given after recrystallization.

** No prestrain given after recrystallization. Strip was in worked condition prior to machining and recrystallizing.

Table 8
Fracture Toughness of Mo-E3 at -100°C

<u>Condition</u>	<u>Hartbower (W/A)</u>		<u>Irwin G_c</u>	
	<u>in-lbs/in²</u>	<u>ergs/cm²</u>	<u>in-lbs/in²</u>	<u>ergs/cm²</u>
as-recrystallized	110	1.9x10 ⁷	120	2.1x10 ⁷
pulled 6% in tension at +25°C	55	9.6x10 ⁶	120	2.1x10 ⁷
reduced 6% by rolling at +25°C	25	4.4x10 ⁶	85	1.5x10 ⁷

Assuming that the geometrical effect of necking is to cause a decrease of 30%, it appears that the necking prestrain per se effectively increases σ_F by about 60%.

4. Slow Bend Tests at -100°C

Slow bend tests were carried out on Mo-E3 in the following conditions: a) as-recrystallized, b) deformed 6% at $+25^\circ\text{C}$ by tensile pulling, c) deformed 6% at $+25^\circ\text{C}$ by rolling. V-notch Charpy specimens were machined to the following dimensions: 0.030 inch thick, 0.394 inch wide, and 2 1/8 inches long.

A 0.079 inch deep, 45° V-notch was machined perpendicular to the rolling direction of the strip (parallel to length direction of specimen). These specimens were precracked by room temperature cyclic bending in compression from zero to about 50 ksi (calculated maximum compressive fiber stress at root of the V-notch). The average depth of a fatigue crack as obtained by this procedure was about 0.025 inch. Slow bend tests were carried out at -100°C and measurements of load vs deflection were obtained.

Both the Hartbower and Irwin methods were used to determine resistance to crack propagation from the slow bend test measurements. The Hartbower (9) method of determining the fracture toughness parameter W/A involves dividing the energy (W) corresponding to the integral of the load vs deflection curve by the area (A) of the fractured surface (below the fatigue crack). The Irwin (10) method of determining the fracture toughness parameter G_c involves use of the following relation:

$$G_c = \frac{(P_m)^2}{B} \frac{d(M^{-1})}{da} \quad (19)$$

where P_m = maximum load
 B = specimen thickness
 M = spring constant (P/e) where e = deflection
 a = notch depth

An approximate value of dM^{-1}/da was obtained from the initial slopes of the P vs e plots corresponding to different initial crack lengths (a).

The fracture toughness values determined from the slow bend tests at -100°C are given in Table 8. The W/A and G_c values for the as-recrystallized condition show good agreement. However, although decreases in (W/A) of 50 to 75% resulted from plastic strains of 0.06 at $+25^\circ\text{C}$, the corresponding decreases in G_c are only 0 to 30%. The fracture toughness values at -100°C fall in the range of 25 to 120 in-lbs/in² or 0.4 to 2.1×10^7 ergs/cm².

C. Flow and Fracture Characteristics of Mo-E4 Strip

The effect of test temperature on the tensile properties of Mo-E4 strip is shown in Fig. 17. For this high oxygen material of fine grain size ($l = 0.020$ mm), T_b and T_d appear to coincide at about -35°C , and T_m occurs at about $+25^\circ\text{C}$. These are higher temperatures than found for the fine grain Mo-E2 and Mo-E3 materials (Table 3). The Mo-E4 also differs from the Mo-E2 and Mo-E3 materials in that $\epsilon_F = 0$ below T_d and σ_F reaches a constant value at about -100°C . No evidence was found that twinning is responsible for the levelling-off in σ_F . Therefore, this phenomenon remains unexplained.

As shown in Table 9, prestraining the Mo-E4 at $+25^\circ\text{C}$ was found to result in increases in fracture stress of about 14 and 20% at -100 and -196°C respectively. The specimens were observed to fracture without any additional plastic strain at these test temperatures. This differs from the Mo-E3 behavior after prestraining since an appreciable amount of strain occurred prior to fracture at -100°C .

The variations of the strain hardening exponent (n) and strain hardening coefficient (K) of Mo-E4 strip with test temperature in the range of -25 to $+50^\circ\text{C}$ are shown in Fig. 18. The strain hardening exponent (n) of Mo-E4 decreases markedly with decrease in test temperature, which is opposite to that found for the Mo-E2 and Mo-E3 materials. On the other hand, the strain hardening coefficient (K) increases with decrease in test temperature similar to the Mo-E2 and Mo-E3 materials.

Using the ϵ_F , n , and K values for Mo-E4 shown in Figs. 17 and 18 respectively, calculations were made of the uniform fracture stress (σ_{fs}) and the substructural strengthening factor (q_s). As shown in Table 4, q_s for Mo-E4 was found to be considerably higher than for the Mo-E2 and Mo-E3 materials in the range of 0°C to 25°C . This is attributed to the relatively high strain hardening characteristics of Mo-E4, presumably due to its high oxygen content. The predicted values of σ_F for Mo-E4 under actual necking conditions are shown in Table 5. The predicted values were found to be 27 to 37% higher than the observed values of σ_F in the range of -25 to $+50^\circ\text{C}$. The agreement is relatively poor as compared to that obtained for the Mo-E2 and Mo-E3 materials. This may be due to a difference between high and relatively low oxygen materials with respect to the degree of plastic constraint for the same reduction in area.

D. Fractographic Characteristics

1. Broken Mo-E2 Tensile Specimens

Based on light and electron microscopic observations, the fractographic characteristics of the fine, medium, and coarse grain Mo-E2 tensile specimens were determined. As shown in Figs. 19 to 22, the fractures of the fine grain Mo-E2 specimens tested at $+25$ to -30°C consist of both cleavage (transgranular) facets and intergranular facets. The cleavage facets contain what are called cleavage steps or river markings, which indicate the direction of crack propagation. On the other hand the intergranular facets

Table 9
Effect of Prestrain on the Fracture Stress of Mo-E4 Strip at -100°C and -196°C

<u>Amount of Prestrain at +25°C</u>	<u>Test Temp. °C</u>	<u>Fracture Strain (after prestrain)</u>	<u>Fracture Stress (after prestrain) ksi</u>	<u>Ratio of Fracture Stresses With and Without Prestrain</u>
0.28	-100	0	140	1.14
0.25	-196	0	148	1.20

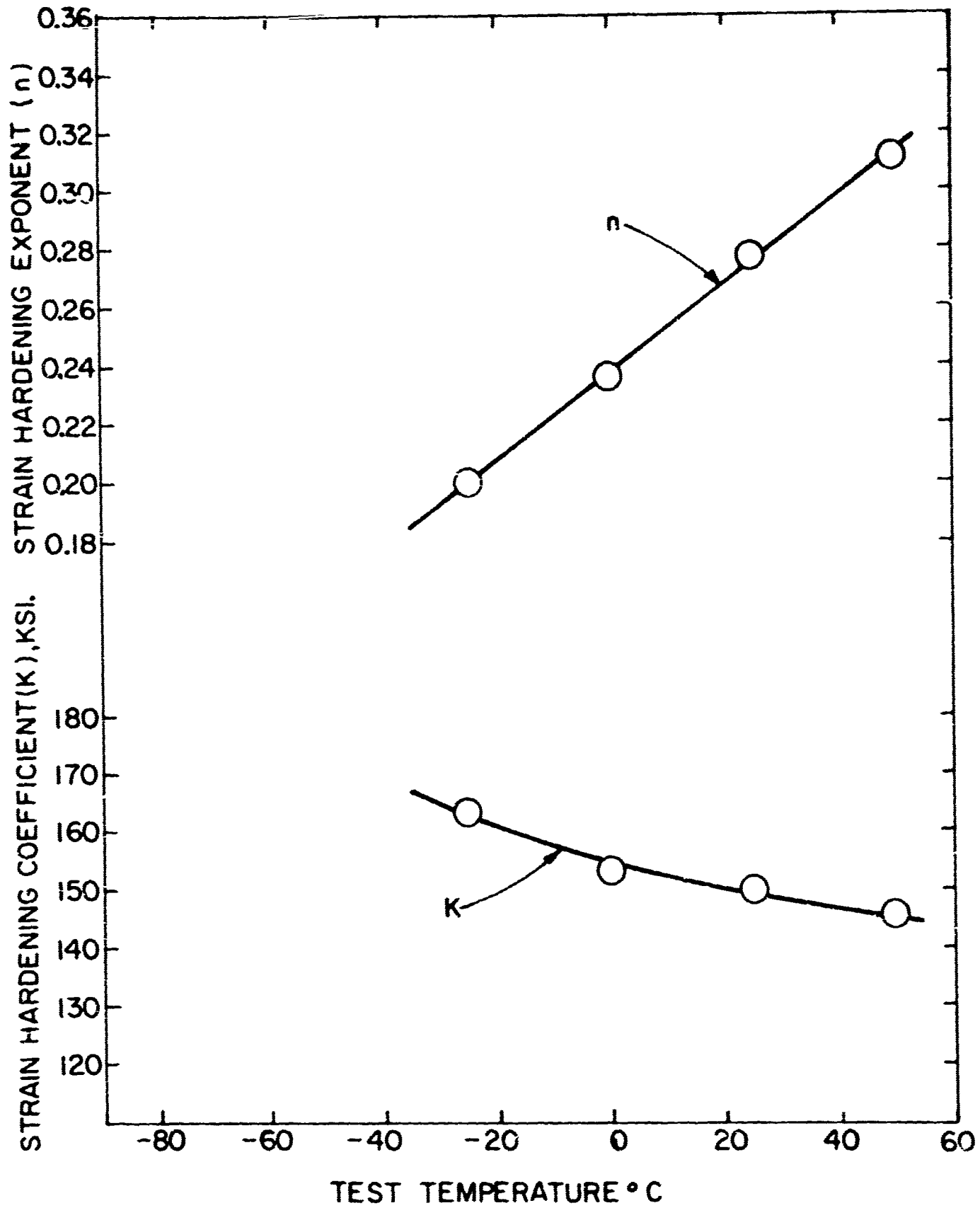


Fig. 18 - Variation of Strain Hardening Exponent (n) and Strain Hardening Coefficient (K) with Test Temperature for Recrystallized Molybdenum (Mo-E4) Strip ($t = 0.020$ mm).

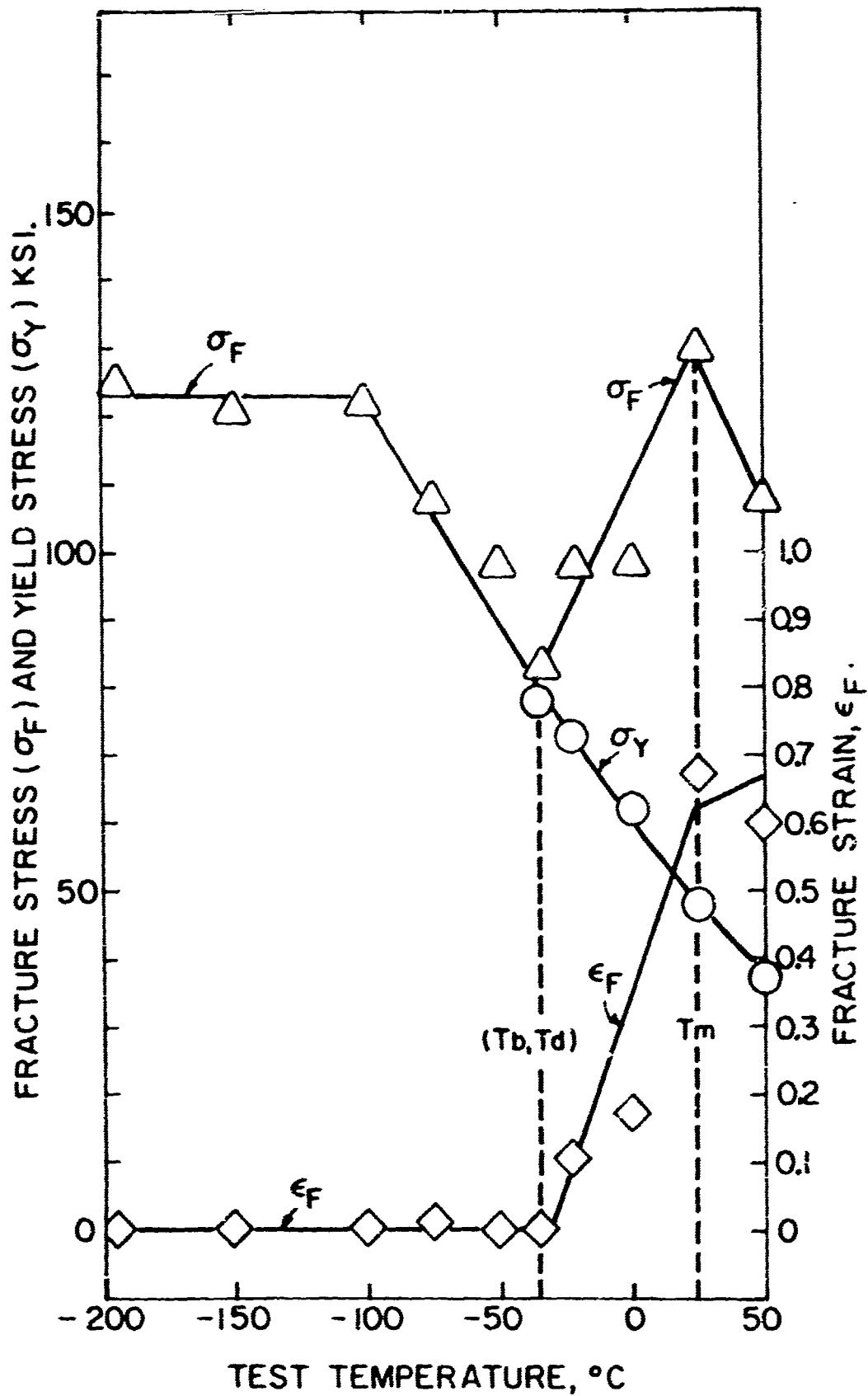


Fig. 17 - Effect of Test Temperature on Tensile Properties of Recrystallized Molybdenum (Mo-E4) Strip ($t = 0.020$ mm).



Light Fractograph

750X

Fig. 19 -

Tensile Fracture of Mo-E2 (0.026 mm grain size)
at +25°C Showing Several Cleavage Facets (with
Cleavage steps) and Two Intergranular Facets (smooth).



Electron Fractograph

2000X

Fig. 20 -

Same Specimen as Fig. 19 - Showing Intergranular
Facets Which Apparently Contains Fine Precipitates.



Light Fractograph

1000X

Fig. 21 -

Tensile Fracture of Mo-E2 (0.026 mm grain size)
at -30°C Showing Several Cleavage Facets.



Electron Fractograph

2000X

Fig. 22 -

Same Specimen as Fig. 21 - Showing Cleavage
Steps and Smooth Intergranular Facets Which
Apparently Contains Fine Precipitates.

are generally smooth, and sometimes contain what appear to be fine precipitates (Figs. 20 and 22). The fractures of the medium grain Mo-E2 was found to be similar to the fine grain Mo-E2. Examples of the coarse grain Mo-E2 fractures in the range of +25 to -196°C are shown in Figs. 23 to 28. At +25°C, the fracture consists predominantly of high distorted cleavage facets (Fig. 23) although a few intergranular facets were observed (Fig. 24). Evidence of what is considered to be initiation of fracture at an intergranular facet at -196°C is shown in Fig. 28.

Table 10 gives a summary of the fractographic characteristics of the Mo-E2 tensile specimens broken in the range of +25° to 196°C. With decrease in test temperature, the relative amount of intergranular facets increases from <1 to about 2% for the fine grain size, from <1 to about 6% for the medium grain size, and from <1 to about 4% for the coarse grain size. The ratio of the average cleavage facet size to the grain size (corrected for total reduction in area prior to fracture) varies from 0.7 to 1.4 for the fine grain size, 0.6 to 1.1 for the medium grain size, and 0.4 to 0.5 for the coarse grain size. The corresponding ratio for the average intergranular facet size varies from 0.7 to 0.9 for both the fine and medium grain size, and 0.1 to 0.3 for the coarse grain size. Thus it appears that although the cleavage and intergranular facet sizes are approximately equal to the grain size for the fine and medium grain size Mo-E2, the cleavage and intergranular facet sizes are significantly smaller than the grain size for the coarse grain Mo-E2.

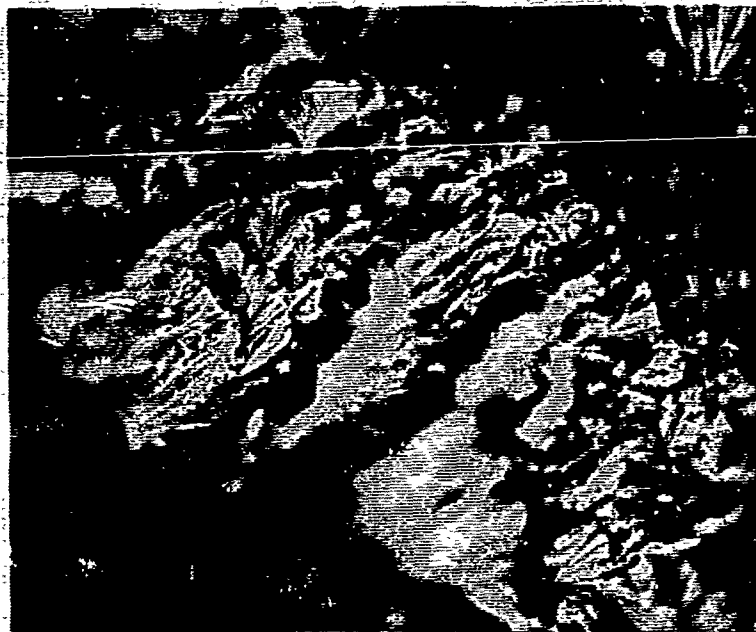
For the coarse grain size Mo-E2, the origin of fracture was traced to a particular intergranular facet from -196°C to T_d ; whereas for the fine and medium grain size Mo-E2, it was traced to a group of both intergranular and cleavage facets. However, above T_d the origin of fracture of the three grain sizes was traced to a group consisting of only cleavage facets. It is therefore concluded that the mode of fracture initiation in Mo-E2 is intergranular at T_d and below, and cleavage above T_d .

The geometrical location of fracture initiation with respect to the specimen cross section was also determined. It was found that fracture generally initiated in the interior of the specimen. The approximate locations can be expressed by the following coordinates: in the width (w) direction, from $w/8$ to $w/2$; and in the thickness (t) direction, from $t/4$ to $t/2$. There were only three cases in which fracture initiated at the surface, one at $w/3$ and the other two at $t/2$ and $t/3$.

2. Broken Mo-E3 Tensile Specimens

As shown in Figs. 29 and 30, the fractures of the broken fine grain Mo-E3 tensile specimens at -20 and -100°C consist of both cleavage and intergranular facets. Prestraining at +25°C followed by breaking at -100°C results in a greater amount of highly distorted cleavage facets (Figs. 31, 33 and 34) as compared to prestraining at -20°C and breaking at -100°C (Fig. 32). Predominantly intergranular fractures (Figs. 35 and 36) were produced by the simulated necking experiments carried out at -100°C.

The fractographic characteristics of the Mo-E3 tensile

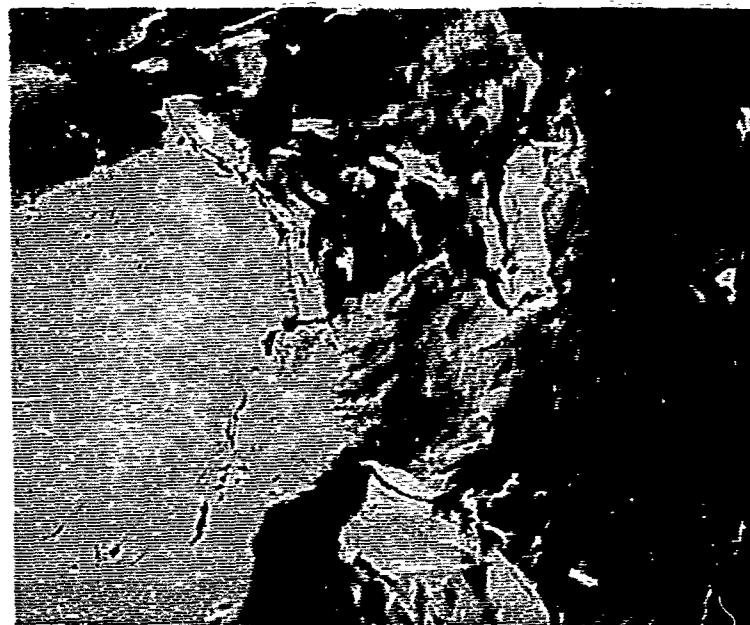


Light Fractograph

500X

Fig. 23 -

Tensile Fracture of Mo-E2 (0.174 mm grain size)
at +25°C Showing Highly Distorted Cleavage Facets.

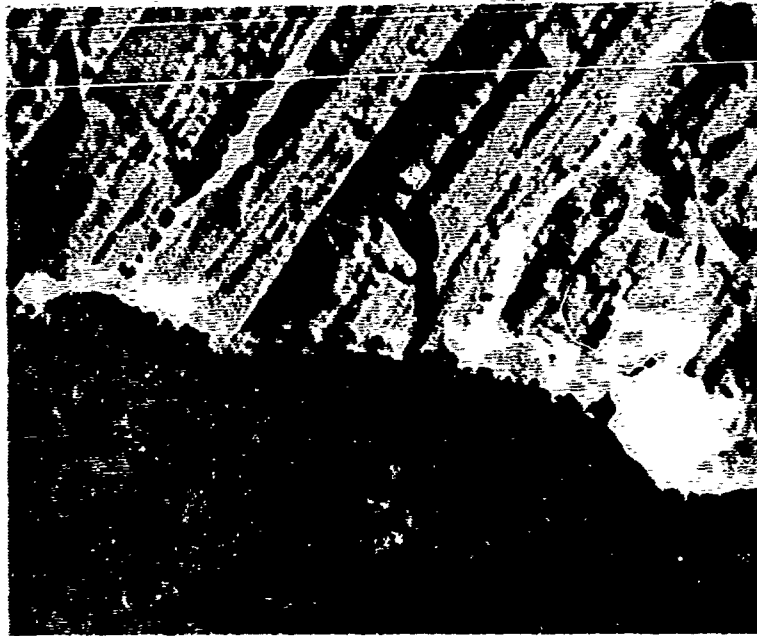


Electron Fractograph

2000X

Fig. 24 -

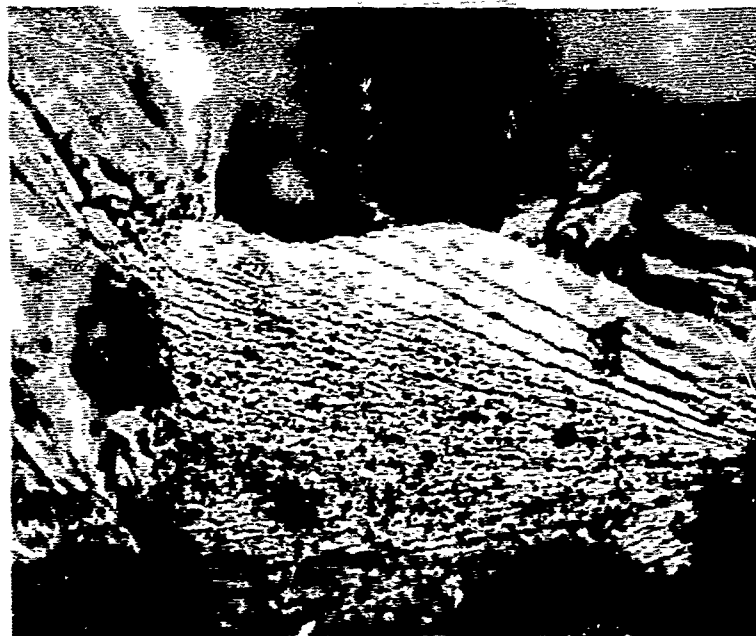
Tensile Fracture of Mo-E2 (0.174 mm grain size)
at +25°C Showing a Portion of a Smooth Intergranular
Facet (Left) Which Apparently Contains Fine Precipitates.



Electron Fractograph

2000X

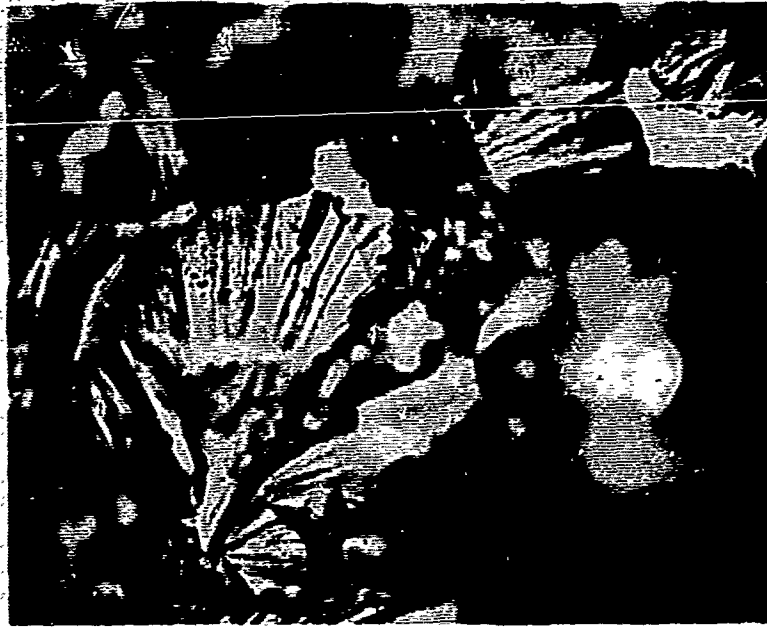
Fig. 25 - Tensile Fracture of Mo-E2 (0.174 mm grain size) at 0°C Showing a Cleavage Facet (upper) and an Intergranular Facet (lower).



Light Fractograph

500X

Fig. 26 - Tensile Fracture of Mo-E2 (0.174 mm grain size) at -40°C Showing a Cleavage Facet Containing Many Cleavage Steps.



Light Fractograph

500X

Fig. 27 - Tensile Fracture of Mo-E2 (0.174 mm grain size) at -100°C Showing One Intergranular Facet (Smooth) and Several Cleavage Facets.



Light Fractograph

650X

Fig. 28 - Tensile Fracture of Mo-E2 (0.174 mm grain size) at -196°C Showing One Intergranular Facet (Smooth) Surrounded by Several Cleavage Facets with "River" Markings Radiating from Intergranular Facet (Possible Fracture Origin).

Table 10

Fractographic Characteristics of Mo-E2 Broken Tensile Specimens

Grain Size mm	Test Temp., °C	Fracture Strain, ϵ F	Cleavage Facets		Intergranular Facets		Fracture Initiation		
			Relative Amount %	Average Size mm	Relative Amount %	Average Size mm	Mode	Location**	
0.018	+25	0.98	>99	0.016	<1	0.017	-	-	(w/2, t/4)
0.021	-30	0.78	>99	0.015	<1	0.019	-	cleavage	(w/4, t/3)
0.024	-70	0.05	99	0.033	1	0.022	-	cleavage	(w/8, t/2)
0.026	-100	0.03	97	0.026	3	0.019	-	intergran.	(0, t/3)
0.026	-196	0.02	98	0.035	2	0.022	-	intergran.	(w/3, t/2)
0.030	+25	1.00	>99	0.018	<1	0.026	-	-	(w/3, 0)
0.035	-25	0.55	98	0.035	2	0.024	-	cleavage	(w/3, t/2)
0.042	-75	0.06	93	0.046	7	0.035	-	intergran.	(w/2, t/4)
0.044	-150	0.03	91	0.033	9	0.032	-	intergran.	(w/3, t/2)
0.044	-196	0.01	95	0.034	5	0.038	-	intergran.	(w/3, t/2)
0.018	+25	1.00	>99	0.049	<1	-	-	-	-
0.020	0	0.97	98	0.042	2	0.025	-	cleavage	(w/3, t/3)
0.139	-25	0.46	98	0.067	2	0.035	-	-	-
0.160	-40	0.20	98	0.078	2	0.058	-	cleavage	(w/3, t/2)
0.167	-80	0.10	97	0.090	3	0.034	-	intergran.	(w/8, t/3)
0.168	-100	0.05	97	0.085	3	0.043	-	intergran.	(0, t/2)
0.170	-125	0.03	97	0.085	3	0.029	-	intergran.	(w/4, t/3)
0.174	-150	0.02	97	0.089	3	0.020	-	intergran.	-
0.174	-196	0.01	96	0.085	4	0.025	-	intergran.	(w/5, t/4)

* Corrected for reduction in area prior to fracture.

** Location of fracture initiation is given in terms of w and t coordinates which are the width and thickness specimen dimensions respectively.



Light Fractograph

1000X

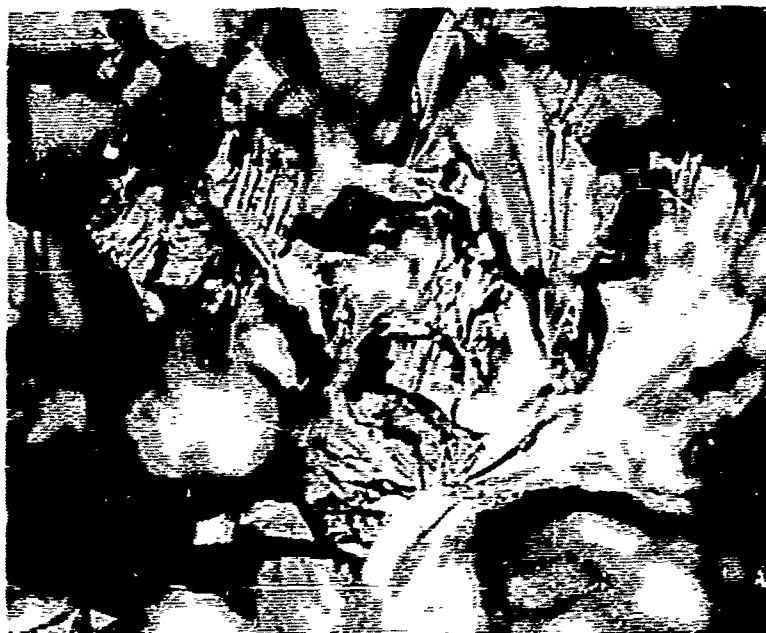
Fig. 29 - Tensile Fracture of Mo-E3 (0.023 mm grain size) at -20°C Showing Several Cleavage Facets and an Intergranular Facet (Smooth).



Light Fractograph

1000X

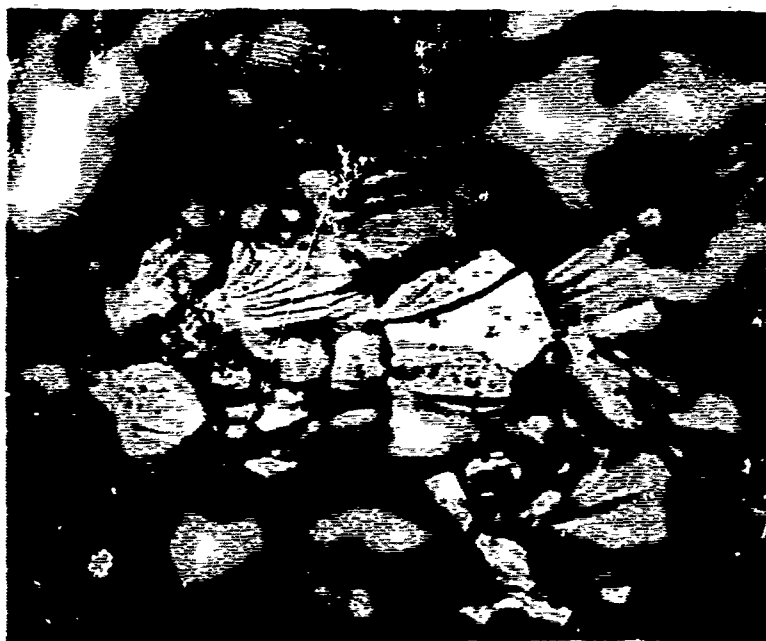
Fig. 30 - Tensile Fracture of Mo-E3 (0.023 mm grain size) at -100°C Showing Several Cleavage and Intergranular Facets.



Light Fractograph

750X

Fig. 31 - Tensile Fracture of Mo-E3 (0.023 mm grain size) Uniformly Prestrained ($\epsilon = 0.115$) at $+25^{\circ}\text{C}$ and Broken at -100°C Showing Several Highly Distorted Cleavage Facets.



Light Fractograph

750X

Fig. 32 - Tensile Fracture of Mo-E3 (0.023 mm grain size) Uniformly Prestrained ($\epsilon = 0.110$) at -20°C and Broken at -100°C Showing Several Cleavage Facets.



Light Fractograph

650X

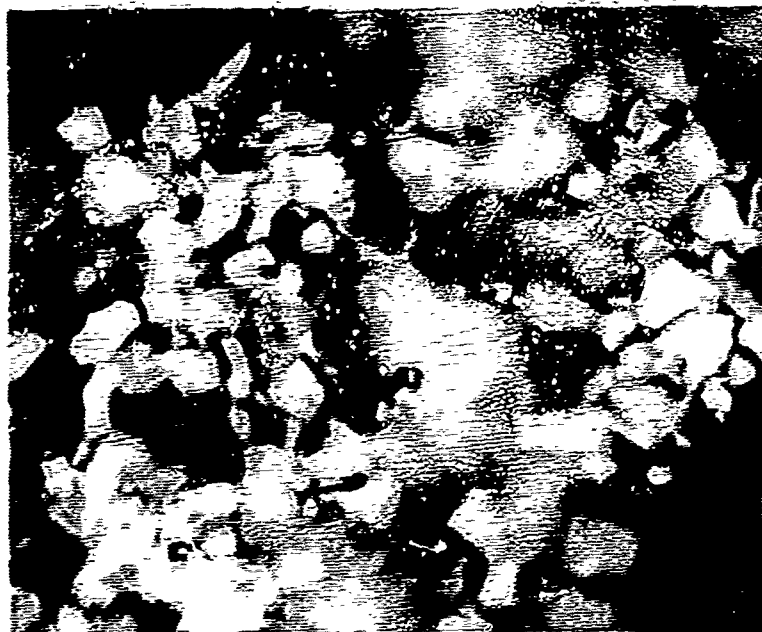
Fig. 33 - Tensile Fracture of Mo-E3 (0.023 mm grain size) Prestrained by Necking ($\epsilon = 0.28$) at +25°C and Broken at -100°C Showing Several Cleavage Facets.



Light Fractograph

650X

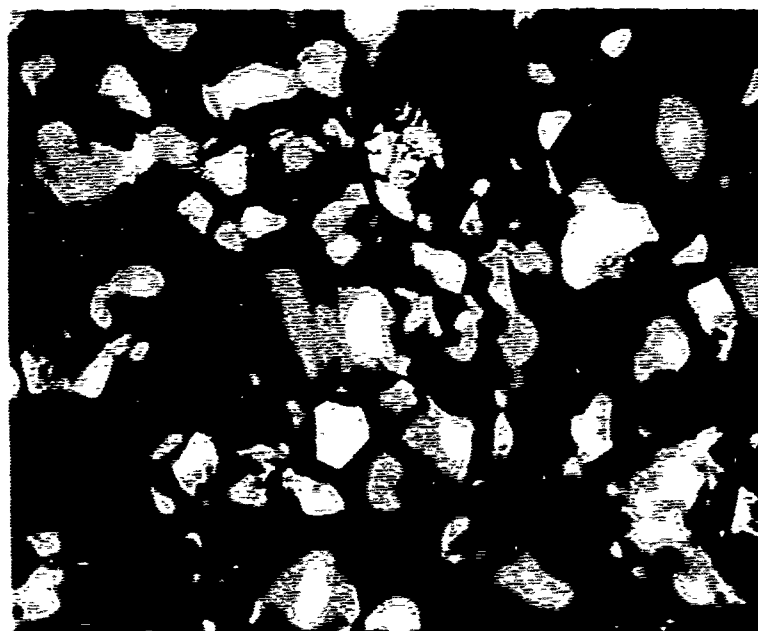
Fig. 34 - Tensile Fracture of Mo-E3 (0.023 mm grain size) Prestrained by Necking ($\epsilon = 0.64$) at +25°C and Broken at -100°C Showing One Intergranular Facet (lower right) and Several Cleavage Facets.



Light Fractograph

650X

Fig. 35 - Tensile Fracture of Mo-E3 (0.023 mm grain size) Prestrained by Necking ($\epsilon = 0.64$) at $+25^{\circ}\text{C}$, Recrystallized, and Broken at -100°C Showing Predominantly Intergranular Facets.



Light Fractograph

650X

Fig. 36 - Tensile Fracture of Mo-E3 (0.023 mm grain size) Having Neck Machined Corresponding to a Necking Prestrain of $\epsilon = 0.64$, Recrystallized and Broken at -100°C Showing Predominantly Intergranular Facets.

specimens in the range of +25 to -196°C are summarized in Table 11. For specimens that were not prestrained, the fractures are similar to the fine grain Mo-E2 material except that considerably more intergranular facets were found in the Mo-E3 specimens broken at -85 and at -196°C (10 and 40% respectively).

After subjecting the Mo-E3 to a uniform prestrain at either -20 or $+25^{\circ}\text{C}$ and breaking at -100°C or -196°C , the fracture consists of only 5-10% intergranular facets. This represents a considerable decrease in intergranular facets as compared to the non-prestrain results. This would seem to correlate with the higher fracture stress at -100°C as compared to that obtained without prestraining. However, a lower fracture stress was found at -196°C after prestraining.

After a necking prestrain at $+25^{\circ}\text{C}$ followed by breaking at -100°C , the amount of intergranular facets (10-20%) is also lower than that obtained without prestraining. However, simulated necking (as accomplished by forming a neck either by prestraining or machining followed by recrystallization) results in a large increase in the amount of intergranular facets (80-90%) after breaking at -100°C . This correlates with the lower fracture stress at -100°C due to simulated necking as compared to the results for either no prestrain or a necking prestrain.

Similar to the Mo-E2 fine grain size, both the intergranular and cleavage facet size in the Mo-E3 broken tensile specimens are approximately equal to the grain size as corrected for the total reduction in area prior to fracture. This holds for both the non-prestrained and prestrained specimens.

3. Broken Mo-E3 Precracked Charpy Slow Bend Specimens

Examples of fractures of Mo-E3 precracked Charpy slow bend specimens broken at -100°C are shown in Figs. 37 and 38, and the observed fractographic characteristics are summarized in Table 12. For tests carried out without prestrain, a greater amount of intergranular facets was found in the bend than in the tensile fracture at -100°C (50 vs 30%). After prestraining about 6% at $+25^{\circ}\text{C}$ either by tensile pulling or by rolling, the bend fracture at -100°C consists of considerably less intergranular facets than without prestraining (5 vs 50%), which is similar to the tensile results (Table 11).

4. Broken Mo-E4 Tensile Specimens

Examples of the fractures of broken Mo-E4 tensile specimens are shown in Figs. 39 and 40 and the fractographic characteristics are summarized in Table 13. A sharp change occurs from a predominantly cleavage fracture (<1% intergranular facets) at $+25^{\circ}\text{C}$ to a predominantly intergranular fracture (80% intergranular facets) at 0°C . A further increase in the amount of intergranular facets to >99% occurs at T_d (-35°C), and the intergranular fracture remains the same down to -196°C . It was found that fracture at

Table 11

Fractographic Characteristics of Mo-E3 Broken Tensile Specimens

Grain Size* mm	Test Temperature		Plastic Strain(ϵ) Prestrain Fracture ϵ_F	Cleavage Facets		Intergranular Facets		Fracture Initiation	
	Prestrain $^{\circ}\text{C}$	Fracture $^{\circ}\text{C}$		Relative Amount %	Average Size mm	Relative Amount %	Average Size mm	Mode	Location**
0.015	-	+25	none	99	0.016	1	0.015	cleavage	(w/2, t/4)
0.013	-	-20	none	99	0.015	1	0.015	cleavage	(w/3, 0)
0.023	-	-85	none	90	0.021	10	0.012	intergran.	(w/3, t/4)
0.023	-	-196	none	60	0.021	40	0.017	intergran.	(w/4, t/5)
0.022	+25	-100	0.077***	90	0.022	10	0.021	cleavage	(w/8, t/2)
0.021	+25	-100	0.115***	95	0.019	5	0.020	cleavage	(w/8, t/4)
0.022	-20	-100	0.055***	90	0.025	10	0.017	-	(w/3, 0)
0.021	-20	-100	0.115***	95	0.025	5	0.024	cleavage	(w/3, t/2)
0.019	+25	-100	0.280***	90	0.018	10	0.013	cleavage	(w/3, t/2)
0.014	+25	-100	0.640***	95	0.016	5	0.013	cleavage	(w/8, t/3)
0.023	-	-100	*****	10	0.022	90	0.020	intergran.	-
0.023	-	-100	*****	20	0.019	80	0.019	intergran.	-
0.021	+25	-196	0.113	95	0.026	5	0.021	cleavage	(w/2, t/3)
0.021	-20	-196	0.115	95	0.022	5	0.018	cleavage	(w/4, 0)

* Corrected for reduction in area prior to fracture.

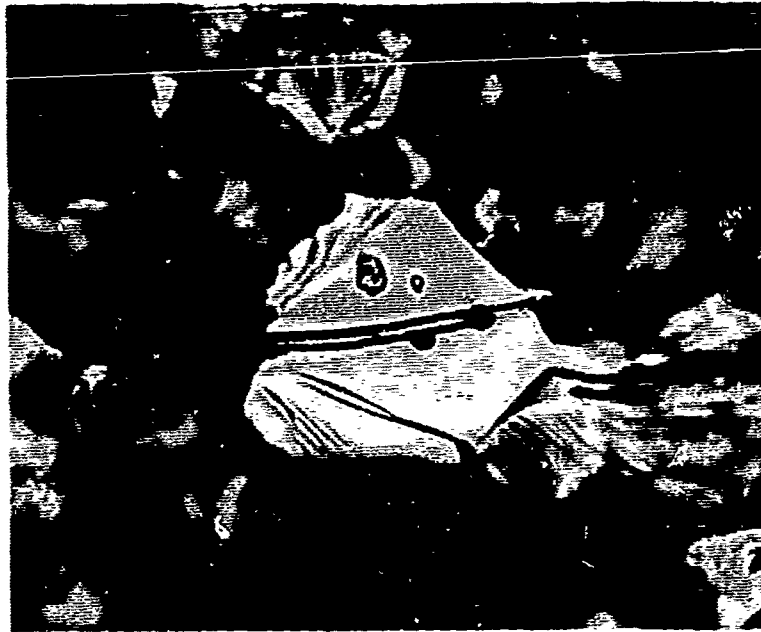
** Location of fracture initiation is given in terms of w and t coordinates, which are the width and thickness specimen dimensions respectively.

*** Uniform prestrain.

**** Necking prestrain.

***** Simulated necking by prestraining followed by recrystallization.

***** Simulated necking by machining followed by recrystallization.



Light Fractograph

1000X

Fig. 37 - Precracked Slow Bend Charpy Fracture of Mo-E3 (0.023 mm grain size) at -100°C Showing a Cleavage Facet Containing a Few Cleavage Steps.



Light Fractograph

1000X

Fig. 38 - Precracked Slow Bend Charpy Fracture of Mo-E3 (0.023 mm grain size) Prestrained (6% by rolling) at $+25^{\circ}\text{C}$ and Broken at -100°C Showing Cleavage Facets Containing Many Cleavage Steps.

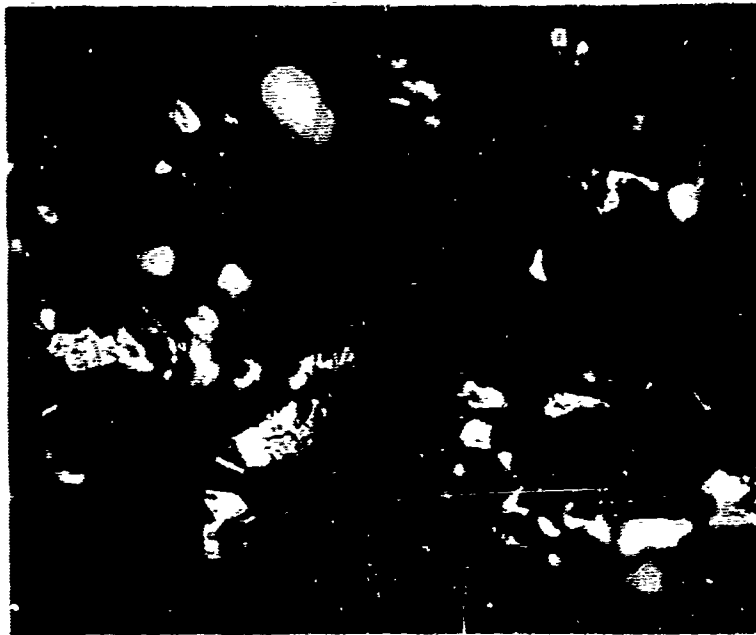
Table 12
Fractographic Characteristics of M.-F. Broken Pre-cracked Charpy Slow Bend Test Specimens

Grain Size* mm	Test Temperature		Amount of Prestrain ϵ_{pr}	Cleavage Facets		Intergran. Facets		Fracture Initiation	
	Prestrain $^{\circ}\text{C}$	Fracture $^{\circ}\text{C}$		Relative Average Amount %	Average Size mm	Relative Average Amount %	Average Size mm	Mode	Location
0.023	-	-100	none	50	0.021	50	0.017	-	at precrack
0.022	+25	-100	0.06**	95	0.018	5	0.013	cleavage	at precrack
0.022	+25	-100	0.06***	95	0.013	5	0.015	cleavage	at precrack

* Corrected for reduction in area prior to fracture.

** By tensile pulling.

*** By rolling.

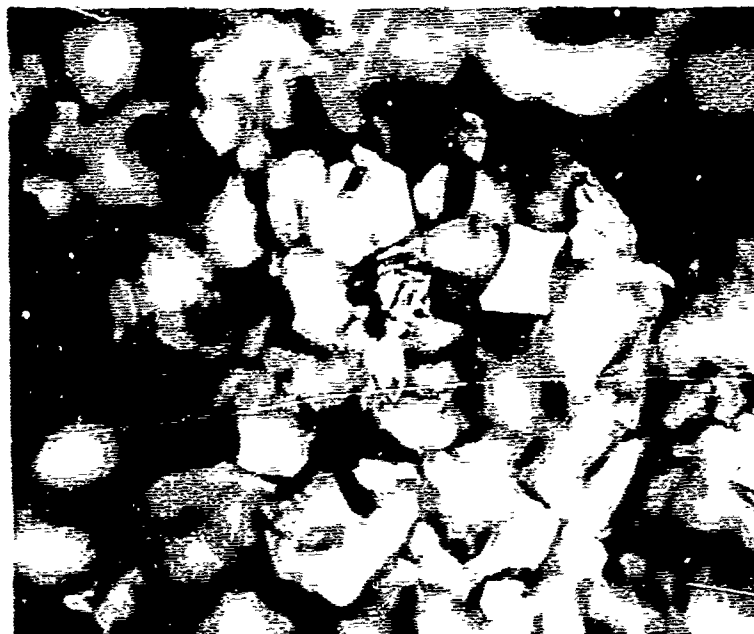


Light Fractograph

500X

Fig. 39 -

Tensile Fracture of Mo-E4 (0.020 mm grain size)
at +25°C Showing Several Cleavage Facets.



Light Fractograph

500X

Fig. 40 -

Tensile Fracture of Mo-E4 (0.020 mm grain size)
at -35°C Showing Two Cleavage Facets and Many
Intergranular Facets.

Table 13

Fractographic Characteristic of Mo-E4 Broken Tensile Specimens

Grain Size* mm	Test Temperature		Plastic Strain		Cleavage Facets		Intergran. Facets		Fracture Initiation	
	Prestrain °C	Fracture °C	Prestrain	Fracture	Relative Average Amount %	Average Size mm	Relative Average Amount %	Average Size mm	Mode	Location**
0.014	-	+25	-	0.67	>99	0.021	<1	0.020	cleavage	(w/8, t/3)
0.017	-	0	-	0.35	20	0.019	80	0.020	intergran.	-
0.020	-	-35	-	0.01	<1	0.020	>99	0.018	intergran.	-
0.020	-	-100	-	0	<1	0.020	>99	0.023	intergran.	-
0.020	-	-196	-	0	<1	0.016	>99	0.020	intergran.	-
0.017	+25	-100	0.28***	0	50	0.018	50	0.015	-	-
0.017	+25	-196	0.25***	0	25	0.019	75	0.014	-	-

* Corrected for reduction in area prior to fracture.

** Location of fracture initiation is given in terms of w and t coordinates which are the final width and the final thickness of the specimen dimensions respectively.

*** Subjected to uniform prestrain at +25° C.

+25°C initiates by a cleavage mode and by an intergranular mode at 0°C. No definite evidence was obtained with respect to the location of fracture initiation at -35 to -196°C; however, it is presumed that the fracture initiation mode is intergranular since only a few cleavage facets were found present. Prestraining at +25°C and breaking at -100°C and at -196°C was found to increase the amount of cleavage facets (50 and 25% respectively), which correlates with the increases in fracture stress obtained by prestraining. Similar to the fine grain Mo-E2 and Mo-E3 materials, both the cleavage and intergranular facet sizes are approximately equal to the grain size as corrected for the reduction in area prior to fracture.

5. Other Observations

Examinations were carried out for the occurrence of microcracks and twins in the vicinity of the fractures of the Mo-E2, Mo-E3, and Mo-E4 materials. No evidence of isolated microcracks was found, although branching of secondary cracks from the main fractures was observed. Likewise, no definite evidence of twinning could be found.

E. Theoretical Considerations

1. Relation of Yield Stress to Fracture Stress

As illustrated schematically in Fig. 41, the brittleness transition temperature (T_b) corresponds to the intersection of curves representing the variation with temperature of the observed fracture stress (σ_F) and a yield stress parameter (σ_y). For each of the molybdenum strip materials studied, it was found that the values of proportional limit (σ_{pl}), lower yield stress (σ_{lys}) or upper yield stress (σ_{uys}) corresponding to a given test temperature are within about 15% of each other. Considering that the probable accuracy of measurement is about $\pm 10\%$ for these three stress parameters, it does not seem to matter whether σ_y represents σ_{pl} , σ_{lys} or σ_{uys} . In Figs. 42 to 46, the locations of T_b for Mo-E2 (3 grain sizes), Mo-E3, and Mo-E4 are shown by the intersections of a band that represents the accuracy of σ_F and a σ_y band that represents the combined variation of σ_{pl} , σ_{uys} , and σ_{lys} .

2. Relation of Necking Stress at Fracture Stress

Also illustrated schematically in Fig. 41 is the intersection of the observed fracture stress (σ_F) and the necking stress (σ_n), where the latter is the true stress corresponding to maximum load. This intersection is shown to occur at the minimum in the σ_F vs. temperature plot. The temperature at which the minimum occurs has been previously defined as the tensile ductility transition temperature (T_d). It was hypothesized by Lement (3) that σ_n intersects σ_F at T_d because below T_d the elongation at fracture was found to be uniform whereas above T_d necking occurs prior to fracture. This situation is schematically indicated in Fig. 41 by the intersection of the fracture strain (ϵ_F) and the maximum uniform strain (ϵ_u) curves at T_d .

STRESS (σ)

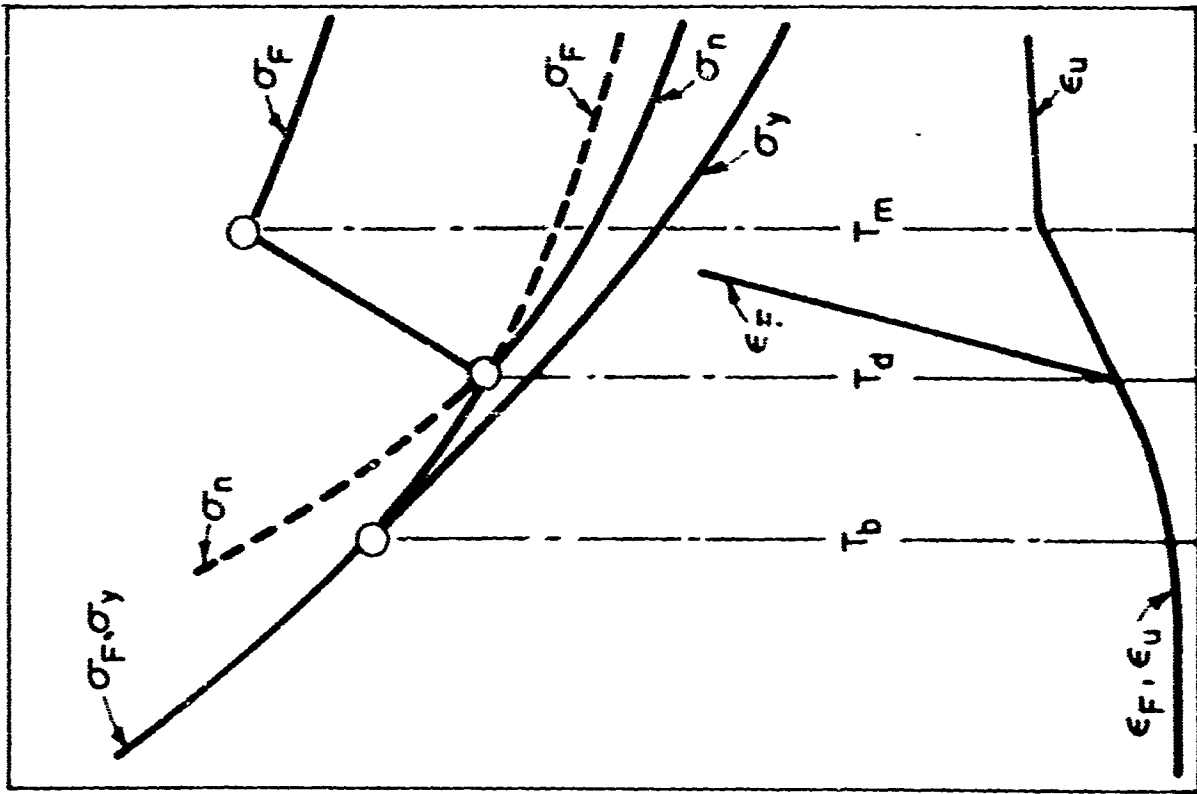
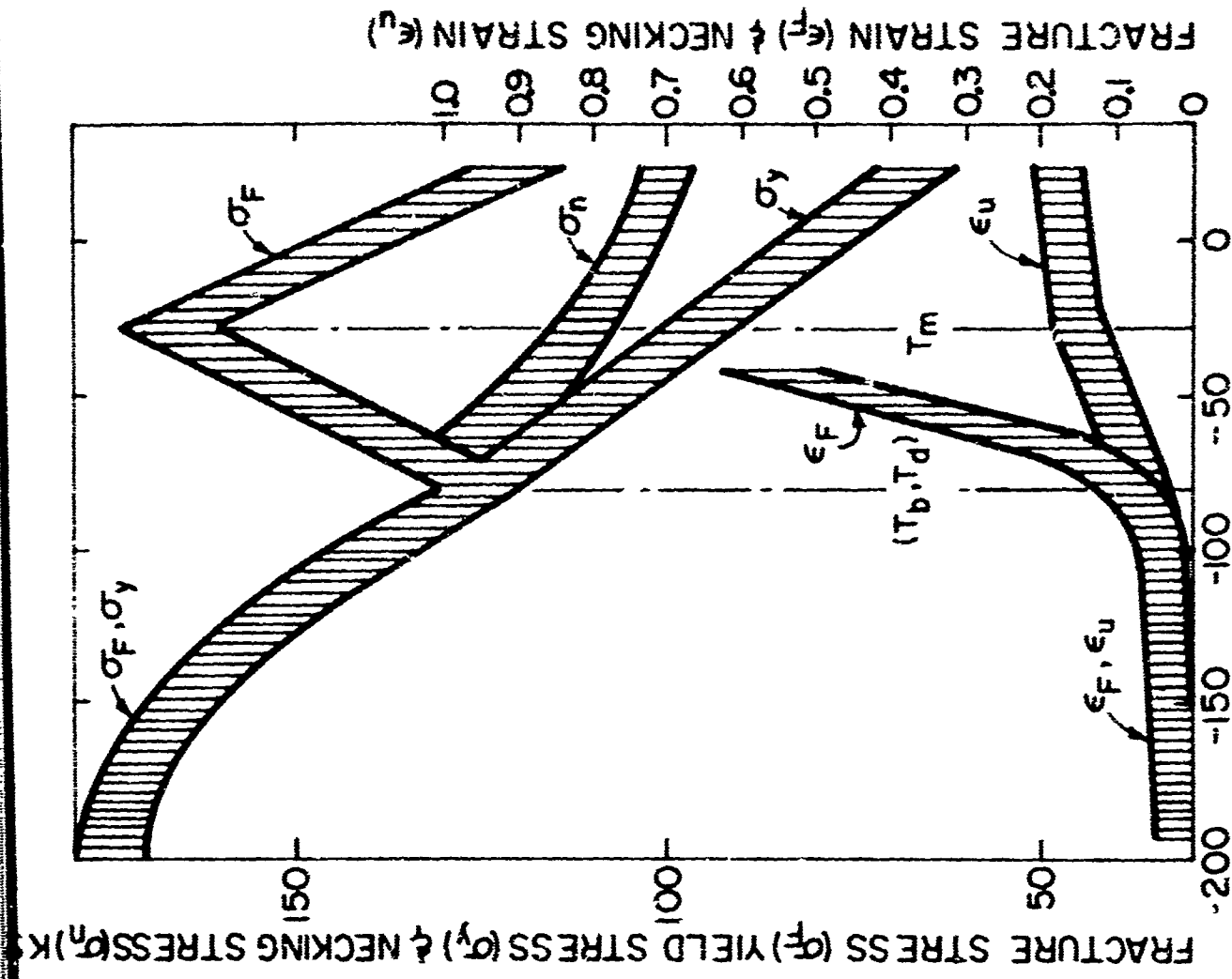


Fig. 41 - Schematic Plots of Variation of Fracture Stress (σ_F), Yield Stress (σ_Y), Necking Stress (σ_n), Fracture Strain (ϵ_F) and Max. Uniform Strain (ϵ_U) with Temperature.

TEST TEMPERATURE (T) \rightarrow



TEST TEMPERATURE (°C)

Fig. 42 - Plot of Stress and Strain Parameter Bands vs. Temperature for Mo-E2 Bands ($l = 0.026$ mm).

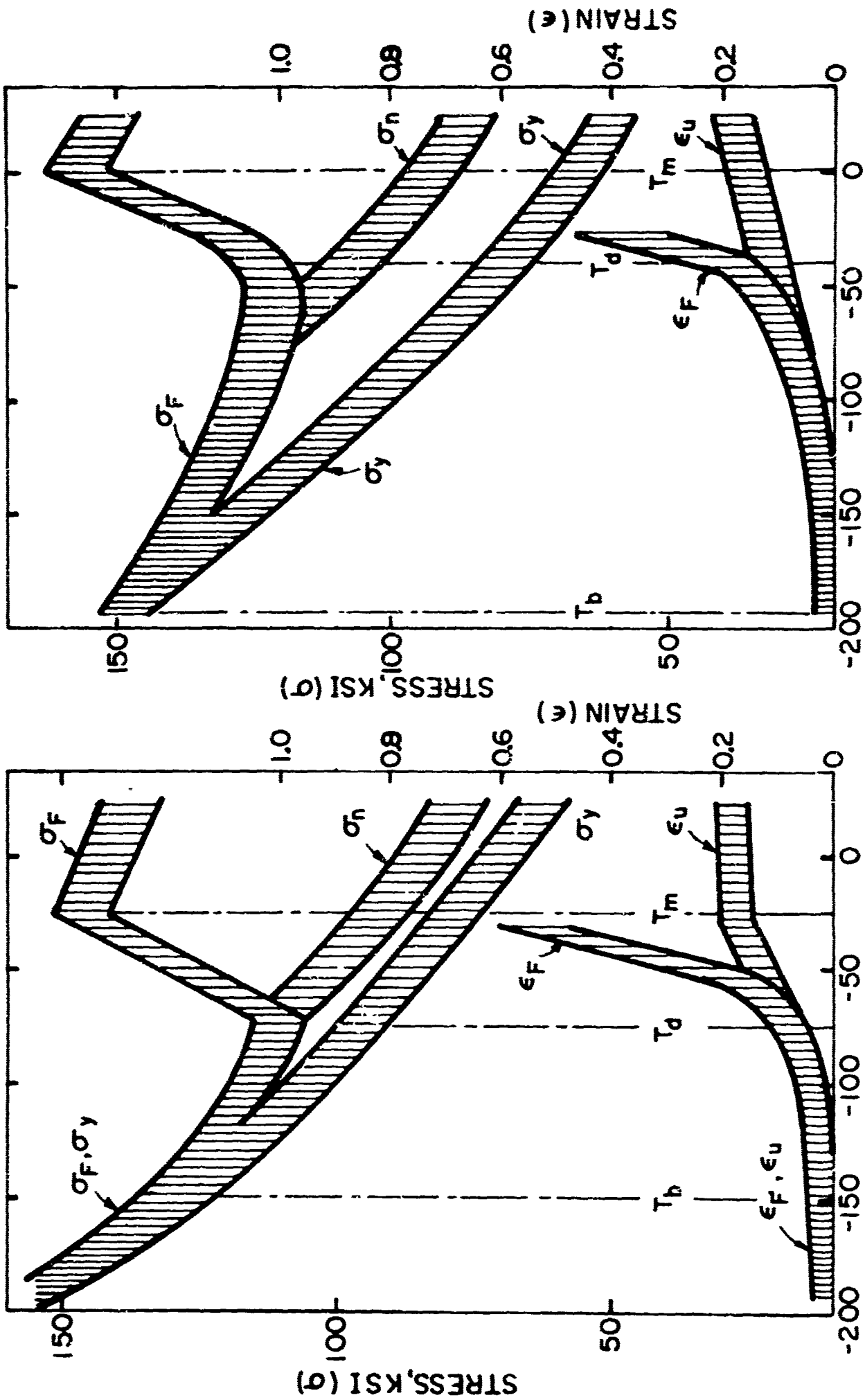


Fig. 43 - Plot of Stress and Strain Parameter Bands vs. Test Temperature for Mo-E2 ($l = 0.044$ mm) .

Fig. 44 - Plot of Stress and Strain Parameter Bands vs. Test Temperature for Mo-E2 ($l = 0.174$ mm) .

Bands vs. Test Temperature for
Mo-E2 ($l = 0.014$ mm).

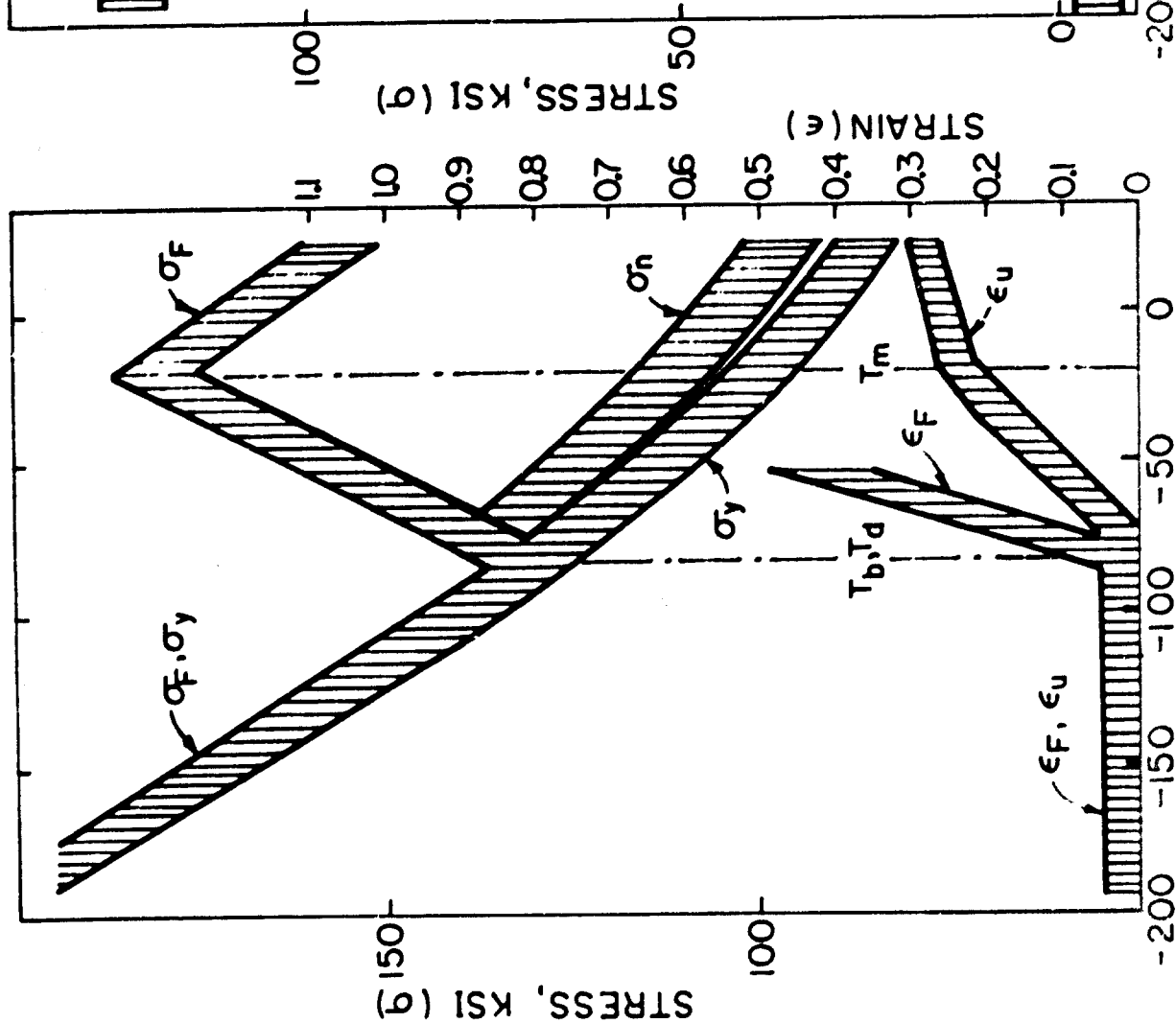


Fig. 45 - Plot of Stress and Strain Parameter Bands vs. Test Temperature for Mo-E3 ($l = 0.023$ mm).

Mo-E2 ($l = 0.174$ mm).

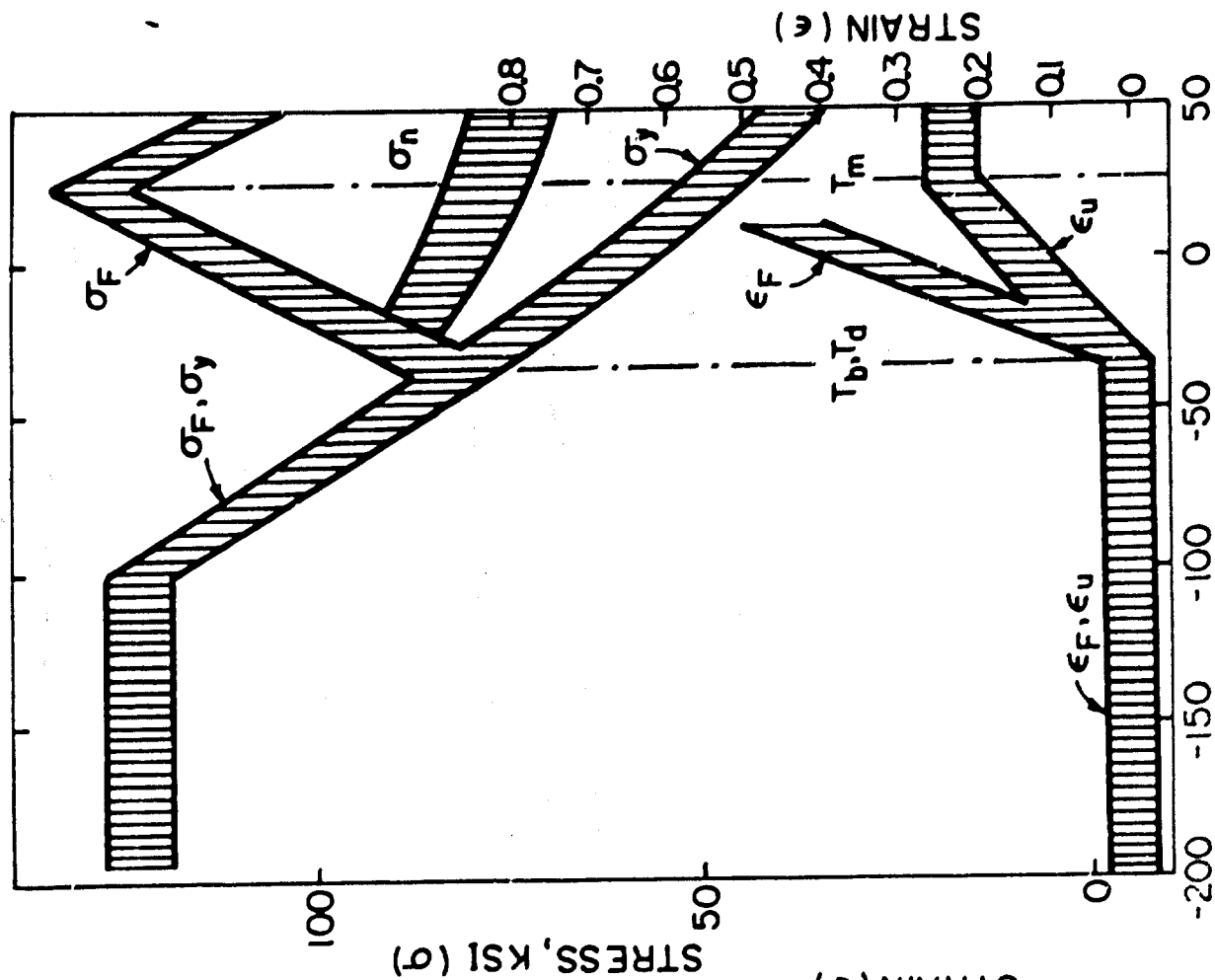


Fig. 46 - Plot of Stress and Strain Parameter Bands vs. Test Temperature for Mo-E4 ($l = 0.020$ mm).

Bands representing the probably accuracy of σ_F , σ_n , ϵ_F , and ϵ_u for the various molybdenum strip materials are shown in Figs. 42 to 46 as a function of test temperature. For the fine grain Mo-E2, Mo-E3 and Mo-E4 materials, T_b and T_d were found to approximately coincide. This is indicated by the intersection of the σ_y , σ_n , and σ_F bands at T_d Figs. 42, 45, and 46. On the other hand, T_b falls below T_d for the intermediate and coarse grain Mo-E2 materials. This is indicated by the fact that the intersection of the σ_y and σ_F bands occurs below that of the σ_n and σ_F bands Figs. 43 and 44. For all the materials studied, the ϵ_u and ϵ_F bands intersect at T_d Figs. 42 to 46.

According to Ault (11), who investigated the tensile properties of a fine grain and relatively impure molybdenum strip material, σ_{ys} intersects σ_F at the minimum in the σ_F vs. temperature plot (which is defined here as T_d). Based on the present study, this should occur if T_d and T_b are equal as was found for the fine grain molybdenum strip materials. However, the more general condition for T_d is the intersection of σ_F and σ_n as indicated by the results for the intermediate and coarse grain strip materials Figs 42 and 43. For these grain sizes, T_d occurs above T_b and σ_n intersects σ_F at T_d .

3. Locking Parameters

3.1 Yield Locking Parameter

According to Cottrell (5), $\sigma_F = \sigma_y$ at T_b and σ_F is inversely proportional to the yield locking parameter (k_y) at T_b . The variation of k_y with test temperature for Mo-E2 as determined by the Petch grain size method was shown in Fig. 5. An alternative method of determining k_y is by the Owen (12) extrapolation method. This first involves extrapolating the flow stress curve (beyond the Lüders strain) back to the elastic line to determine the frictional stress (σ_i). Based on the power law, σ_i at the intersection of the plastic and elastic curves is given by

$$\sigma_i = K \left(\frac{\sigma_i}{E} \right)^n \quad (20)$$

From the Petch relation,

$$k_y = \frac{\sigma_y - \sigma_i}{d - 1/2} \quad (21)$$

Using Eq. (20) and (21), calculations were made of k_y and σ_i at test temperatures of +25° C, T_d , and T_b for all of the molybdenum strip materials and the results are given in Table 14. The T_b values of k_y and σ_i for the intermediate and coarse grain Mo-E2 given in this table are based on rough extrapolations of the K and n curves down to -150 and -196° C

Table 14

Yield Locking Parameter (k_y) and Frictional Stress (σ_i) for Mo-E2, Mo-E3, and Mo-E4 Strip

Table 14

Yield Locking Parameter (k_y) and Frictional Stress (σ_j) for Mo-E2, Mo-E3, and Mo-E4 Strip

Material and Grain Size	Test Temp. °C	σ_{lys} dynes/cm ²	Strain Hardening Coefficient (K)	Strain Hardening Exponent (n)	By Petch		By Owen	
					Grain Size Method (σ_j) dynes/cm ²	(k_y) dynes/cm ^{3/2}	Extrapolation Method (σ_j) dynes/cm ²	(k_y) dynes/cm ^{3/2}
Mo-E2 (0.026mm)	+25	4.6x10 ⁹	7.0x10 ⁹	0.065	3.9x10 ⁷	4.5x10 ⁷	4.3x10 ⁷	1.8x10 ⁷
	-80(T _b)	8.8x10 ⁹	14.0x10 ⁹	0.115	5.3x10 ⁷	16x10 ⁷	6.8x10 ⁷	10x10 ⁷
Mo-E2 (0.044mm)	+25	4.5x10 ⁹	6.1x10 ⁹	0.090	3.9x10 ⁷	4.5x10 ⁷	3.3x10 ⁷	7.9x10 ⁷
	-75(T _d)	7.0x10 ⁹	12.6x10 ⁹	0.110	5.2x10 ⁷	15x10 ⁷	6.5x10 ⁷	3.3x10 ⁷
	-150(T _b)	9.3x10 ⁹	18.2x10 ⁹	0.160	6.4x10 ⁷	24x10 ⁷	6.7x10 ⁷	17x10 ⁷
Mo-E2 (0.174mm)	+25	4.3x10 ⁹	6.6x10 ⁹	0.073	3.9x10 ⁷	4.5x10 ⁷	3.9x10 ⁷	4.1x10 ⁷
	-40(T _d)	5.7x10 ⁹	10.0x10 ⁹	0.087	4.6x10 ⁷	12x10 ⁷	5.4x10 ⁷	4.1x10 ⁷
	-196(T _b)	10.7x10 ⁹	14.1x10 ⁹	0.22	7.1x10 ⁷	29x10 ⁷	5.6x10 ⁷	68x10 ⁷
Mo-E3 (0.023mm)	+25	5.7x10 ⁹	7.1x10 ⁹	0.048	-	2.2x10 ^{7*}	5.3x10 ⁷	1.1x10 ⁷
	-80(T _b)	9.3x10 ⁹	14.8x10 ⁹	0.090	-	7.0x10 ^{7*}	8.5x10 ⁷	3.5x10 ⁷
Mo-E4 (0.020mm)	+25	3.4x10 ⁹	10.7x10 ⁹	0.276	-	19x10 ^{7*}	1.3x10 ⁷	9.4x10 ⁷
	-35(T _b)	5.9x10 ⁹	11.9x10 ⁹	0.185	-	22x10 ^{7*}	3.4x10 ⁷	11x10 ⁷

* Approximate grain size k_y value.

respectively. Corresponding values are given in Table 14 for k_y and σ_i as determined by the Petch grain size method for the Mo-E2 materials (Figs. 4 and 5), which also required extrapolation down to -196°C . For the Mo-E2 materials, relatively good agreement (within 30%) was found between the σ_i values as determined by the Owen extrapolation and the Petch grain size methods. On the other hand, there are much larger discrepancies between the k_y values as obtained by these two methods. Furthermore, the extrapolation k_y values exhibit anomalous variations with test temperature.

Since the Petch grain size k_y values appear to be more reasonable, it was decided to use these values in subsequent calculations of the effective surface energy for crack initiation. However, this raised the difficulty that only the Owen extrapolation k_y values were determined for the Mo-E3 and Mo-E4 materials. As an approximation, it was decided to use the ratio of the grain size k_y to the extrapolation k_y for the fine grain Mo-E2 in order to convert the extrapolation k_y values for the fine grain Mo-E3 and Mo-E4 materials to grain size k_y values. For the fine grain Mo-E3, this ratio is about 2; and values of grain size k_y for Mo-E3 and Mo-E4 as converted on this basis are given in Table 14.

3.2 Flow Locking Parameter

The flow locking parameter (k_f) was determined as a function of plastic strain (ϵ_p) and test temperature for Mo-E2. This involved determination of the variation with grain size of the uniform flow stress (σ_{fs}) as determined by the power law:

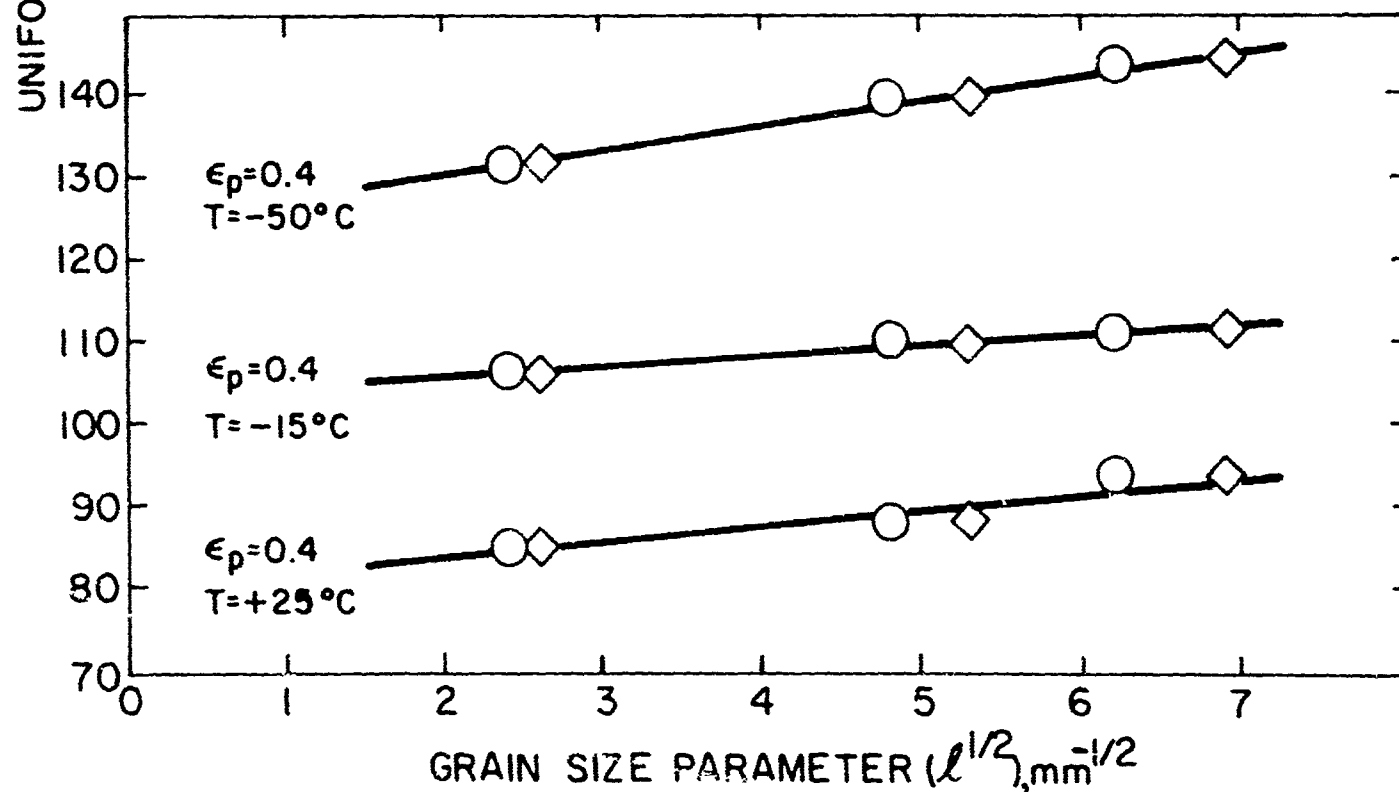
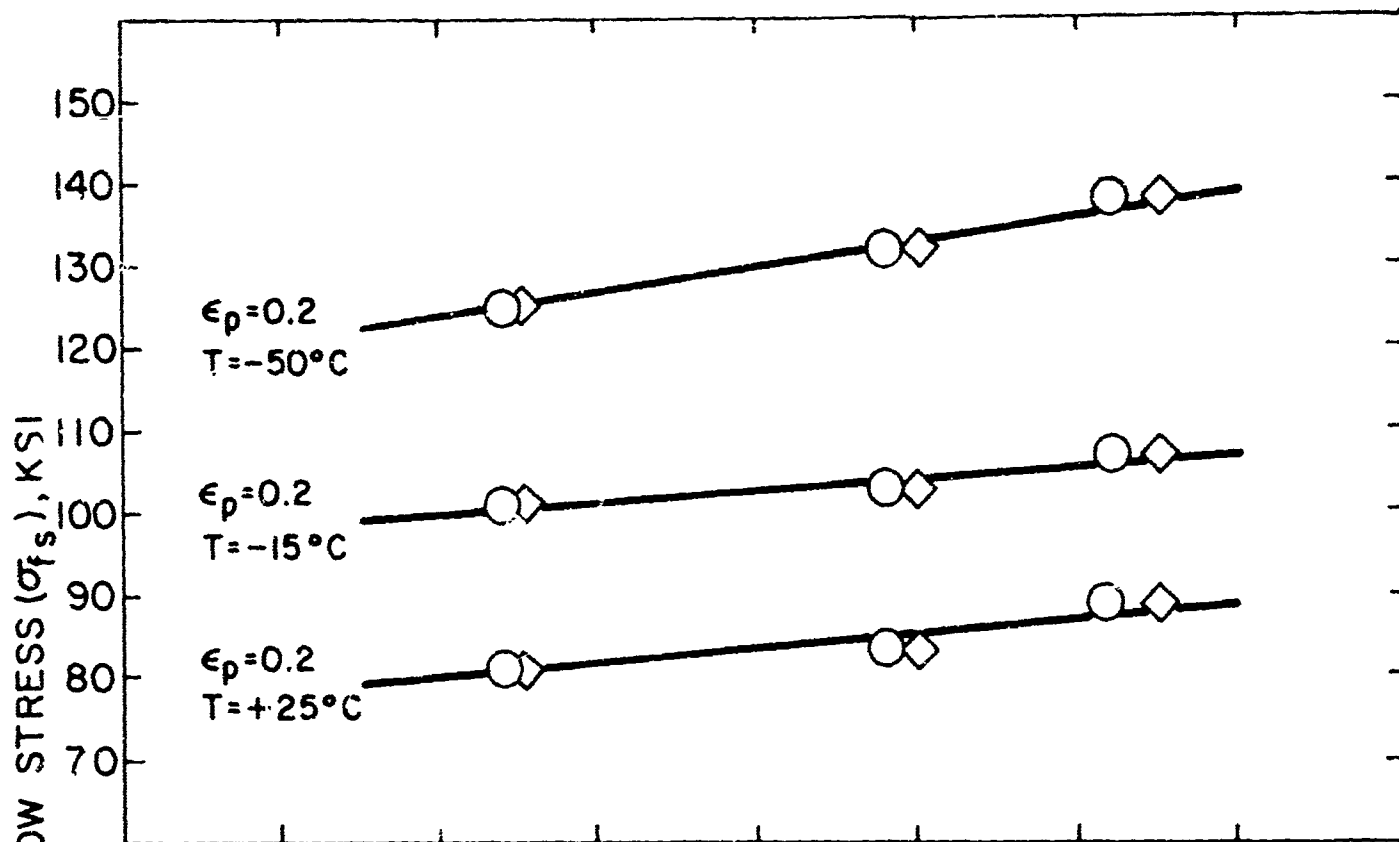
$$\sigma_{fs} = K (\epsilon_p)^n \quad (22)$$

In Figs. 47 and 48, the values of σ_{fs} corresponding to ϵ_p values of 0.2 to 1.0 are plotted as a function of the grain size parameter ($l^{-1/2}$) for test temperatures of -50 , -15 , and $+25^\circ\text{C}$. The slopes of these σ_{fs} vs $l^{-1/2}$ plots give k_f as defined by the following relation:

$$k_f = \frac{\sigma_{fs} - \sigma_o}{l^{-1/2}} \quad (23)$$

Where σ_o is a constant for a given value of ϵ_p and temperature. As is apparent from Figs 47 and 48, the value of k_f for a given strain and temperature is not significantly affected by plotting σ_{fs} against the final rather than the initial grain size.

Values of k_f based on Fig. 47 are given in Table 15. For each ϵ_p , k_f is approximately equal to k_y at $+25^\circ\text{C}$ and with decrease in test temperature goes through a minimum at about -15°C . The ratio of k_f to k_y was found to decrease from about 1.0 to about 0.4 in the range of $+25$ to -15°C , and from -15 to -50°C there is little change. These results differ from the work of Armstrong (13), who reported that k_f/k_y equals about 0.3 for molybdenum at room temperature.



(○ initial grain size)

(◇ final grain size)

Fig. 47 - Plots of Uniform Flow Stress (σ_{fs}) vs. Grain Size Parameter for Recrystallized Mo-E2 Strip at Plastic Strains (ϵ_p) of 0.2 and 0.4.

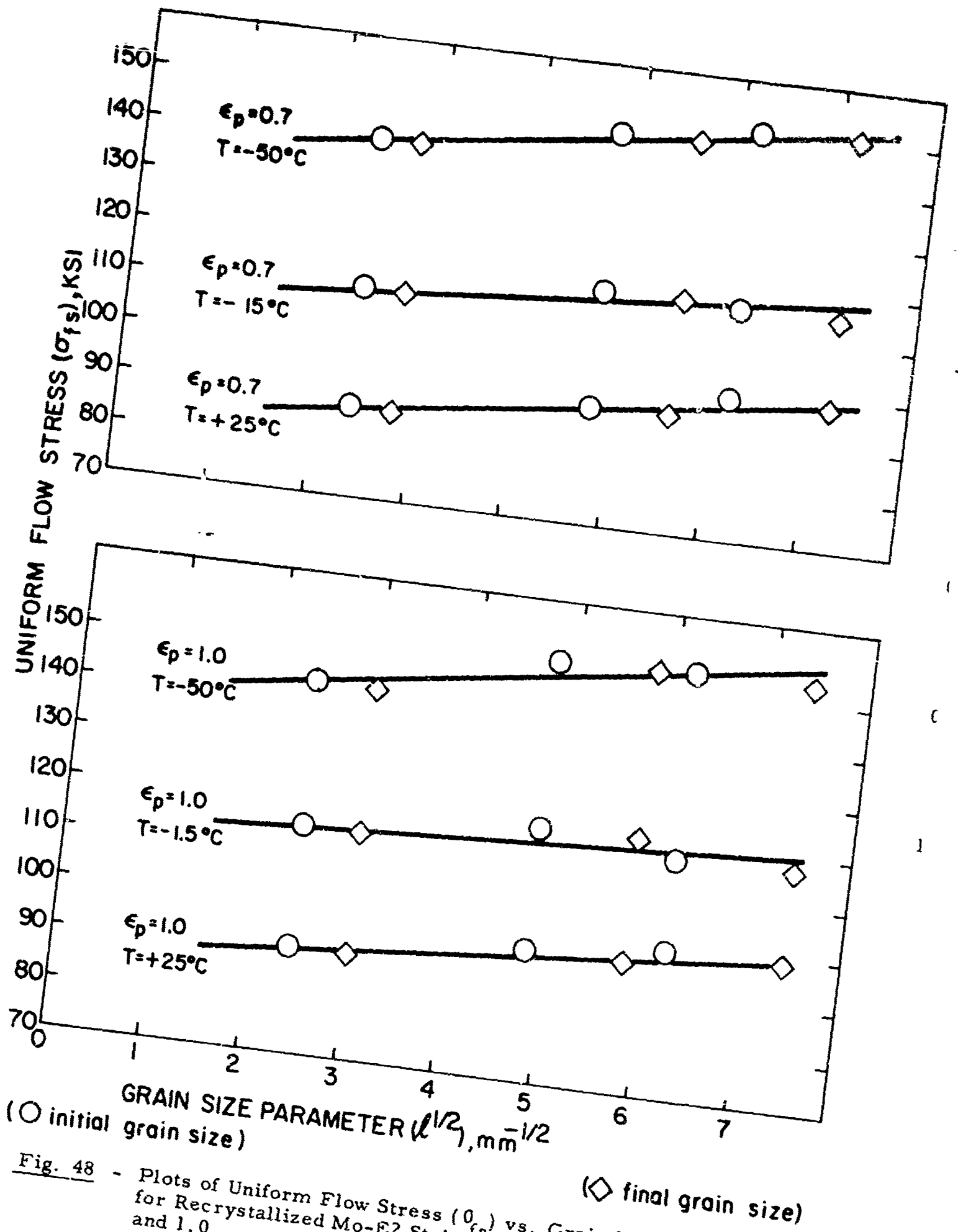


Fig. 48 - Plots of Uniform Flow Stress (σ_{fs}) vs. Grain Size Parameter for Recrystallized Mo-E2 Strip at Plastic Strains (ϵ_p) of 0.7 and 1.0.

Table 15

Flow Locking Parameter (k_f) for Mo-E2 Strip

<u>Plastic Strain (ϵ_p)</u>	<u>Test Temp. (T) °C</u>	<u>Flow Locking Parameter (k_f) dynes/cm^{3/2}</u>	<u>Yield Locking Parameter (k_y) dynes/cm^{3/2}</u>	<u>Ratio k_f/k_y</u>
0.2	+25	6.0×10^7	4.5×10^7	1.3
	-15	3.5×10^7	8.0×10^7	0.4
	-50	4.0×10^7	13×10^7	0.3
0.4	+25	4.5×10^7	4.5×10^7	1.0
	-15	3.0×10^7	8.0×10^7	0.4
	-50	6.5×10^7	13×10^7	0.5
0.7	+25	5.0×10^7	4.5×10^7	1.1
	-15	3.0×10^7	8.0×10^7	0.4
	-50	5.5×10^7	13×10^7	0.4
1.0	+25	4.0×10^7	4.5×10^7	0.9
	-15	2.5×10^7	8.0×10^7	0.3
	-50	6.6×10^7	13×10^7	0.5

Values of k_f were not determined for the Mo-E3 and Mo-E4 materials because these were recrystallized to a fine grain size only. However, k_f for these materials can be approximated by using the k_f/k_y ratio determined for Mo-E2 and the k_y values for Mo-E3 and Mo-E4 given in Table 14 (converted from extrapolation to grain size k_y values). Approximate values of k_f for Mo-E3 and Mo-E4 as determined on this basis are given in Table 16. These values also show a minimum at -15°C .

4. Calculation of Effective Surface Energy for Crack Initiation

The Cottrell (5) fracture relation for crack initiation at the brittleness-transition temperature (T_b) is as follows:

$$\gamma_i' = \frac{k_y \ell^{1/2} \sigma_F}{8G} \quad (24)$$

where γ_i' = effective surface energy for crack initiation

k_y = yield locking parameter based on normal stress and full grain diameter

G = shear modulus and is equal to $\frac{E}{2(1+\nu)}$ where ν is Poisson's ratio (0.3)

ℓ = full grain diameter

The effective surface energy for crack initiation (γ_i') in Mo-E2, Mo-E3 and Mo-E4 at the brittleness transition temperature (T_b) was calculated using a) values of σ_F at T_b given in Figs. 1, 2, 3, 11 and 17; b) values of k_y at T_b based on the Petch grain size method (Table 14); and c) values of G at T_b as determined from the variation of the elastic modulus (E) with temperature for molybdenum (Fig. 49), i. e. $G = 0.38 E$. Calculations were also made of γ_i' at temperatures above T_b based on a modification of Eq. (24) which involves substituting the flow locking parameter (k_f) for k_y in order to take into account the relatively large plastic strains that occur prior to fracture. Values of k_f were obtained from Tables 15 and 16, and the results of γ_i' calculations are given in Table 17.

As shown in Table 17, the values of γ_i' at T_b (based on k_y) are in the range of 0.7×10^4 to 3.5×10^4 ergs/cm². With increase in temperature, an initial decrease in γ_i' (based on k_f) occurs which is a mathematical consequence of k_f being lower than k_y . Since a lower value of γ_i' would be expected if the initiation mode is intergranular as compared to cleavage, this casts doubt on the validity of Eq. (24) based on k_y . Above T_d , γ_i' for Mo-E2 and Mo-E3 remains essentially constant up to at least $+25^\circ\text{C}$ and the mode of crack initiation is cleavage over this range. On the other hand, there is about a 75% increase in γ_i' for Mo-E4 between 0°C and $+25^\circ\text{C}$ where the initiation mode changes from intergranular to cleavage. It therefore appears that the high oxygen content of Mo-E4 results in different γ_i' as well as fracture initiation characteristics than the relatively low oxygen content materials (Mo-E2 and Mo-E3).

Table 16

Approximate Values of Flow Locking Parameter (k_f) for Mo-E3 and Mo-E4 Strip

<u>Material</u>	<u>Plastic Strain (ϵ_p)</u>	<u>Test Temp. (T)</u> °C	<u>Approx. k_f/k_y *</u>	<u>Approx. k_y **</u> dynes/cm ^{3/2}	<u>Approx. k_f</u> dynes/cm ^{3/2}
Mo-E3	0.2-1.0	+25	1.0	2.2×10^7	2.2×10^7
		-15	0.4	3.9×10^7	1.6×10^7
		-50	0.4	5.3×10^7	2.1×10^7
Mo-E4	0.2-1.0	+25	1.0	19×10^7	19×10^7
		-15	0.4	21×10^7	8.4×10^7
		-50	0.4	23×10^7	9.0×10^7

* Assumed to be the same as for Mo-E2 strip given in Table 15.

** Approximate grain size k_y values given in Table 14 and linear extrapolations.

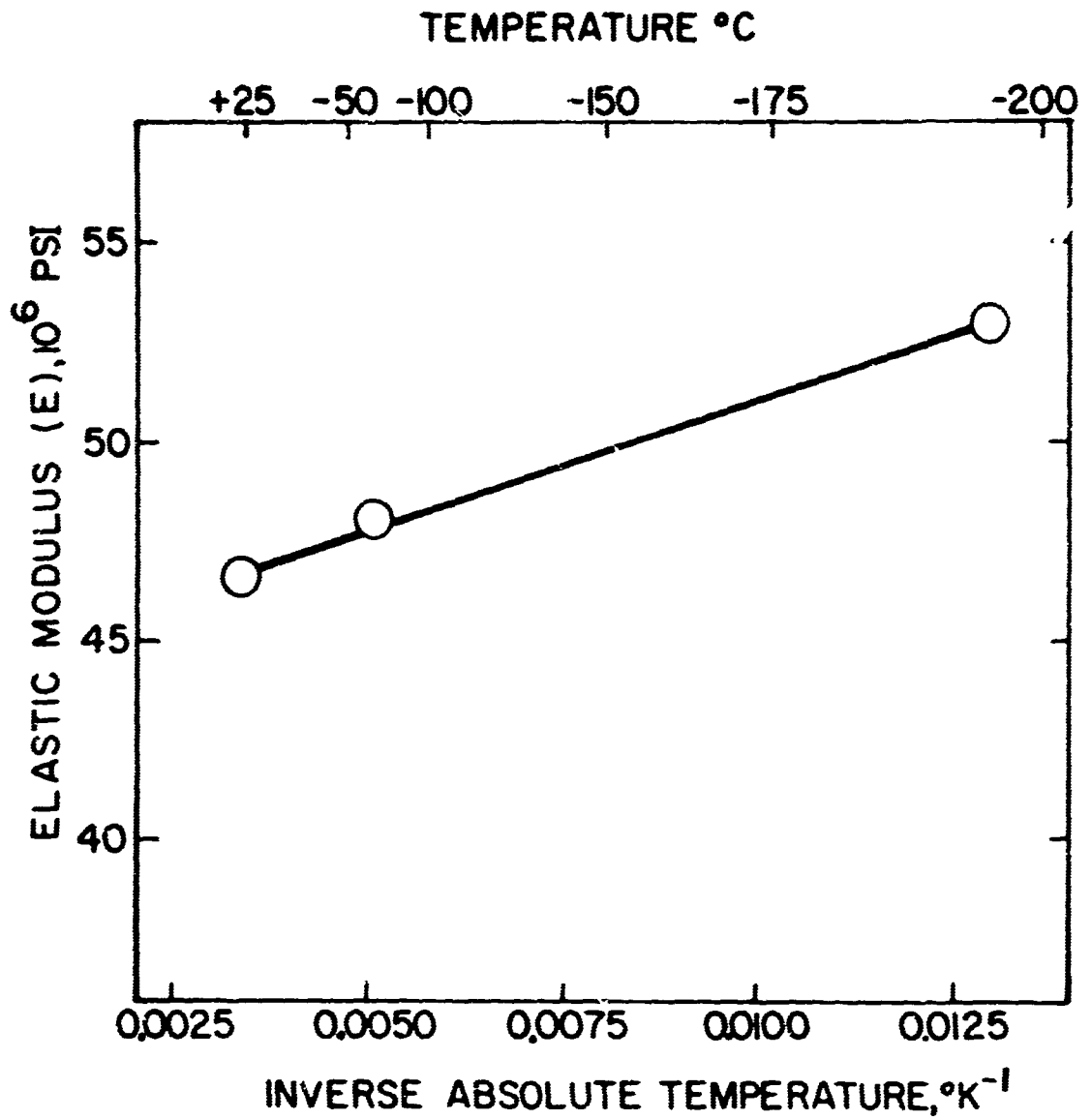


Fig. 49 - Variation of Elastic Modulus of Molybdenum (Mo-E1 Rod) with Temperature.

Table 17

Calculated Effective Surface Energy for Crack Initiation in Mo-E2, Mo-E3 and Mo-E4 Strip

Material and Original Grain Size	Test Temp. °C	Fracture Strain (ϵ_F)	Shear Modulus (G)	Grain Size*	Fracture Stress (σ_F)	Locking Parameter (k_y) or (k_f)	Effective Surface Energy (γ_i)	Fracture Initiation Mode
			dynes/cm ²	mm	dynes/cm ²	dynes/cm ^{3/2}	ergs/cm ²	
Mo-E2 (0.026 mm)	-80	0.04	1.25x10 ¹²	0.026	8.6x10 ⁹	1.6x10 ^{7**}	0.7 x10 ⁴	intergran.
	-55	0.35	1.25x10 ¹²	0.022	10.0x10 ⁹	6.5x10 ⁷	0.3x10 ⁴	cleavage
	-30	0.80	1.2x10 ¹²	0.019	11.6x10 ⁹	4.3x10 ⁷	0.25x10 ⁴	cleavage
	+25	0.98	1.2x10 ¹²	0.018	8.4x10 ⁹	4.5x10 ⁷	0.2x10 ⁴	cleavage
Mo-E2 (0.044 mm)	-150	0.02	1.3x10 ¹²	0.044	9.0x10 ⁹	2.4x10 ^{7**}	1.4x10 ⁴	intergran.
	-75	0.07	1.25x10 ¹²	0.043	7.6x10 ⁹	4.5x10 ⁷	0.25x10 ⁴	intergran.
	-50	0.20	1.25x10 ¹²	0.040	8.8x10 ⁹	4.0x10 ⁷	0.25x10 ⁴	cleavage
	-25	0.65	1.2x10 ¹²	0.034	10.1x10 ⁹	3.7x10 ⁷	0.25x10 ⁴	cleavage
	+25	1.00	1.2x10 ¹²	0.030	9.6x10 ⁹	4.5x10 ⁷	0.25x10 ⁴	cleavage
Mo-E2 (0.174 mm)	-196	0.02	1.4x10 ¹²	0.174	10.3x10 ⁹	2.9x10 ^{7**}	3.5 x10 ⁴	intergran.
	-40	0.17	1.2x10 ¹²	0.160	8.4x10 ⁹	3.8x10 ⁷	0.4x10 ⁴	intergran.
	-20	0.62	1.2x10 ¹²	0.134	9.7x10 ⁹	3.4x10 ⁷	0.4x10 ⁴	cleavage
	0	0.95	1.2x10 ¹²	0.120	11.0x10 ⁹	3.1x10 ⁷	0.4x10 ⁴	cleavage
	+25	1.00	1.2x10 ¹²	0.118	10.5x10 ⁹	4.5x10 ⁷	0.5x10 ⁴	cleavage

Table 17 (Continued)
Calculated Effective Surface Energy for Crack Initiation in Mo-E2, Mo-E3 and Mo-E4 Strip

Material and Original Grain Size	Test Temp. °C	Fracture Strain (ϵ_F)	Shear Modulus (G) dynes/cm ²	Grain Size* mm	Fracture Stress (σ_F) dynes/cm ²	Locking Parameter (k_y) or (k_f) dynes/cm ^{3/2}	Effective Surface Energy (γ_i) ergs/cm ²	Fracture Initiation Mode
Mo-E3 (0.023 mm)	-85	0.03	1.25×10^{12}	0.023	9.0×10^9	$7.0 \times 10^{7**}$	0.3×10^4	intergran.
	-45	0.54	1.25×10^{12}	0.018	11.2×10^9	2.0×10^7	0.1×10^4	cleavage
	-20	0.91	1.2×10^{12}	0.016	12.4×10^9	1.7×10^7	0.1×10^4	cleavage
	+25	1.06	1.2×10^{12}	0.015	10.7×10^9	2.2×10^7	0.1×10^4	cleavage
Mo-E4 (0.020 mm)	-35	0.00	1.2×10^{12}	0.020	5.5×10^9	$22 \times 10^{7**}$	0.8×10^4	intergran.
	-25	0.10	1.2×10^{12}	0.019	6.2×10^9	8.6×10^7	0.25×10^4	intergran.
	0	0.36	1.2×10^{12}	0.017	7.6×10^9	12×10^7	0.4×10^4	intergran.
	+25	0.68	1.2×10^{12}	0.015	9.0×10^9	19×10^7	0.7×10^4	cleavage
	+50	0.61	1.2×10^{12}	0.015	7.5×10^9	19×10^7	0.55×10^4	cleavage

* Corrected for reduction in area prior to fracture.

** Yield locking parameter (k_y) values; other values given in this column are flow locking parameter (k_f) values.

5. Effective Surface Energy for Crack Propagation

5.1 Based on Tensile Tests

Assuming that fracture of the molybdenum materials is controlled by crack initiation rather than crack propagation, it follows that using the value of the observed fracture stress in a Griffith-Orowan type of relation should give an upper limit to the probable value of the effective surface energy for crack propagation (γ_p). Accepting this restriction, calculations were made of γ_p under plane strain conditions using the Irwin (14) relation for an interior crack of radius c that is small with respect to the section area:

$$\gamma_p = \frac{4(1 - \nu^2) \sigma_F^2 c}{\pi E} \quad (25)$$

For the crack radius (c), it was decided to use one-half the measured cleavage facet size for test temperatures above T_d and one-half the measured intergranular facet size for test temperatures of T_d and below.

As shown in Table 18, the γ_p values are in the range of 1.0×10^4 to 12.3×10^4 ergs/cm². Starting at -196°C for Mo-E2 and Mo-E3 and at -100°C for Mo-E4, γ_p first decreases with increase in temperature up to T_d , then increases from T_d to T_m , and finally decreases above T_m . This variation is similar to that of σ_F with temperature. The ratio of γ_p to γ_i at the same temperature varies from 1 to 43. This indicates the possibility that γ_p may be larger than γ_i even though fracture is controlled by crack initiation.

According to Barrett (15) crack initiation involves the growth of a critical size crack until it encounters a major barrier (typically a grain boundary). In order for the crack to cross the boundary and continue to propagate, an increase in effective surface energy is involved. Thus, it seems reasonable to expect that γ_p is generally greater than γ_i . For fracture to be controlled by crack initiation rather than crack propagation, the condition to be satisfied is $(\sigma_F)_p \leq (\sigma_F)_i$. Based on the results given in Table 17, it appears possible for the ratio of $(\sigma_F)_p$ to $(\sigma_F)_i$ to be as low as 1/43 with $\gamma_p \geq \gamma_i$.

5.2 Based on Precracked Charpy Slow Bend Tests

As was shown in Table 10, the fracture toughness values of Mo-E3 as determined by precracked Charpy slow bend tests fall in the range of 0.4×10^7 to 2.1×10^7 ergs/cm². These values are approximately 10^3 times larger than either the calculated effective surface energy for crack initiation (γ_i) or for crack propagation (γ_p) based on the tensile test results for Mo-E3 as given in Tables 17 and 18 respectively. This difference may be due to a greater amount of plastic deformation at

Table 18

Calculated Effective Surface Energy for Crack Propagation in Mo-E2, Mo-E3, and Mo-E4 Strip

Material and Original Grain Size	Test Temp. °C	Fracture Strain (ϵ_F)	Elastic Modulus (E) dynes/cm ²	Facet Semi-Size (c) cm	Fracture Stress (σ_F) dynes/cm ²	Effective Surface Energy (γ_p) ergs/cm ²	Fracture Initiation Mode	γ_p/γ_i
Mo-E2 (0.026mm)	-196	0.02	3.65×10^{12}	0.0011	12.3×10^9	5.3×10^4	intergran.	-
	-80	0.04	3.3×10^{12}	0.0010	8.6×10^9	2.6×10^4	intergran.	4
	-55	0.35	3.3×10^{12}	0.0010	10.0×10^9	3.5×10^4	cleavage	12
	-30	0.80	3.25×10^{12}	0.0008	11.6×10^9	3.8×10^4	cleavage	15
	-25	0.98	3.2×10^{12}	0.0008	8.4×10^9	2.0×10^4	cleavage	10
Mo-E2 (0.044mm)	-196	0.02	3.6×10^{12}	0.0019	10.9×10^9	7.2×10^4	intergran.	-
	-75	0.07	3.3×10^{12}	0.0018	7.6×10^9	3.6×10^4	intergran.	14
	-50	0.20	3.3×10^{12}	0.0020	8.8×10^9	5.4×10^4	cleavage	22
	-25	0.65	3.2×10^{12}	0.0018	10.1×10^9	6.6×10^4	cleavage	26
	+25	1.00	3.2×10^{12}	0.0019	9.6×10^9	3.0×10^4	cleavage	12
Mo-E2 (0.174mm)	-196	0.02	3.65×10^{12}	0.0013	10.3×10^9	4.3×10^4	intergran.	1
	-40	0.17	3.3×10^{12}	0.0029	8.4×10^9	7.1×10^4	intergran.	18
	-20	0.62	3.25×10^{12}	0.0034	9.7×10^9	11.3×10^4	cleavage	28
	0	0.95	3.2×10^{12}	0.0021	11.0×10^9	9.1×10^4	cleavage	23
	+25	1.00	3.2×10^{12}	0.0025	10.5×10^9	1.0×10^4	cleavage	20

Table 18 (Continued)

Calculated Effective Surface Energy for Crack Propagation in Mo-E2, Mo-E3, and Mo-E4 Strip

Material and Original Grain Size	Test Temp. °C	Fracture Strain (ϵ_F)	Elastic Modulus (E) dynes/cm ²	Facet Semi-Size (c) cm	Fracture Stress (σ_F) dynes/cm ²	Effective Surface Energy (γ_p) ergs/cm ²	Fracture Initiation Mode	γ_p/γ_i
Mo-E3 (0.023mm)	-196	0.02	3.65×10^{12}	0.0009	14.8×10^9	4.2×10^4	intergran.	-
	-85	0.03	3.3×10^{12}	0.0006	6.1×10^9	1.7×10^4	intergran.	6
	-45	0.54	3.25×10^{12}	0.0008	11.2×10^9	3.6×10^4	cleavage	36
	-20	0.91	3.25×10^{12}	0.0008	12.4×10^9	4.3×10^4	cleavage	43
	+25	1.06	3.2×10^{12}	0.0008	10.7×10^9	3.3×10^4	cleavage	33
Mo-E4 (0.020mm)	-100	0.00	3.35×10^{12}	0.0012	8.6×10^9	3.1×10^4	intergran.	-
	-35	0.00	3.25×10^{12}	0.0009	5.5×10^9	1.0×10^4	intergran.	2
	-25	0.10	3.2×10^{12}	0.0009	6.2×10^9	1.2×10^4	intergran.	5
	0	0.36	3.2×10^{12}	0.0010	7.6×10^9	2.1×10^4	intergran.	5
	+25	0.68	3.2×10^{12}	0.0011	9.0×10^9	3.2×10^4	cleavage	5
+50	0.61	3.2×10^{12}	0.0011	7.5×10^9	2.2×10^4	cleavage	4	

the tip of the fatigue precrack in the Charpy specimen as compared to the tip of the crack that initiates in a tensile specimen. In other words, the fatigue action at +25°C may produce a relatively "blunt" crack tip corresponding to much lower stress concentration as compared to that for the tip of a tensile test crack formed at -100°C.

6. Variation of Fracture Stress with Temperature

6.1 Decrease in Fracture Stress up to T_d

Starting from a relatively low temperature, -196°C, the fracture stress (σ_F) of the various recrystallized molybdenum materials studied in this investigation was found to decrease with increase in test temperature and reach a minimum value at the tensile ductility transition temperature (T_d). Since σ_F is slightly higher than the proportional limit over most of this temperature range, it seems likely that a) σ_F corresponds to crack nucleation rather than to crack propagation, and b) crack nucleation requires the prior occurrence of at least a small amount of plastic deformation. A crack that initiates at a stress level higher than that required for propagation would be expected to immediately propagate completely through the specimen section. On this basis, the observed decrease in σ_F up to T_d is considered to be essentially a consequence of the decrease in yield stress (σ_y) which occurs with increase in test temperature.

6.2 Increase in Fracture Stress T_d to T_m

In the range from T_d to T_m , σ_F increases from a minimum to a maximum even though σ_y continues to decrease. These changes are accompanied by an increase in ductility from a relatively low level at T_d to a relatively high level at T_m . It was observed that below T_d the elongation takes place uniformly over the entire gage length, whereas above T_d necking occurs prior to fracture. These fracture and necking observations indicate that T_d represents the intersection of the fracture stress corresponding to uniform elongation (i. e., the σ_F curve below T_d) with the necking stress (σ_n) which is the tensile strength on a true stress basis.

As an aid in understanding the increase in σ_F in the range from T_d to T_m , σ_F can be considered as a flow stress, i. e., the particular flow stress that corresponds to the fracture strain (ϵ_F) at a given test temperature. On this basis, it was shown that the increase in σ_F above T_d can be attributed to the following effects: a) strain hardening due to increased substructure formation, b) plastic constraint due to the necking that occurs above T_d , and c) increase in strain rate due to the localized nature of necking. This approach was first used by Bechtold (8) and more recently by Ault (11), although the latter neglected the strain hardening effect.

For a more complete understanding of the increase in σ_F from T_d to T_m , an explanation is needed for the increase in fracture stress per se which permits the flow stress corresponding to ϵ_F to increase in the observed manner. Although the plastic constraint and increased local

strain rate effects due to necking both increase the flow stress corresponding to a given amount of plastic strain, it seems doubtful whether these effects also raise the fracture stress per se. It is generally found that an increase in plastic constraint results in a decrease in fracture stress, which is attributed to an increase in the flow stress relative to the fracture stress such that fracture occurs at a smaller plastic strain value than without plastic constraint. Likewise, an increase in strain rate raises the applied stress required for a given amount of plastic strain, and appears to act similar to plastic constraint in that the fracture stress is lowered.

Since no micro-cracks were observed above T_d , it appears likely that crack initiation rather than crack propagation is the controlling step in the fracture of the molybdenum materials studied. In order to explain the increase in σ_F in the range of T_d to T_m on the basis of crack initiation, one might hypothesize that an increase occurs in the effective surface energy for crack initiation (γ_i). However, calculations of γ_i made on the basis of a modified Cottrell relation using the flow locking parameter (k_f) instead of the yield locking parameter (k_y) indicate that, with the possible exception of the Mo-E4 material, there is no significant change in γ_i in this range. Instead, the increase in σ_F appears to be associated in most cases with a decrease in both k_f and the effective grain size (l) corrected for the reduction in area that occurs prior to fracture. The decrease in k_f with increase in temperature can be attributed to decreased association of interstitials with dislocations.

6.3 Decrease in Fracture Stress above T_m

It was found that σ_F reaches a maximum at T_m and then decreases above this temperature. Since no evidence of fibrous fracture was found at the highest test temperature employed (+25°C or +50°C), it does not seem likely that the decrease in σ_F can be associated with a change in fracture mode from cleavage to fibrous. However, a change does take place from comparatively undistorted to highly distorted cleavage facets. This is accompanied by an increase in k_f , which based on the Cottrell relation for crack initiation should tend to lower σ_F . Further work is necessary to account for the increase in k_f above T_m .

IV. CONCLUSIONS

1. As determined by tensile tests, the ductility transition temperature (T_d) and the brittleness transition temperature (T_b) approximately coincide in fine grain, recrystallized molybdenum. With increase in grain size, T_b is lowered whereas T_d is raised.

2. The occurrence of a minimum in the observed fracture stress (σ_F) at T_d is associated with the intersection of the necking stress (σ_n) and the fracture stress corresponding to uniform fracture strain, i. e. necking occurs above T_d but not below T_d . If T_d and T_b happen to coincide, the yield stress (σ_y) also intersects at the minimum in σ_F since T_b is defined as the intersection of σ_F and σ_y .

3. Taking into account strain hardening due to substructural changes in addition to necking effects such as plastic constraint and increased strain rate, the predicted variation of σ_F with test temperature above T_d was found to agree (within 15%) with the observed values in most cases.

4. For the molybdenum materials with relatively low oxygen contents, the fracture initiation mode is intergranular at or below T_d and cleavage above T_d . For a relatively high oxygen content (145 ppm), the fracture initiation mode is intergranular up to a temperature that is intermediate between T_d and that corresponding to the maximum in σ_F (T_m).

5. By prestraining at a temperature above T_d and breaking below T_d , it is possible to increase σ_F by as much as 20% as compared to without prestraining. The increase in σ_F due to prestraining correlates with an increase in cleavage facets in most cases.

6. For test temperature below T_d , fracture occurs after a relatively small amount of plastic strain and is apparently controlled by crack initiation. For test temperatures above T_d , crack initiation also appears to be the controlling step even though the amount of plastic strain prior to fracture increases markedly.

7. The ratio of the flow locking parameter (k_f) to the yield locking parameter (k_y) is approximately unity at room temperature and decreases to at least 0.3 with lowering of temperature. A minimum in k_f was found to occur between T_d and T_m .

8. Based on the Cottrell relation for crack initiation, the increase in σ_F from T_d to T_m is attributed to decreases in both k_f and the effective grain size. The maximum in σ_F at T_m is associated with the increase in k_f after passing through a minimum below T_m .

9. The calculated upper limit of the probable value of the effective surface energy for crack propagation (γ_p^1) was found to be up to about 40 times greater than the corresponding γ_i^1 value.

References

1. Lement, B.S., Thomas, D.A., Weissmann, S., Owen, W.S. and Hirsch, P.B., "Substructure and Mechanical Properties of Refractory Metals," WADD-TR-61-181, (August, 1961).
2. Lement, B.S., Thomas, D.A., Weissmann, S., Owen, W.S. and Hirsch, P.B., "Substructure and Mechanical Properties of Refractory Metals," WADD-TR-61-181, Part II (October 1, 1962).
3. Lement, B.S., Thomas, D.A., Weissmann, S., Owen, W.S., and Hirsch, P.B., "Substructure and Mechanical Properties of Refractory Metals," WADD-TR-61-181, Part III (April, 1963).
4. Wronski, A.S., and Johnson, A.A., "The Deformation and Fracture Properties of Polycrystalline Molybdenum," *Phil. Mag.* 7 (1962) 213.
5. Cottrell, A.H., "Theory of Brittle Fracture in Steel and Similar Metals," *Trans. AIME*, 212 (1958) 192.
6. Bridgeman, P.W., "The Stress Distribution at the Neck of a Tension Specimen," *Trans. ASM*, 32 (1944) 553.
7. Aronofsky, A., "Evaluation of Stress Distribution in the Symmetrical Neck of Flat Tensile Bars," *J. Appl. Mech.*, 18 (1951) 75.
8. Bechtold, J.H., "Effects of Temperature on the Flow and Fracture Characteristics of Molybdenum," *Trans. AIME* 197 (1953) 1469.
9. Hartbower, C.E. and Orner, G.M., "Metallurgical Variables Affecting Fracture Toughness in High-Strength Sheet Alloys," ASD-TR-62-868 (February 1963).
10. Irwin, G.R., Kies, J.A., and Smith, H.L., "Fracture Strength Relative to Onset and Arrest of Crack Propagation," *Proc. ASTM*, 58, (1958).
11. Ault, R.T., "Fracture of Molybdenum," RTD-TDR-63-4088, December, 1963.
12. Owen, W., et al. "Yield Phenomena in Refractory Metals," Ref. no. 3, page 168.
13. Armstrong, R., Codd, I., Douthwaite, R.M., and Petch, N.J., "The Plastic Deformation of Polycrystalline Aggregates," *Phil. Mag.* 7 (1962) 45.
14. Irwin, G.R., "Theoretical Aspects of Fracture Failure Analysis," ASM Metals Congress, New York (1962).
15. Averbach, B.L. et al., "Fracture", Swampscott 1959 Conference, The Technology Press (1959).

Appendix I

Definitions of Transition Temperatures Used in Text

- T_b Brittleness - transition temperature corresponds to intersection of the fracture stress (σ_F) and yield stress (σ_y) curves.
- T_d Ductility - transition temperature corresponds to minimum in the fracture stress (σ_F) curve.
- T_m Corresponds to maximum in fracture stress (σ_F) curve, which occurs at a temperature above T_d .